University of Pécs

Doctoral School of Chemistry

Electrospray ionization tandem mass spectrometry-based structure elucidation of lipid A molecules

PhD thesis

Ibrahim Aissa

Supervisor
Dr. Ágnes Dörnyei

Co-supervisor
Dr. Anikó Kilár

Head of the Doctoral School
Prof. Dr. Attila Felinger

PÉCS, 2023

À mon père (Mounir) et ma mère (Amel)

Aucune dédicace ne saurait exprimer l'amour, l'estime, le dévouement et le respect que j'ai toujours eu pour vous.

Rien au monde ne vaut les efforts fournis jour et nuit pour mon éducation et mon bien être.

Ce travail est le fruit de vous sacrifices que vous avez consentiez pour mon éducation et ma formation.

Je vous dédie aujourd'hui ma réussite.

À mes frères (Mohamed Ali et Riadh)

À tous ceux qui me sont chers

Acknowledgements

First, I sincerely appreciate **Almighty God** to bless me with the opportunity to pursue my studies in a peaceful and charming country "**Hungary**".

Additionally, I am deeply grateful to my supervisor **Dr. Ágnes Dörnyei**, for her permanent support, scientific guidance, constant optimism and encouragement throughout this long walk with all its “ups and downs”. I consider myself very fortunate for being receiving kindness and respect from her. Without her acceptance to be my supervisor, I would not be able to finish my studies in **Hungary**. Thus, I’m highly indebted to her.

I would like to express my gratitude and appreciation to my co-supervisor **Dr. Anikó Kilár** who made this work possible, she continuously provided encouragement and was always willing and enthusiastic to assist in any way she could throughout the research project. Her positive outlook, cheerful mood and support in my research inspired me and gave me confidence. Her careful editing contributed enormously to the production of the papers.

I am thankful to my colleague **Dr. Viktor Sándor** for his help and contribution in research. I am especially thankful to him for the excellent training as well as to share with me his expertise and competences. We really had a great time during the measurements full of jokes and spectacular moments that we will remember forever.

I am thankful to the former head of our doctoral school **Prof. Dr. Ferenc Kilár** and the head of our department **Prof. Dr. Attila Felinger** for their invaluable advice,

continuous support during my PhD study. Their immense knowledge and plentiful experience have encouraged me in all the time of my academic research and daily life.

I would like to express my deepest gratitude to **Prof. Bela Kocsis** for preparing natural lipid A samples.

I also grab the opportunity to thank my best friend **Dr. Sami Chniti** who is one of the few people in my life who has helped me become who I am today. I'm so thankful for this friendship.

I must not forget my friend **Péter Noveczky**, who helped me a lot at the beginning of my journey. I wish him the best for his career and life.

Finally, I appreciate the **Stipendium Hungaricum Scholarship Programme** for funding my doctoral study.

Ibrahim

List of Abbreviations

AcOH.....acetic acid

Ara4N.....4-amino-4-deoxy-L-arabinose

BGE.....background electrolyte

C10:0.....decanoic acid or capric acid

C12:0.....dodecanoic acid or lauric acid

C14:0.....tetradecanoic acid or myristic acid

C14:1.....tetradecenoic acid or unsaturated myristic acid

C10:0(3-OH) .....3-hydroxydecanoic acid or hydroxycapric acid

C12:0(2-OH) .....2-hdroxydodecanoic acid or hydroxylauric acid

C12:0(3-OH) .....3-hydroxydodecanoic acid or hydroxylauric acid

C14:0(3-OH) .....3-hydroxytetradecanoic acid or hydroxymyristic acid

CE.....capillary electrophoresis

CID.....collision induced dissociation

DCM.....dichloromethane

EIE.....extracted ion electropherogram

ESI….....electrospray ionization

Et_3N.....triethylamine

FDA.....Food and Drug Administration

GlcN 2-amino-2-deoxy-D-glucopyranose

HPLC .....high performance liquid chromatography

IT.....ion trap

Kdo.....3-deoxy-D-*manno*-oct-2-ulosonic acid

LC .....liquid chromatography

LPSs.....lipopolysaccharides

MALDI.....matrix assisted laser desorption ionization

MS .....mass spectrometry

MS/MS .....tandem mass spectrometry

MS^n .....multistage mass spectrometry

NACE .....non-aqueous capillary electrophoresis

OS .....oligosaccharide

Q.....quadrupole

q.....collision cell

QqQ.....triple quadrupole

Th1.....T helper cell type 1

TLC.....thin layer chromatography

TLR4/MD-2.....toll-like receptor 4/myeloid differentiation factor 2

TOF.....time-of-flight

UVPD.....ultraviolet photodissociation

Contents

1. Introduction

The main cause of death in intensive care units in hospitals around the world is septicemia, a serious bloodstream infection that may progress to sepsis and septic shock (Beutler and Rietschel, 2003). Septicemia happens when bacteria and their toxins enter the bloodstream from a bacterial infection in another part of the body, commonly the skin, lungs, kidneys, or bladder. People with chronic health conditions and weakened immune system are at a higher risk of septicemia due to their increased susceptibility to bacterial infections. In case of a Gram-negative bacterial infection, the uncontrolled growth and membrane lysis of bacteria results in the release of large amounts of membrane-associated lipopolysaccharide (LPS, endotoxin) in the bloodsream, which can, in turn, lead to exaggerated immune responses, called sepsis (Rietschel and Brade, 1992; Cavaillon, 2018). In serious cases, sepsis can result in dangerously low blood pressure, called septic shock, which can be fatal to the host.

Paradoxically, under normal circumstances, Gram-negative bacteria (e.g., intestinal bacteria, or bacteria in home dust) have been known by upregulating the immune system by releasing small amounts of LPS that act as immunostimulants (Galanos and Delves, 1998; Gehring et al., 2020; Mbongue et al., 2022). Thus, in order to understand the diverse effects of LPS molecules on the human body, detection of their chemical structure, especially their lipid A portion – the primary immunostimulator of LPS (Zahringer et al., 1994) – is essential.

At present, mass spectrometry is the most efficient method for exposing chemical structures of bacterial lipid A (Kilár et al., 2013) . Soft ionization techniques such as electrospray (ESI) and matrix-assisted laser desorption/ionization (MALDI) are used extensively to investigate the structural characteristics of these biomolecules. Tandem

mass spectrometry (MS/MS), and particularly, higher order tandem mass spectrometry (MS^n) in an ion trap mass analyzer is a powerful technique to demonstrate structural heterogeneity present in a lipid A extract. Not least, chemical structure information is especially important for the development of lipid A-based vaccine adjuvants.

2. Literature review

2.1. Lipopolysaccharides

A variety of amphiphilic macromolecules are present in the outer membrane of a Gram-negative bacterium. Lipopolysaccharides (LPSs), also called endotoxins, are regarded as one of those exceptionally important outer membrane-forming macromolecules of bacteria (Rietschel and Brade, 1992; Caroff and Novikov, 2020) (Fig. 1). Besides being implicated in regular membrane functions, LPS also has a unique role related to immune response (Alexander and Rietschel, 2001), as they are recognized by the host's defense system during an infection (Rietschel et al., 1996).

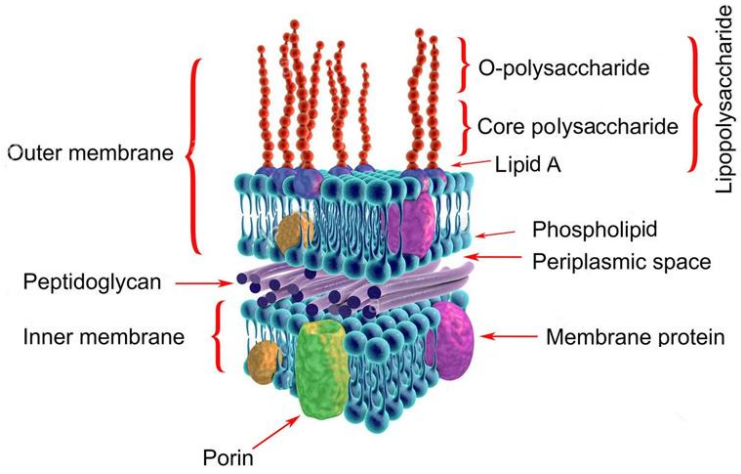

Figure 1. Gram-negative bacterial cell wall, labeled, 3D illustration.

2.1.1. Structure of lipopolysaccharides

The overall structure of LPS is illustrated in Fig. 2. A full LPS molecule consists of three structural components that are covalently linked with each other: (i) a long "O-

specific" polysaccharide, (ii) a central oligosaccharide region (OS core), and (iii) a hydrophobic region known as lipid A (Rietschel et al., 1994). This latter anchors LPS to the outer leaflet of the outer membrane of Gram-negative bacteria through hydrophobic interactions.

LPSs are also divided into three types based on their structural components (Hitchcock and Brown, 1983; Pupo et al., 2013). A smooth LPS (type S) includes all three domains; these are common in wild-type bacterial strains. They are also referred to as long-chain LPS. A semi-rough LPS (type SR) (also called short-chain LPS) has only one O-chain repeater unit attached to the core oligosaccharide. Rough LPS (type R) are completely free of the O-specific polysaccharide chain. Endotoxic activity was compared between S-type LPS and R-type LPS and it was reported that the endotoxic activity is caused by the lipid A portion only (Zahringer et al., 1994).

The O-specific antigen is composed of repetitive units of monosaccharides responsible for the antigenic specificity. It exhibits high structural variability depending on the nature, sequence, substitution and binding types of monosaccharides, and the structure of the repetitive oligosaccharide units varies from strain to strain (Luderitz et al., 1982; Kabanov and Prokhorenko, 2010).

The core oligosaccharides are structurally very similar and thus present less variability (Mayer et al., 1989; Kabanov and Prokhorenko, 2010). The core is made up of two regions: an internal core and an external core. The outer core consists of hexoses, whereas the inner core contains heptapyranoses and 3-deoxy-2-manno-2-octulosonic acid (Kdo). The high density of negatively charged residues has a physiological significance of concentrating the bivalent cations (Ca^{2+} and Mg^{2+}) at the cell surface which are necessary for structural and functional integrity of the external membrane (Rietschel et al., 1994).

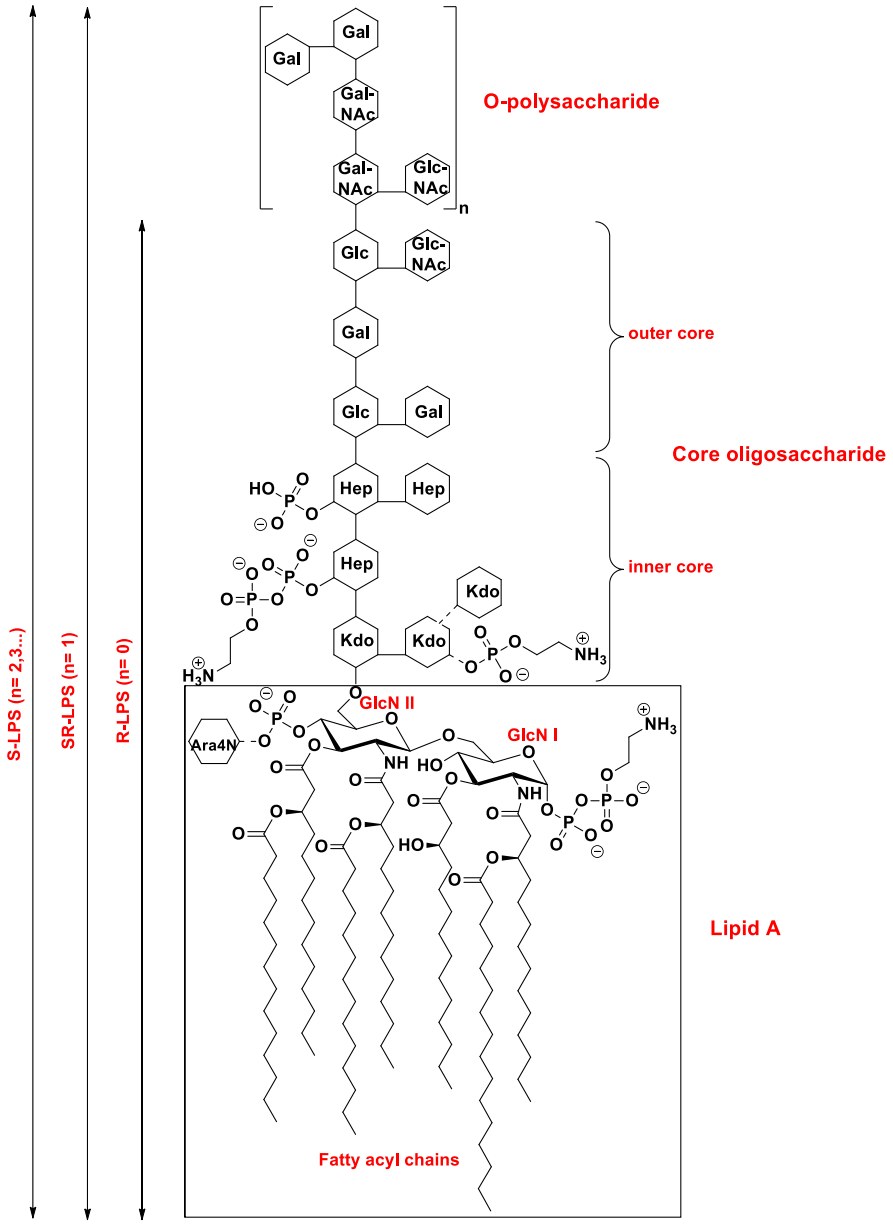

Figure 2. General architecture of an intact smooth type endotoxin (lipopolysaccharide) (Kilár et al., 2013). Abbreviations: Gal: D-galactose, GalNAc: *N*-acetyl-D-galactosamine, Glc: D-glucose, GlcNAc: *N*-acetyl-D-glucosamine, Hep: L-*glycero*-D-*manno*-heptose, Kdo: 3-deoxy-D-manno-oct-2-ulosonic acid, Ara4N: 4-amino-4-deoxy-L-arabinose; GlcN, D-glucosamine. GlcN I and II indicate the reducing and non-reducing terminus of disaccharide, respectively. Some common fatty acids of bacterial lipid A are lauric acid (12:0), myristic acid (14:0), palmitic acid (16:0), stearic acid (18:0), and/or their hydroxyl derivatives.

Lipid A constitutes the toxic and immunomodulating component of LPS (Caroff and Novikov, 2020). Lipid A is a phosphoglycolipid that is pathophysiologically important, because it has intense effects when injected into a mammal. The most common effects

include the induction of endotoxin shock, pyrogenicity, macrophage activation, and interferon production (Youngner et al., 1973; Galanos et al., 1985).

The general structure of lipid A moiety is shown in Figure 3. Mostly, it is composed of a β-D-Glc*p*N-(1→6)-α-D-Glc*p*N disaccharide backbone, but in some bacteria 2,3-diamino-2,3-deoxy-glycopyranose residues have also been observed (Moran et al., 1991; Zahringer et al., 2004). To the disaccharide spine, a variety of acyl chains are attached (chain lengths generally range from 10 to 30 carbon atoms), as well as phosphoryl residues, which can be decorated by ethanolamine phosphate or 4-amino-4-deoxy-arabinose. One of the phosphoryl residues is linked to the hydroxyl group of the reducing glucosaminyl residue and the other one is attached at position 4′ of the non-reducing glucosamine group.

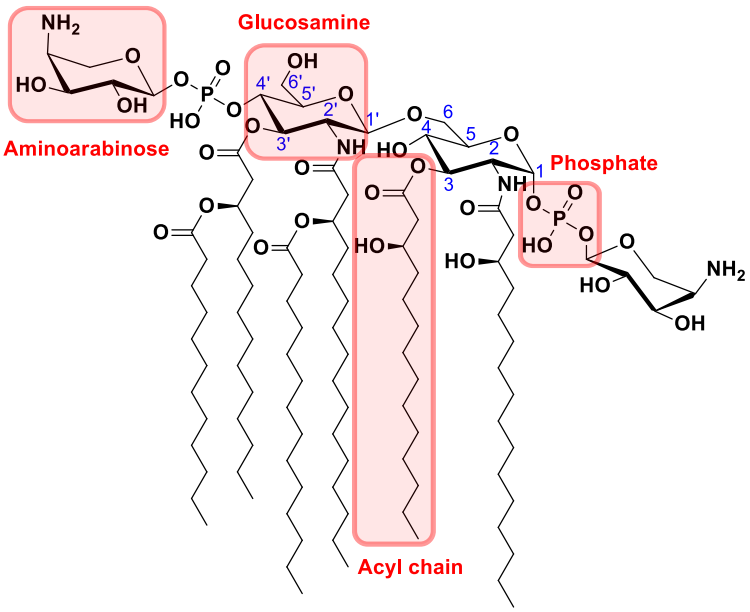

Figure 3. General structure of lipid A.

Usually, four acyl chains are attached to the carbohydrate backbone at positions 2, 3, 2′, and 3′. The acyl chains at positions 2, 2′ and 3′ can be further acylated (depending on the bacterial strain) at their 3-hydroxyl group. In an *Escherichia coli* type lipid A, these

secondary acylations consist of dodecanoic acid (C12:0), tetradecanoic acid (C14:0), and in a *Salmonella* type lipid A, an extra hexadecanoic acid (C16:0) is present.

2.1.2. Recognition of lipid A by the innate immune receptor TLR4/MD-2

When the immune system or antibiotics attack the invading bacteria and destroy their cell wall, the membrane-bound LPS is set free, and the lipid A part of endotoxins is sensed by the mammalian toll-like receptor 4 (TLR4)/MD-2 complex present on macrophages. However, depending on the structure and amount of lipid A, this recognition can generate toxic effects to the host body. The most toxic *E. coli* type lipid A, carrying 6 fatty acids and 2 phosphate groups, is most sensitively recognized by the TLR4/MD-2 complex (Park et al., 2009) (Fig. 4a). After activation it triggers an excessive production of inflammatory cytokines leading to septic shock and death.

On this lipid A, as shown in Fig. 4, the amide linked primary fatty acyl chain at C-2 is labelled R2, the ester linked primary fatty acyl chain at C-3 is labelled R3, the amide linked primary fatty acyl chain at C-2' is labelled R2', the ester linked primary fatty acyl chain at C-3' is labelled R3', the R2" chain is matched to the secondary fatty acid at C-2' position and the R3" chain is matched to the secondary fatty acid at C-3' position. In the crystal structure these lipid chains interact with the hydrophobic pocket in MD-2 (Fig. 4b). The acyl chains of lipids R3, R2', R3', R2" and R3" are completely buried inside the pocket, but the R2 chain is partially exposed to the MD-2 surface composing the core hydrophobic interface for interaction with TLR4*. The amide (at C-2 and C-2' positions) and ester (at C-3 and C-3' positions) groups linked to the two glucosamine backbones are exposed to the surface of MD-2. They interact with hydrophilic side chains situated on the βG strand of the MD-2 pocket and on the surface of TLR4 and TLR4* (Fig. 4c). Both phosphate groups of lipid A bind to the TLR4–MD-2 complex through interaction with

positively charged residues in TLR4, TLR4* and MD-2 and establishing a hydrogen bond to S118 of MD-2 (Fig. 4d).

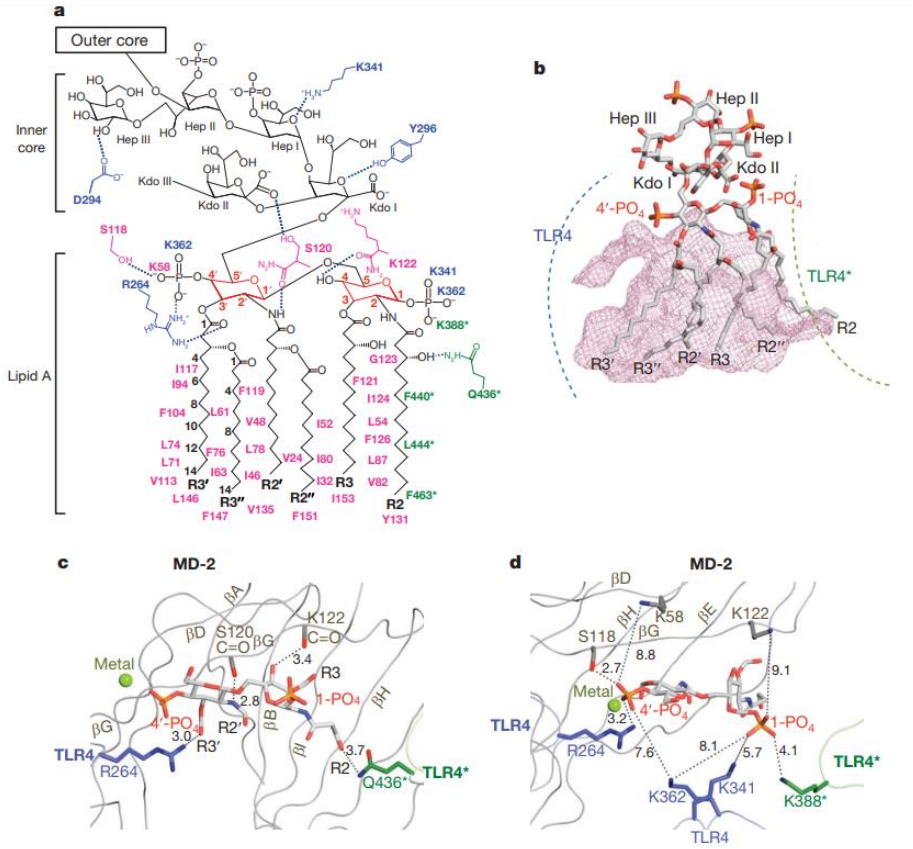

Figure 4. Binding of LPS to TLR4/MD-2 receptor complex (Park et al., 2009).
a) Chemical structure of the R type *E. coli* LPS. Fatty acyl chains are labelled, glucosamines and fatty acyl chains are numbered. Hydrogen bonds are represented as broken blue lines.
b) The molecular surface of the MD-2 pocket is traced in mesh. c) Hydrogen bonds between lipid A and TLR4–MD-2. d) Ionic and hydrogen bond interactions of both phosphate groups of lipid A. Interaction distances in Ångström are written.

Changes in the acylation, phosphorylation, or glycosylation profile affect the endotoxic activity of the lipid A in the Gram-negative bacterium (Rietschel et al., 1994; Trent et al., 2006). Any deviation from the classical bisphosphorylated hexa-acyl lipid A could lead to reduced toxicity or even antitumor activity. For instance, endotoxicity is reduced by removal of one phosphate group. Interestingly, it has been shown that lipid A with a reducing terminal phosphate (at the 1 position) was more highly inflammatory than lipid A with a non-reducing terminal phosphate (at the 4’ position) (Coats et al., 2011).

Any substitution in the phosphate group could also modify the endotoxic activity. An aminoarabinose sugar (Ara4N) attached to the phosphate group increases the bacterial resistance to the host's cationic antimicrobial peptides (Trent et al., 2006). Some tetra-acylated lipid A could even possess antagonistic properties (Peri and Calabrese, 2014). A selection of natural lipid A structures are summarized in Figure 5.

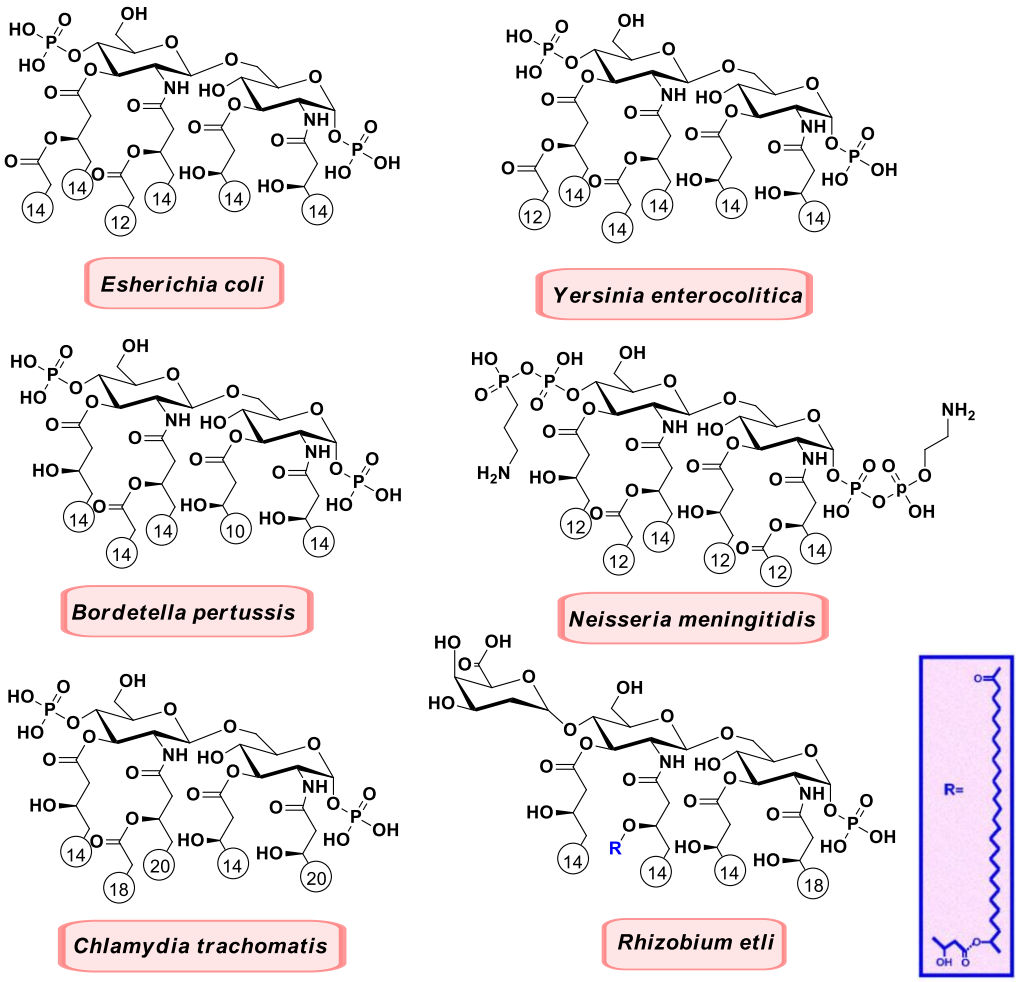

Figure 5. A collection of natural lipid A structures. Fatty acyl chain lengths are given by numbers in circles (Caroff and Karibian, 2003).

2.1.3. Chemical differences in the structural architecture of lipid A in *Pseudomonas aeruginosa*

Pseudomonas aeruginosa (*P. aeruginosa*) is a human opportunistic pathogen and a major cause of nosocomial infections, affecting immunocompromised (e.g., AIDS or

cancer) patients and those with tissue injuries or cystic fibrosis. Control against *P. aeruginosa* infection is difficult due to its high intrinsic resistance to antibiotics (Potron et al., 2015; Moradali et al., 2017). Resistance acquisition is partly due to alterations of the lipid A component present in the external membrane of this Gram-negative bacterium. The major lipid A produced by laboratory strains of *P. aeruginosa* has a doubly phosphorylated pentaacylated (75% of the molecules) and a hexaacylated form (25% of the molecules) (Fig. 6), which latter differs from the classical *E. coli* type hexaacylated structure (Fig. 5) in the type and position of acyl chains. Therefore, the inflammatory response elicited by *P. aeruginosa* lipid A would be expected to be less than that of enterobacterial LPS, and this is indeed the case (Backhed et al., 2003).

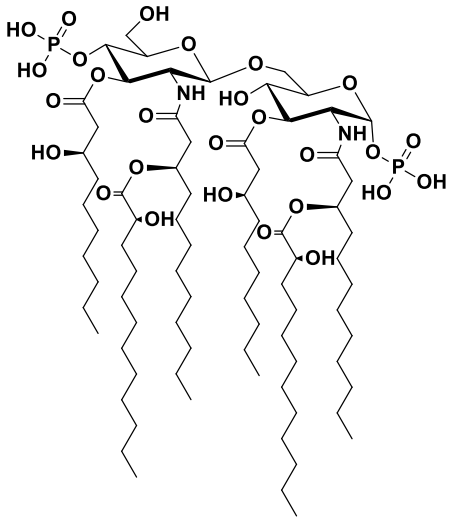

Figure 6. Typical lipid A produced by laboratory strains of *Pseudomonas aeruginosa* PAO1. The 3-hydroxydecanoyl chain at the C-3-position is absent in approximately 75% of LPS molecules. The secondary lauroyl chains are non-stoichiometrically 2-hydroxylated.

However, when lipid A from clinical isolates of *P. aeruginosa* (from cystic fibrosis patients) has been characterized, modified structures were found, arising from the addition of a secondary palmitoyl group (C16:0) to the primary fatty acid at C-3' on GlcN II, and addition of Ara4N to either of the phosphates (Ernst et al., 1999; King et al., 2009). This hyperacylated lipid A can induce an enhanced inflammatory response that most probably contributes to the severity of lung damage (Ernst et al., 2003).

2.1.4. Chemically modified natural and fully synthetic lipid A as monotherapeutics

Of particular note among lipid A structures is the nontoxic 3-O-deacyl-4'-monophosphoryl lipid A (MPL) (Casella and Mitchell, 2008), which is an FDA-approved vaccine adjuvant for clinical use. MPL is of natural origin, derived from the lipopolysaccharide of *Salmonella minnesota* R595. In the eighties, scientists from Ribi Immunochem Research investigated methods of chemically modifying lipid A in order to distinguish its toxic effects from potentially useful immunomodulatory effects. This led to the identification of 3-O-deacyl-4'-monophosphoryl lipid A. Its structure is depicted on Fig. 7.

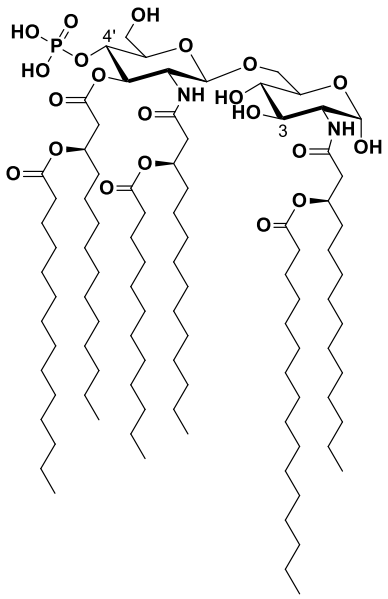

Figure 7. Structure of 3-O-deacyl-4'-monophosphoryl lipid A (MPL).

This non-endotoxic material was obtained by, first, treatment of *Salmonella minnesota* R595 LPS with 0.1 N HCl at 100 °C for 30 min, which caused the removal of the glycosidic phosphate at the position 1 and the inner core residues attached via the 6' position, thus generating 4'-monophosphoryl lipid A. Next, this substance was dissolved in organic solvents and exposed to very mild alkaline treatment, which selectively

removed the base-labile fatty acyl residue attached to the 3 position, yielding 3-O-deacyl-4'-monophosphoryl lipid A. The resulting product was then purified and converted to the monobasic triethylammonium salt and lyophilized.

MPL expresses antagonistic activity towards the immune system by activating only part of the TLR4-MD-2 signal pathway (Casella and Mitchell, 2008). This ligand has the ability to induce strong Th1-type proinflammatory immune responses, but without causing pathological inflammation. Apart from the use of MPL as an adjuvant e.g., in the human papilloma virus vaccine Cervarix™ and in the hepatitis B virus vaccine FENDrix® (Tagliabue and Rappuoli, 2008), further research is also being carried out on their use for health promotion and disease prevention, such as for treatment of endotoxaemia and septicaemia, as well as reducing risk of Alzheimer's disease (Rego et al., 2016). Moreover, it has also been subjected to clinical trials in humans for herpes, metastatic melanoma, malaria, breast cancer and colorectal cancer vaccines (Baldridge et al., 2004; Neidhart et al., 2004; Wu et al., 2021).

It should be pointed out that analysis of MPL (Hagen et al., 1997; Hopkins et al., 2001) revealed that it is not a single chemical entity, but a mixture of 3-O-deacyl-4′-monophosphoryl lipid A analogues that contain 4, 5 and 6 fatty acids. It is believed that all structures contribute to the adjuvant activity of MPL, although to a different extent (Ribi et al., 1984; Ulrich and Myers, 1995) . The individual species and the total content of the analogues are assessed in all adjuvant preparations, for which usually reversed-phase high-performance liquid chromatography (RP-HPLC) with fluorescence detection is used, since retention on RP columns are sensitive to differences in fatty acid substitution (Hagen et al., 1997; Hopkins et al., 2001). However, concerning the production of MPL, it's native heterogeneity poses challenges for both the standardization

and the scale up to an expected world-wide demand. Thus, the study of other LPS-based molecules is also important.

Synthetic structural analogues of MPL containing just one molecular species prove to be useful candidates in various developmental studies of adjuvant formulation (Arenas, 2012). An advantage of these molecules over MPL is that the synthesis can be done resulting in higher purity and lower costs. Moreover, homogeneous lipid A is particularly desirable for therapeutics development in biological model systems, since it leads to a better understanding of the cellular response after stimulation with a well-defined reference lipid A product with known chemical structure.

Multiple studies have revealed that synthetic analogues of MPL are as safe and effective as biological types (Fox et al., 2010; Arenas, 2012; Fox et al., 2017). Currently, four synthetic structural analogues of MPL, including 3D-PHAD, 3D-(6-acyl)-PHAD, PHAD and PHAD-504 (Fig. 8), all manufactured in accordance with current Good Manufacturing Practice guidelines are commercially available. Such synthetic MPLs have been used as adjuvants in numerous commercialized human vaccines (Fox et al., 2010; Coler et al., 2011).

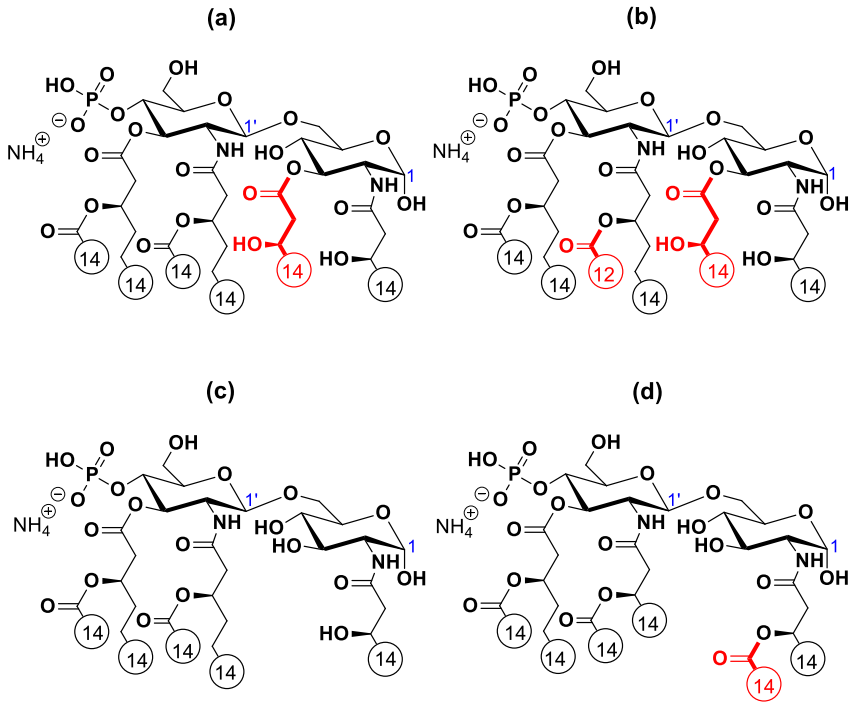

Figure 8. Structures of the four synthetic lipid A standards: (a) PHAD, (b) PHAD-504, (c) 3D-PHAD, and (d) 3D(6-acyl)PHAD. The colored structural parts indicate the differences between the four structures**.**

3D(6-acyl)-PHAD is most closely related to the reported structure of MPL adjuvant (but both secondary fatty acids on the non-reducing sugar are C14). It is structurally homogeneous and highly purified and mimics the TLR4 agonist activity of bacterial MPL. The 3D-PHAD (3-deacyl monophosphorylated penta-acyl disaccharide, differing from 3D(6-acyl)-PHAD by the lack of the secondary fatty acid on the reducing sugar), besides being comparable to bacterial MPL and other synthetic MPL analogues at eliciting an immune response in a liposomal adjuvant system, it is less pyrogenic than its bacterial-derived mimic. PHAD is an adjuvant that has been given to more than 1000 human subjects with no serious adverse effects. PHAD-504 was designed as a synthetic structural analog of detoxified MPL derived from *E. coli*. It is structurally similar to PHAD, differing only in the length of secondary fatty acid chain at C-2' position (being C12). As anticipated, the activity of PHAD-504 is fairly similar to that of PHAD, making both products interchangeable as adjuvants in vaccine or immunotherapy formulations.

2.2. Mass Spectrometry in the analysis of lipid A

To accurately decipher the relationship between the functional groups and bioactivity of lipid A, a detailed characterization of its chemical structure is essential. Modern mass spectrometric methods, in general, have high mass resolution and mass accuracy, and permits fragmentation analysis needed for structure elucidation. To date, the modern soft ionization techniques, such as electrospray ionization (ESI) and matrix assisted laser desorption ionization (MALDI) in combination with tandem (MS/MS) or multistage mass spectrometry (MS^n) have become the most effective and sensitive analytical tools for collecting structural information about lipid A molecules (Boue and Cole, 2000; Kussak and Weintraub, 2002; Lukasiewicz et al., 2006; Madalinski et al., 2006; Schilling et al., 2007; Silipo et al., 2008; Basheer et al., 2011). Before analysis, lipid A isolates are derived by mild acid hydrolysis of the native LPS sample (*i.e.*, a chemical degradation of LPSs at around pH 4, at 100 °C, for 1-2 h needs to be carried out). Then, the lyophilized lipid A can be dissolved in a mixture of methanol and chloroform, or methanol and dichloromethane, which provides proper dissolution of lipid A molecules, making it compatible for ionization in the ESI ion source. The biggest advantage of ESI is that it can be combined with high efficiency separation techniques (HPLC, CE), compared to the off-line MALDI system. Although direct and coupled MS techniques have been applied with increasing success to the analysis of lipid A, there are still some major challenges in precisely determining the structure of individual lipid A compounds in a heterogeneous bacterial extract, especially when lipid A isomers are present simultaneously.

2.2.1. Negative ion mode mass spectrometry in the study of lipid A molecules

For tandem mass spectrometric analysis of lipid A, most often the negative-ionization mode is employed, because phosphate groups in lipid A can be readily deprotonated and the resulting singly or doubly charged anions ($[M - H]^-$ or $[M - 2H]^{2-}$) show high detection susceptibility in MALDI or ESI MS. Specifically, MS/MS analysis following ESI in negative ion mode proved to be useful for obtaining information about the acylation profile of bis-phosphorylated, 4'-mono-phosphorylated (Kussak and Weintraub, 2002; Madalinski et al., 2006; Sándor et al., 2016), and even non-phosphorylated (Sándor et al., 2016) lipid A molecules in deprotonated form.

Collisional activation studies in the negative ion mode of selected precursor ions (with a specific *m/z*) of any of the above-mentioned lipid A types result in a series of ions due to serial fatty acid cleavages. Since the acyl residues are usually of different mass, one can determine the type of cleaved acyl chain based on the mass difference between the product ions, and of the precursor, of course. Moreover, the position of the acyl chain greatly affects its lability, meaning that there is an elimination order between the acyl chains based on their exact position on the disaccharide. For this reason, ESI–MS/MS in the negative ion mode provides an effective and sensitive technique for clarifying acyl groups on bacterial lipid A.

Uniquely, only in the case of a 4'-monophosphorylated lipid A precursor ion, the loss of the primary acyl chain at the C-3' position gives a pair of product ions, which are highly characteristic for this fatty acyl loss. Based on low-energy CID experiments, Kussak and Weintraub (Kussak and Weintraub, 2002) proposed that this elimination occurs in two ways. One is a charge-driven process for the neutral loss of an acyl group as a ketene derivative (Scheme 1), and the other is a charge-remote process for the neutral loss of an

acyl group as a free fatty acid (Scheme 2). For other type of lipid A (like the bis-, 1-mono-, or non-phosphorylated), such ion pairs have not been detected.

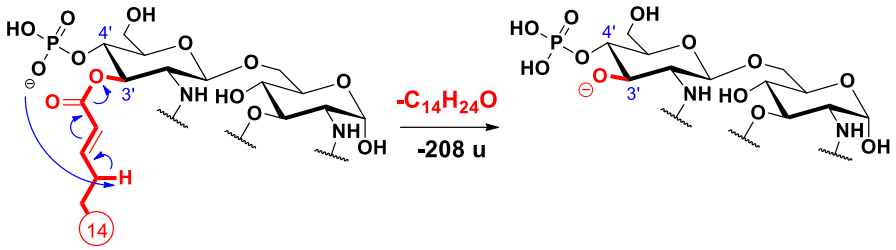

Scheme 1. Proposed fragmentation mechanism for the loss of the C-3' primary acyl chain as a ketene, along with a proton transfer (Kussak and Weintraub, 2002).

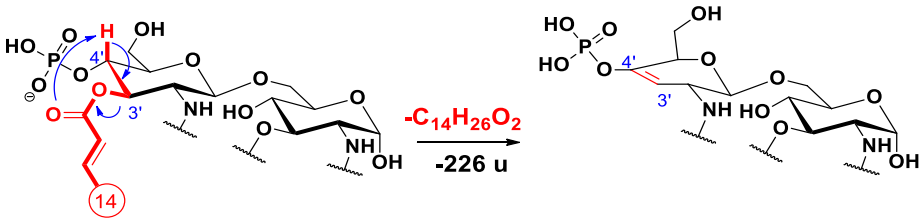

Scheme 2. Proposed fragmentation mechanism for the loss of the C-3' primary acyl chain as an acid, leading to the creation of a double bond between the C-3' and C-4' carbon atoms (Kussak and Weintraub, 2002).

Seminal negative mode ESI–MS/MS applications about the structural analyses of 4'-mono-, 1-mono-, and 1,4'-bis-phosphorylated lipid A molecules from different bacterial strains can be found in the literature, such as from *Salmonella minnesota* R595 (Chan and Reinhold, 1994), *Shigella flexneri* (Chan and Reinhold, 1994; Kussak and Weintraub, 2002), *Burkholderia pseudomallei* (Novem et al., 2009), *Burkholderia thailandensis* (Novem et al., 2009), *Escherichia coli* (Madalinski et al., 2006), *Yersinia pestis* (Jones et al., 2010), and many others.

In the studies mentioned above, different mass analyzers were used, such as an IT, a QqQ and a QTOF. Among them, only the IT analyzer has the advantage of performing different levels of fragmentation (MS^n), with n up to even 6. This is called multistage tandem MS in time. First, ions of a variety of masses are trapped together within the trap;

then, the selected precursor ion is retained in the trap and all other ions are expelled; next, fragmentation of selected ion is induced by collisional activation; and then the product ions are expelled according to their masses in order to get the fragmentation mass spectrum. However, if a product ion is trapped again, it can be subjected to an additional CID experiment (MS^3), and the resulting product ions are analyzed in stage 3. This process can be repeated until enough precursor ions are available in the trap.

In lipid A analysis, several stages of MS (*i.e.*, the MS^n) can be particularly useful to determine the genealogical relationship between product ions (Madalinski et al., 2006), which is not possible with a QqQ or a QqTOF instrument. For example, with sequential CID measurements, it has been demonstrated that the cleavage of amide bonds only occurs at higher MS^n stages (where n = 3 or higher), indicating that fatty acyl amides are more stable than fatty acyl esters (Lukasiewicz et al., 2006; Silipo et al., 2008). Nevertheless, there is a critical drawback of the usage of IT, which is the low mass "cut-off" when using resonance activation during the collision-induced dissociation. The low mass "cut-off" phenomena practically results, that the IT fails to trap and consequently, it is not able to detect fragment ions below a certain *m*/*z* limit (e.g., the 27% of the *m/z* of the precursor ion).

On the contrary, with QqQ and QTOF analyzers which are representative of MS/MS in space, the collision cell (q) is placed between two analyzers (e.g., for QqTOF, q is between the quadrupole and TOF analyzers). There are also systems which combine the structural power of the ion trap with the quantitative accuracy of the quadrupole. The QqQ is capable of functioning in four MS/MS modes: product ion scan, precursor ion scan, neutral loss scan and selected reaction monitoring (SRM). The latter mode is quicker than the product ion scan (used in IT) and it allows the simultaneous measurement of high

number of MS/MS transitions or reactions. Currently, this is a very important question in common applications when selecting and developing an analytical method.

In addition to CID (which is the benchmark tandem MS technique in lipid A analysis), there are other alternative methods, such as Infrared multiple photon dissociation (Madsen et al., 2011) or ultraviolet photodissociation (UVPD) (Madsen et al., 2011; O'Brien et al., 2014). While CID mainly involves cleavages of ester-linked acyl chains, the removal of phosphoryl groups, and appearance of inter- and cross-ring fragments (such as “C”, “Z”, and “A”, “X” ions, respectively), using 193 nm UVPD results in intensive glycan fragments, and dissociation processes that happen along the C–O, C–N and C–C bonds of the alkyl chains (Hankins et al., 2012; O'Brien et al., 2014).

Regardless of the collisional activation strategy, there is a general problem with the detection of a chimera mass spectrum (*i.e.*, a mixture of mass spectra stemming from cofragmenting isobaric lipid A precursor ions) of phosphoisomers (monophosphorylated lipid A having the phosphate group either at C1 or C4’), because of the overlap of the mass spectral peaks of the two isomers. Therefore, the direct detection of isomeric lipid A species present simultaneously in a bacterial sample with conventional negative ion mode MS/MS is not feasible.

2.2.2. Positive ion mode mass spectrometry in the analysis of lipid A molecules

The mass spectra of lipid A in the positive ion mode always comprise intensive Na adduct ions, but low abundant $[M + H]^+$ ions. One way to increase the sensitivity of the protonated form is the addition of an ammonium formate to the sample, by which the basic amidic group is preferentially protonated. Another observation is that after addition of triethylamine (Et_3N) to the sample (and the spray solution), intensive Et_3N adduct ions

are formed in the ion source. MS/MS of these ions lead to the formation of $[M + H]^+$ ions by the neutral loss of Et_3N (Kondakov and Lindner, 2005).

Several studies have been reported on the tandem MS analysis of the monosodium adduct $[M + Na]^+$ of phosphorylated and non-phosphorylated lipid A species (Wang et al., 1992; Harrata et al., 1993; Karibian et al., 1999; Aussel et al., 2000; Coats et al., 2009; Phillips et al., 2011; Nichols et al., 2012). Because mostly, the rupture of the glycosidic bond between the two GlcN rings can be provoked in the positive-ion mode by fragmentation, consequently oxonium ion formation was observed in those studies. Moreover, the oxonium ion was generally used only to confirm the interpretation of negative ion mass spectra for the acylation pattern determination of lipid A species. An oxonium ion is an abundant "B" fragment, assigned as the distal sugar fragment (GlcN II), thus the presence or absence of the phosphate group connected to it (at position C-4') can also be determined. In certain cases, disodiated lipid A adducts, such as $[M – H + 2Na]^+$ or $[M – H – PO_3H + 2Na]^+$, were also seen in positive-ion experiments of mono- and bisphosphorylated lipid A species (Wang et al., 1992; Karibian et al., 1999; Aussel et al., 2000; Phillips et al., 2004; Coats et al., 2009), even though such ions were not fragmented. However, it must be mentioned that the CID fragmentation of the triethylammonium adduct (Sándor et al., 2018) $[M + H + Et_3N]^+$ results in excessive accumulation of Et_3N in the ion source which causes ion suppression and a strong memory effect in mass spectrometers. For this reason, scientists generally do not prefer to perform MS/MS analysis of this type of precursor ion in positive ion mode.

Hence, in general, the application of positive ion mode tandem MS for the structure elucidation of lipid A is less frequent than negative ion mode tandem MS due to the low proton affinity of the phosphorylated lipid A molecules. Most probably, this is the reason

why the use of positive ion mode MS and tandem MS for the structural determination of lipid A species by their sodium adducts or as protonated molecules have not been thoroughly investigated. In particular, in the case of a mixture containing both C1-monophosphorylated and C4′-monophosphorylated species, usually the combination of MS studies with NMR analysis of lipid A was used for the identification of the phosphorylation sites (Kumada et al., 1995; Zhou et al., 2000; Smit et al., 2008; Madala et al., 2011).

2.2.3. Analysis of lipid A heterogeneity using separation techniques and mass spectrometry

An essential problem faced in lipid A research is the multicomponent nature of bacterial lipid A preparations. LPS lipid A, in general, is a mixture of molecules of different but very similar structure. The direct identification of structural microheterogeneities of lipid A analogues is a particular challenge, which is possible by mass spectrometric analyses only after the effective separation of the individual components. The simultaneous presence of several lipid A congeners might result from the intrinsic biological heterogeneity, but it should also be mentioned that the procedures used to extract LPS and then lipid A from bacteria may also lead to the cleavage of fatty acids, phosphate groups and other attachments.

In some studies, we can read about the application of different separation techniques to reveal the heterogeneity of lipid A samples from LPS extracts. Using normal-phase (usually silica gel or aluminum oxide) thin-layer chromatography (TLC) procedures, lipid-A mixtures can be divided into a few fractions according to the degree of acylation and phosphorylation. The spots can then be revealed by destructive (charring after spraying the plate with sulfuric acid) (Qureshi et al., 1983) or non-destructive

visualization (radioisotopic labeling, or different alcohol-water mixtures used for plate-development) (Therisod et al., 2001; Henderson et al., 2013), and further analyzed by MS.

There are also several examples in the literature about the examination of lipid A samples with HPLC, most of these studies using reversed phase (RP) column and a gradient elution process to separate the different lipid A species contained in the native samples. Lipid A does not contain a chromophore group and has a low absorbance that varies depending on the degree of acylation. Therefore, the UV detection of characterized lipid A molecules is not possible on an analytical scale, and their derivatization is unavoidable when using a UV or fluorescence detector. Derivatives include e.g., methylation of the phosphate group with diazomethane (detection at 210 nm)(Qureshi et al., 1985; Qureshi et al., 1988; Beasley et al., 2012) or an oxime derivative formed with dinitrobenzyloxyamine (detection at 254 nm) (Hagen et al., 1997). For fluorescence detection, derivatization with dansylhydrazine is used (excitation wavelength 345 nm, emission wavelength 515 nm) (Hopkins et al., 2001). However, the risk of derivatization is that the sample composition changes as a result of the loss of some functional groups. Therefore, its usage is not so recommended.

Lipid A detection without derivatization was also implemented with an HPLC system equipped with an evaporative light scattering detector. Bobbala et al (Bobbala et al., 2015) used this method to quantify encapsulated monophosphorylated, 3-Odeacylated lipid A (MPL adjuvant) from *Salmonella minnesota* R595.

Adequate analytical methods for examination of lipid A mixtures are essential for a better understanding of structure-activity relationships and profiling of the real microheterogeneity. Not least because the detection of biologically important molecules present in small concentrations can only be achieved with a detection technique that has

high sensitivity and is characterized by a wide dynamic range, such as mass spectrometry (Vekey, 2001). As a result, all recent publications deal with the mass spectrometry of lipid A molecules coupled with high-efficiency separation techniques.

Hamdy et al (Hamdy et al., 2007). developed a liquid chromatography/mass spectrometry (RP-HPLC-MS) method for the quantitative determination of synthetic lipid A-based vaccine adjuvants. Mobile phase A was methanol containing 0.1% glacial acetic acid and 0.1% triethylamine, mobile phase B was 10% methanol in tetrahydrofuran containing 0.1% glacial acetic acid and 0.1% triethylamine. This method was able to solve all difficulties associated with previous methods, such as the poor UV-absorbance, use of radiolabeling, and precolumn derivatization of lipid A compounds. In addition, the sensitivity of the method was three order of magnitude better than for the previously reported HPLC analyses.

Later, O'Brien et al (O'Brien et al., 2014) presented their RP-HPLC-UVPD-MS/MS method, characterized by significantly higher selectivity, for the separation and structural identification of lipid A isolates from a genetically modified *E. coli* strain. mobile phase A was a 50:50 (%) mixture of methanol/water containing 0.05% ammonium hydroxide, mobile phase B was 40:40:20 (%) mixture of 2-propanol/chloroform/methanol. In this study, seven types of lipid A molecules with different acylation (tetra-, penta- and hexa-acylated) and different phosphorylation (bis- and monophosphorylated) were identified by partial separation using a 30-minute gradient elution. These results provided a good basis for the development of even more improved lipid A separation methods, which enable proper structural identification of all type of components present in heterogeneous samples, including even isobaric components.

Recently, Sándor et al. (at University of Pécs) developed a non-aqueous capillary electrophoresis (NACE) method coupled to tandem mass spectrometry (Sándor et al., 2020) for the in-depth separation and structural characterization of both phosphate and acyl chain positional isomers of lipid A. The background electrolyte was a mixture of methanol and dichloromethane, containing a small amount of triethylamine and acetic acid. The separation capillary (bare fused-silica) was rather short (only 55 cm), however the analysis time was as long as 43 min. The NACE can be considered as an orthogonal technique to conventional RP-HPLC strategies, since, by NACE, the phosphorylation isomers are baseline separated in addition to the partially resolved acylation isomers, while by RP-HPLC, the lipid A molecules are primarily separated according to their acylation profile, whereas phosphoisomers are mostly unresolved.

3. Aims of the study

The primary focus of my PhD work was to develop new tandem mass spectrometry-based structural elucidation strategies with the systemic interpretation of fragmentation mass spectra of synthetic and natural lipid A molecules. Since any immunological effect induced by a bacterial lipid A molecule depends on its primary structure, such improved structure elucidation techniques would aid in the search for the treatment of sepsis.

Our specific goals were:

1. To carefully study the fragmentation of three positively charged lipid A ions: $[M + H]^+$ (protonated molecule), $[M + Na]^+$ (monosodium adduct), and $[M – H + 2Na]^+$ (disodium adduct), and to compare results with the commonly detected negatively charged lipid A ions: $[M – H]^–$ (deprotonated molecule).

   - We planned to carry out positive and negative ionization CID experiments with a set of synthetic and natural-sourced monophosporylated lipid A compounds using three mass spectrometers: ESI-Q-TOF, ESI-IT, and ESI-QqQ.

2. To perform a mechanistic study regarding the fragment ion formation through CID multistage mass spectrometry (MS^n).

   - We planned to interpret the formation of fragment ions from deprotonated, protonated and sodiated lipid A, using possible mechanisms consistent with the principles of reactions described in organic chemistry.

3. To identify hitherto unknown isomeric monophosphorylated lipid A species present in *Pseudomonas aeruginosa*, a priority target pathogen in antibiotic research.

   - We planned to use non-aqueous capillary electrophoresis (NACE) for the separation of phosphorylation and acylation isomers, and then tandem mass spectrometry (ESI-

Q-TOF MS/MS) in both positive and negative electrospray ionization modes to demonstrate the confident identification of structurally very similar, isobaric lipid A species in a bacterial extract.

4. Materials and Methods

4.1. Chemicals

Methanol (LC-MS Chromasolv grade), chloroform (Chromasolv Plus, for HPLC, ≥99.9%), triethylamine (Et_3N, eluent additive for LC-MS), acetic acid (AcOH, eluent additive for LC-MS) and sodium hydroxide (NaOH) were bought from Sigma-Aldrich (Steinheim, Germany), and ammonium formate (LC-MS Chromasolv grade) was bought from Fluka (Seelze, Germany).

4.2. Synthetic lipid A standards

Synthetic monophosphoryl lipid A standards were bought from Sigma-Aldrich, the exclusive Avanti Polar Lipids provider (Alabaster, AL, USA) in Hungary. The standards were monophosphoryl lipid A (PHAD), and monophosphoryl lipid A-504 (PHAD-504), monophosphoryl 3-deacyl penta-acyl lipid A (3D-PHAD, Pat No. 9,241,988), monophosphoryl 3-deacyl hexa-acyl lipid A (3D(6-acyl)-PHAD), and all of them were in their ammonium salt forms. The structures of the four standards are depicted in Fig. 8 (Literature review section).

4.3. Bacterial strains and culture conditions

Bacterial strains of *E. coli* O83 and *P. aeruginosa* PAO1 strains were cultured at 37 and 25 °C, respectively, in a 30-litre laboratory fermentor (Braun Melsungen, Germany) on a Mueller-Hinton broth at pH 7.2, until they reached the late logarithmic phase (about 10 h). The bacterial cells were collected by centrifugation and dried with acetone.

4.4. Lipopolysaccharide and lipid A isolation

Cell-wall lipopolysaccharides were extracted from the acetone-dried organisms by the hot phenol/water procedure(Westphal et al., 1952) in a yield of 5% of bacterial cell dry

mass, and were lyophilized. The lipid A part was released from each LPS by mild acid hydrolysis with 1% (v/v) AcOH (pH 3.9) at 100 °C for 1 h. Then, the solution was centrifuged (8000 × g, 4 °C, 20 min). The sediment, containing lipid A, was washed four times with distilled water and lyophilized.

4.5. Lipid A sample preparation

Approximately 0.1 mg of the synthetic lipid A standards and lipid A extracted from *E. coli* was dissolved in 1 mL of a MeOH:DCM (70:30, v/v) mixture. Next, 5 mg of ammonium formate was added, and the sample was vortexed and then placed in an ultrasonic bath for 5 min. Subsequently, 300 µL of the sample and 700 µL of methanol was pipetted into a sealed glass vial. A small amount of NaCl (about 0.5 mg) was added to promote sodium cation attachment to the phosphorylated lipid A molecules extracted from *E. coli O83*. After vortexing for 1 min, the sample was ready for injection. The lipid A (0.1 mg) extracted from *P. aeruginosa* PAO1 was dissolved in 200 µL of a MeOH:$CHCl_3$ (50:50, v/v) mixture and centrifuged (5 min, 21 000 × g).

4.6. Mass spectrometric analysis

Mass spectra of the four lipid A standards and *E. coli* lipid A were recorded in both negative and positive ion modes using a 6530 Accurate-Mass Quadrupole Time-of-Flight (Q-TOF) mass spectrometer (Agilent Technologies, Singapore). The lipid A samples (1 µL) were injected using a UHPLC autosampler (Agilent Technologies, Waldbronn, Germany).

The ESI voltage was adjusted at 3.0 kV for the two ion modes. The nitrogen drying gas flow rate was 5.0 L/min at 200°C with a nebulizer nitrogen gas pressure of 15 psi, except for during the sample injection, when the nebulizer nitrogen gas pressure was reduced to 1 psi in order to prevent the aspiration effect (a process that allows air to be

released from the mould cavity during metal casting), if not, a segment of air could penetrate the capillary to the side of the inlet, and the current could be stopped.. The flow rate and temperature of the Agilent Jet Stream curtain gas were 2 L/min and 90 °C, respectively. The MS data were collected under full scan mode in the range of *m/z* 600–2100 at a rate of 3 spectra/s. Identification of ion peaks was done through CID MS/MS experiments by applying collision energies in the 30–70 V range in both ion modes. MS/MS spectra were acquired in the range of *m/z* 50–2100 at the scan rate of 2 spectra/s.

To investigate the genealogy of the fragments from precursor ion to fragments through all fragment generations, ESI-ion trap MS^n analyses were conducted in both ionization modes using an MSD Trap XCT Plus mass spectrometer (Agilent Technologies, Germany) and the Agilent LC/MSD Trap Software 5.3. A syringe pump with a flow rate of 3 μL/min was used to inject the samples directly into the ion source. The electrospray capillary high voltage was applied at 3500 V. Nitrogen was used both as a nebulizer (15 psi, 5 L/min) and drying gas (at 325 °C). Spectra were scanned in the range of *m/z* 50–2200. The mass isolation window for precursor ion selection was set to 4 Da in the multiple-stage analysis. Each precursor ion was excited by a resonant excitation voltage in the range 0.5 V to 1.5 V, according to the intensity of the precursor ion signal. Negative and positive ion mass spectra and CID spectra, were averaged over 5–20 scans, based on the relative abundances of the precursor ions.

Fragmentation patterns of the lipid A standards and the natural-sourced *E. coli* lipid A were also studied in the negative-ion mode with a SCIEX Triple Quad TM 6500+ mass spectrometer (AB Sciex LP, Concord, ON, Canada) equipped with a built-in syringe pump set at a flow rate of 25 μL/min. Mass spectra were scanned in the range of *m/z* 50–1600. The scan rate was 1000 for both Q1 MS and product ion MS^2. The ion spray voltage and temperature were set at –4500 V and 200 °C, respectively. The curtain gas was set at a

flow rate of 20 psi; gas 1 (nebulizer gas) was set at 3 psi and gas 2 (heater gas) was set at 0 psi. The collision gas (CAD) was set at 8 for most experiments, this corresponds to a pressure of about $8 \cdot 10^{-3}$ mbar in the collision cell. The data was captured using the Analyst software 1.7.2.

4.7. NACE–ESI-Q-TOF MS/MS

Measurements of the *P. aeruginosa* PAO1 lipid A sample were performed with the non-aqueous capillary electrophoresis (NACE) method (Sándor et al., 2020) using a 7100 CE system (Agilent Technologies, Waldbronn, Germany) monitored through Chemstation Rev. B.04.03. software. The CE instrument was connected to a 6530 Q-TOF mass spectrometer (Agilent Technologies, Singapore) with an Agilent Jet Stream electrospray ionization (ESI) interface. The background electrolyte (BGE) composition consisted of MeOH:$CHCl_3$:Et_3N:AcOH (50:50:0.72:0.24, v/v/v/v). For separations, bare fused silica capillaries (50 μm id, 375 μm od; Polymicro Technologies, Phoenix, AZ, USA) with a length of 55 cm were used. The samples were injected by applying 50 mbar of pressure during 15 s, followed by injecting BGE with 50 mbar of pressure for 5 s. The temperature of the capillary was kept at 20 °C. The applied voltage was –30 kV (the cathode was at the inlet capillary end). Initial voltage ramps were applied to slow the development of passively induced pressure flows through axial temperature gradients (Xuan et al., 2006), *i.e.*, the separation voltages increased linearly from 0 to –30 kV under 0.3 min. During the runs, an external pressure of 5 mbar starting at 0 min and 30 mbar starting at 25 min was used to overcome the cathodic mobility of the electroosmotic (counter) flow. Before use, the capillary was preconditioned by flushing with methanol for 5 min, followed by 1 M NaOH for 10 min, then water for 10 min, before rinsing with BGE for 10 min. Between runs, the capillary was washed with the running solution for 5 min.

The capillary outlet end was inserted into the triaxial electrospray interface. The original Agilent stainless steel ESI needle was changed to the Agilent G7100–60041 platinum needle. To keep the electrospray stable, the end of the capillary was positioned 0.3 mm from the end platinum needle. The coaxial sheath liquid consisted of 0.06% (v/v) Et_3N and 0.02% (v/v) AcOH in methanol at 10 µL/min flow rate, supplied with an isocratic pump (Agilent Technologies) via a splitter set at 1:100. The ESI voltage was adjusted to 3.0 kV in both negative and positive ion modes. The nitrogen drying gas flow rate was 5.0 L/min at 200°C with a nebulizer nitrogen gas pressure of 15 psi, except for during the sample injection, when the nebulizer nitrogen gas pressure was reduced to 1 psi. The flow rate and temperature of the Agilent Jet Stream curtain gas were 2 L/min and 90 °C, respectively. The MS data were collected under full scan mode in the range of *m/z* 600–2100 at a rate of 3 spectra/s. Identification of ion peaks was performed by CID MS/MS experiments in both positive and negative ion modes by applying different RF amplitudes. MS/MS spectra were acquired in the range of *m/z* 50–2100 at the scan rate of 2 spectra/s.

4.8. Data evaluation

The evaluation of the CID spectra was made by considering the monoisotopic masses of the fragment ions and the neutral losses, based on the known composition and structure of the precursor ions. Namely, fragment ion identification included the summation of the masses of the sugar, phosphate and fatty acid constituents.

The classical nomenclature for glycoconjugates and cross-ring fragmentation nomenclature described by Domon and Costello (Domon and Costello, 1988) was adopted to label the fragment ions (Fig. 9). According to this nomenclature, the ions corresponding to the intra-ring (also known as cross-ring) and the inter-ring fragments are

called A-type cross-ring fragments ($^{0,2}A_2$ or $^{0,4}A_2$) and B_1, Y_1, Z_1 or C_1 type inter-ring fragments.

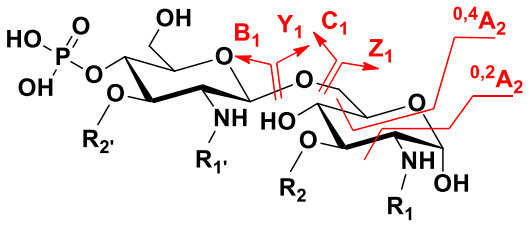

Figure 9. Intra-ring ($^{0,2}A_2$, $^{0,4}A_2$) and inter-ring (B_1, Y_1, Z_1, C_1) cleavage sites in a lipid A.

5. Results

5.1. Examination of CID mass spectra of negatively and positively charged lipid A precursors

5.1.1. Ionization of lipid A in negative and positive ESI modes

The ESI-Q-TOF mass spectrum of each lipid A sample registered in the negative-ion mode displayed one significant peak in the form of a deprotonated molecule $[M - H]^-$ (Fig. 10a), while, in the positive-ion mode, it displayed three signals corresponding to the protonated lipid A molecule $[M + H]^+$, the monosodium adduct $[M + Na]^+$, and the disodium adduct $[M + 2Na - H]^+$ (Fig. 10b). Results of the direct injection ESI-MS in the positive ion mode of all standard samples are depicted in Fig. A1 in the Appendix.

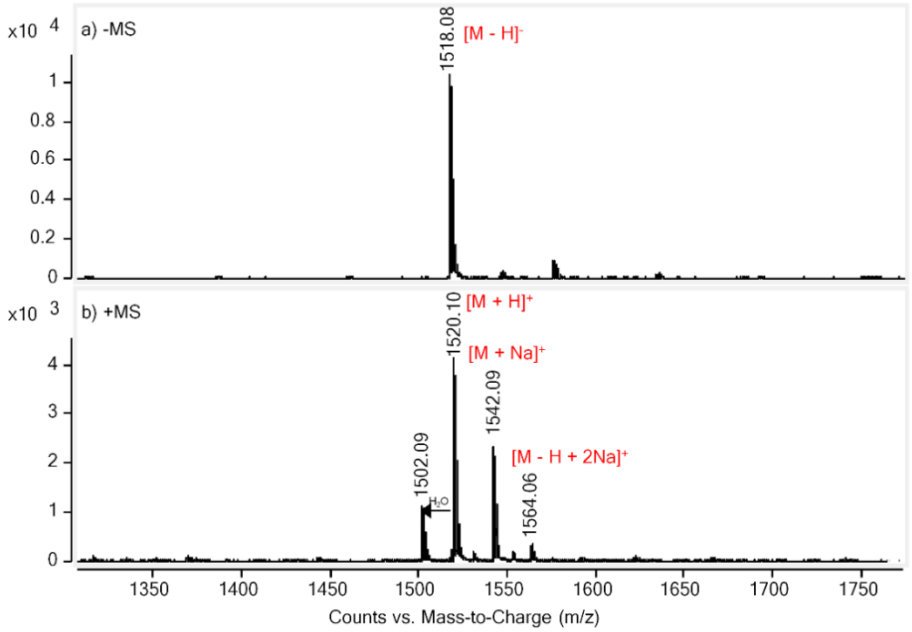

Figure 10. Comparison of the ESI-Q-TOF mass spectra of the 3D-PHAD lipid A (M = 1519 Da) obtained in a) negative and b) positive ion modes (lipid A was dissolved in MeOH/DCM 90/10 v/v) (Aissa et al., 2022).

In the positive ion mode, the $[M + H]^+$ ion was predominant, whereas the $[M - H + 2Na]^+$ ion was the least abundant. it is worth noting here that the formation of $[M + H]^+$ resulted from the decomposition in the ion source of the ammonium adduct of lipid A $[M + NH_4]^+$.

It can be seen that the ionization efficiency (*i.e.*, the quantity of ions produced from a particular compound in the ionization source.) of the two modes was in the same magnitude range; however, because of the formation of multiple ions in the positive mode, the abundance of ions was approximately one to two orders of magnitude less than the negative mode.

The negatively charged and the three positively charged ions described above were chosen as precursors, and their fragmentation patterns obtained by low-energy CID were studied in the case of four lipid A standards (3D-PHAD, 3D(6-acyl)-PHAD, PHAD, PHAD-504) and a bacterial lipid A mixture from *E. coli* O83.

5.1.2. CID fragmentation pattern of the $[M - H]^-$ lipid A precursor ions

Fragmentation patterns of the deprotonated C-4'monophosphorylated synthetic lipid A molecules were investigated, and results obtained with the ESI-QqQ and ESI-IT instruments were compared. In the case of the ion trap (Fig. 11), the first-generation ions are mainly produced from a chosen precursor ion, – in fact, this makes the sequential analysis MS^n of the ions particularly helpful for defining their genealogical relationships – while with QqQ (Fig. 12), especially when using high collision energy, many other higher-generation product ions are formed with high or medium abundance, as well. An important thing to note is that with the QqQ instrument, fragments of ions less than *m/z* 100 can be scanned, as well, whereas with the ion trap analyzer, which has a low-mass cut-off value, the fragment ions are detected only from c.a. 27% of the precursor ion mass. Hence, the PO_3^- (*m/z* 79) and $H_2PO_4^-$ (*m/z* 97) fragment ions could not be observed during the sequential MS^n analyses, although they were formed. On the other hand, it could be seen with the QqQ instrument that as the collision energy increased, the relative intensity of the peaks at *m/z* 79 and 97 also increased, whereas that of the peaks at *m/z* 796 and 778 decreased. The peaks at *m/z* 796 and 778 each represent $^{0,2}A_2$ fragments that had lost the

C-3’ acyloxyacyl group either as a ketene or an acid, respectively. The formation of the $^{0,2}A_2$ fragments and the two phosphate fragment ions from them will be discussed later.

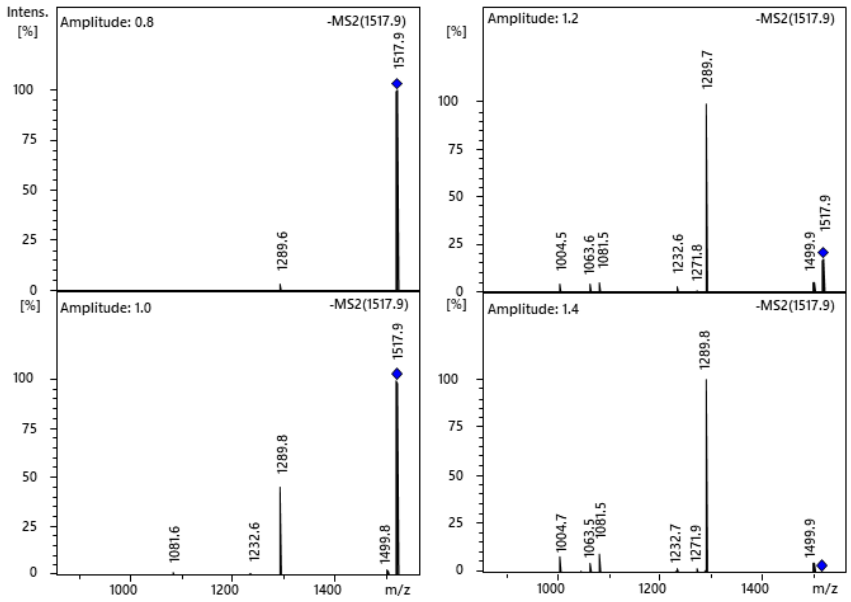

Figure 11. ESI-ion trap MS^2 mass spectra $[M - H]^-$ lipid A precursor ions of 3D-PHAD applying different RF amplitudes (Aissa et al., 2021).

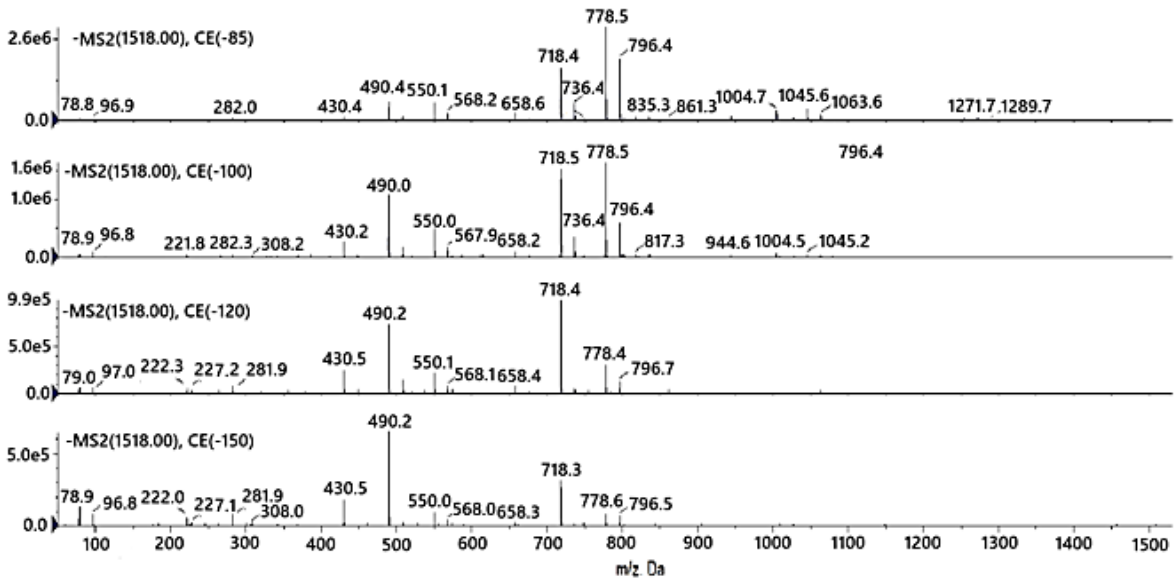

Figure 12. ESI-QqQ MS^2 mass spectra $[M - H]^-$ lipid A precursor ions of 3D-PHAD applying different collision energies (CE) (Aissa et al., 2021).

The ESI-IT MS^2 mass spectra of all four lipid A standards and of *E. coli* lipid A, as well, are shown in Figure 13.

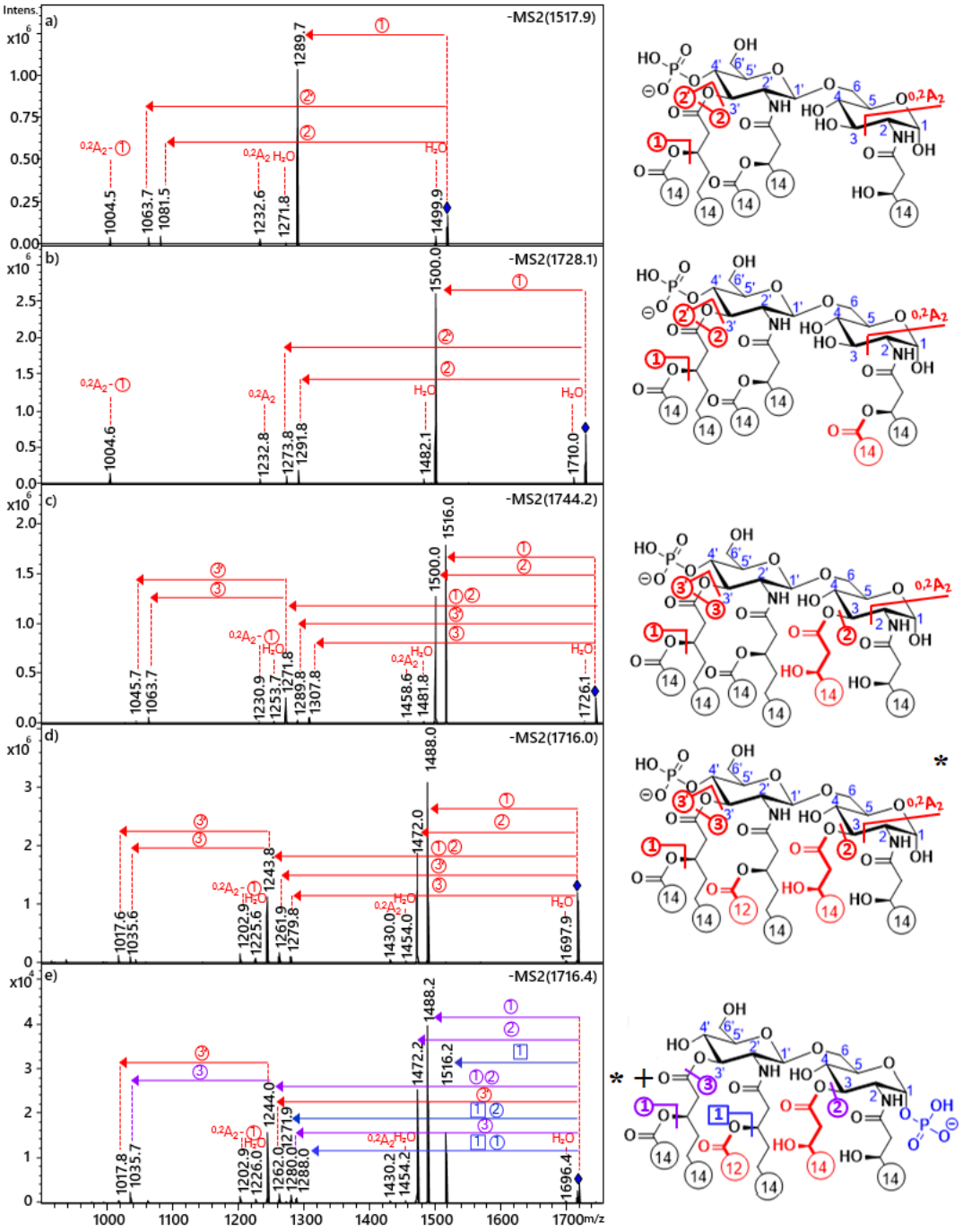

Figure 13. ESI-ion trap MS^2 mass spectra of the $[M - H]^-$ ions of a) 3D-PHAD (*m/z* 1518), b) 3D(6-acyl)-PHAD (*m/z* 1728, c) PHAD (*m/z* 1744), d) PHAD-504 (*m/z* 1716), and e) lipid A extract from *E. coli* O83 (*m/z* 1716) with showing cleavage locations in the structure. Red signs refer to 4'-monophosphoryl species, blue to 1-monophosphoryl species, and purple to both isomeric species. Fatty acyl chain lengths are given by numbers (Aissa et al., 2021).

The identity of the fragment ions was determined using the fragmentation rules described previously (Sándor et al., 2016) for the CID dissociation of lipid molecules A in deprotonated form. Namely, the order of the ester bond cleavages for a deprotonated 4′-monophosphorylated lipid A species is the following: (1) C-3′ secondary ester linkage, (2) C-3 primary ester linkage, (3) C-3′ primary ester linkage (resulting in 2 product ions by the elimination of an acid and a ketene at the same time), (4) C-2 secondary ester linkage, and (5) C-2′ secondary ester linkage. Accordingly, the most intensive peak in Fig. 13 (*i.e.*, appearing at *m/z* 1290 for 3D-PHAD, *m/z* 1500 for 3D-(6-acyl)-PHAD, *m/z* 1516 for PHAD, and *m/z* 1488 for PHAD-504 and for *E. coli* lipid A) was generated by releasing the fatty acid (C14:0, 228 u) from the C-3' secondary position for all samples. The other intense peak appearing only for the 3-acyl lipid As (at *m/z* 1500 and *m/z* 1472 in Fig. 13c and d/e, respectively), was due to the removal of a C14:0(3-OH) (244 u) fatty acid from the C-3 primary position.

It is important to highlight that only in the case of the *E. coli* lipid A (Fig. 13e), a third fragment was also detected, but that peak was due to the loss of fatty acid at the C-2' secondary position from the isomeric precursor, *i.e.*, the 1-monophosphoryl hexaacylated isomer, which was also present in the native lipid A mixture. However, for the pure PHAD-504 standard, which has the same structure as the 4'-monophosphoryl lipid A isomer produced by *E. coli*, a fragment ion peak at *m/z* 1516 was clearly missing (Fig. 13d).

This was a direct indication that there was no release of lauric acid (C12:0, 200 u) from the C-2' branched position from the pure, synthetic sample. On the other hand, from 1-monophosphoryl species, the loss of fatty acid from the C-2' secondary position is the most favored cleavage process according to previous observations (Sándor et al., 2018).

For the 3-acyl standards, a further peak of moderate intensity was observed (at *m/z* 1272 and 1244 in Fig. 13c and d/e, respectively), coming from the combined losses of the C-3' secondary and C-3 primary fatty acids (472 u). An additional loss of a C14:1 in the form of a ketene and an acid (208 or 226 u, respectively) from the C-3' primary position led to pairs of low-intensity fragment ions (at *m/z* 1064 and *m/z* 1046 in Fig. 13c, and *m/z* 1036 and *m/z* 1018 in Fig. 13d and e).

The loss of the C-3' linked C14:0(3-O-C14:0) acyloxyacyl chain both as a ketene and an acid (436 or 454 u) resulted in pairs of peaks detected with very low intensities for all precursor ions (at *m/z* 1082/1064, *m/z* 1292/1274, *m/z* 1308/1290, and *m/z* 1280/1262 in Fig. 13a, b, c, and d/e, respectively). Water losses (18 u) were also detected at low intensities from precursors and from certain acyl fragment ions.

Within each MS^2 mass spectrum, multiple $^{0,2}A_2$ diagnostic cross-ring fragments were observed. Since the non-reducing GlcN structures of the 3-deacyl standards were comparable, they exhibited the same $^{0,2}A_2$ fragment ion peak pairs (at *m/z* 1233 and *m/z* 1005 in both Fig. 13a and b), of which the latter was formed following the loss of a C14:0 from the C-3' secondary position. In addition, different $^{0,2}A_2$-type ions were detected for the 3-acyl standards (at *m/z* 1459 and *m/z* 1231 in Fig. 13c, and *m/z* 1431 and *m/z* 1203 in Fig. 13d and e), before and following the C-3' secondary acyl loss, respectively.

Thereafter, all the fragment ions listed above were subjected to sequential mass analysis measurements in the ion trap instrument. The MS^n mass spectra (n = 3–6) showed additional cleavage products, including $^{0,4}A_2$-type cross-ring fragments and the release of fatty acids from the C-2' secondary and C-2' and C-2 primary positions.

5.1.3. CID fragmentation pattern of the $[M + H]^+$ lipid A precursor ions

The ESI-Q-TOF MS/MS mass spectra of the $[M + H]^+$ precursor ions of the four lipid A standards and hexaacylated *E. coli* O83 lipid A is shown in Fig. 14.

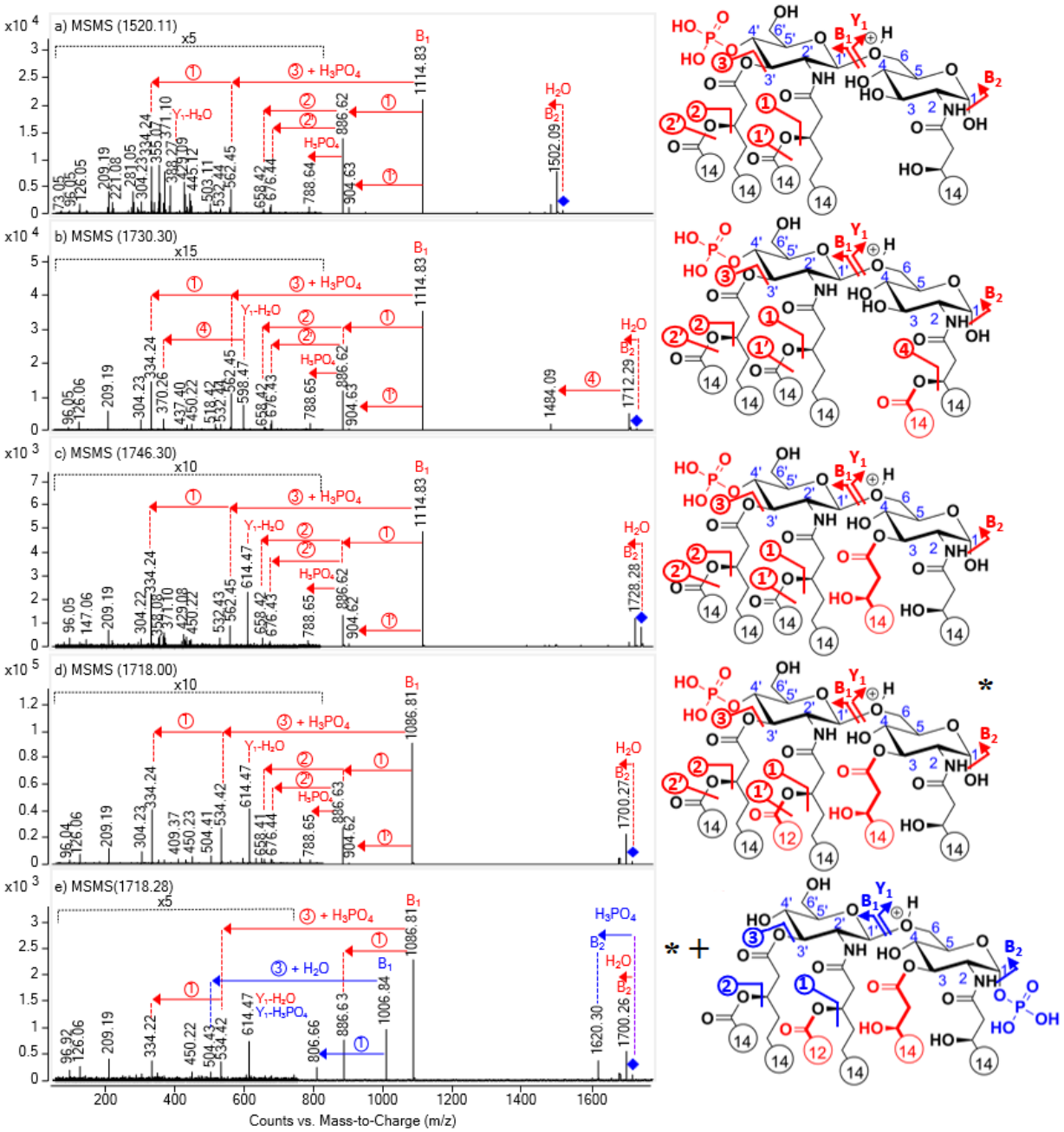

Figure 14. ESI-Q-TOF MS/MS mass spectra of the $[M + H]^+$ lipid A precursor ion of a) 3D-PHAD (*m/z* 1520), b) 3D(6-acyl)-PHAD (*m/z* 1730), c) PHAD (*m/z* 1746), d) PHAD-504 (*m/z* 1718) and e) *E.coli* O83 (*m/z* 1718) with showing cleavage locations in the structure. Red signs match with 4'-monophosphoryl species, blue signs with 1-monophosphoryl species, and purple signs refer to both isomeric species. Fatty acyl chain lengths are given by numbers, and the colored parts of the structure show the differences among the four lipid congener (Aissa et al., 2022).

Typically, the highest fragment ion peak (at *m/z* 1115, except for PHAD-504 and *E. coli*, for which it was at *m/z* 1087) was the B_1 ion (inter-ring cleavage). Since the native sample consists of a mixture of 1- and 4'-monophosphoryl species, two B_1 ions – a phosphorylated one (*m/z* 1087) and a nonphosphorylated one (*m/z* 1007) – showed up (although the latter was less intense). Starting with the B_1 ion, the secondary fatty acyl loss at C-2' occurred for all compounds, resulting in the moderate-intensity fragment ion at *m/z* 887, apart from the 1-monophosphoryl lipid A species present in the *E. coli* sample (Fig. 14e), for which it gave a peak at *m/z* 807.

The position of this fatty acid could be readily determined by comparing the mass difference associated with this removal for PHAD-504 (200 u, reflecting the loss of a C12:0 from the C-2' secondary position) with that observed for the remaining three lipid A standards (228 u, corresponding to the removal of a C14:0 in the same position). The C-2' secondary fatty acid was also lost in the form of ketene, leading to the small-intensity peak at *m/z* 905. In addition, for all synthetic derivatives, low-intensity peaks occurred at *m/z* 789, 677 and 659 due to the loss of phosphoric acid (98 u), the C-3' secondary fatty acid as a ketene (210 u) and an acid (228 u), respectively, from the triacylated B_1 ion (*m/z* 887). The fragment ion at *m/z* 562 (or at *m/z* 534 for PHAD-504 and *E. coli*) resulted *via* the cleavage of the C14:0(3-O-C14:0) at the C-3' position (454 u) together with the removal of phosphoric acid (98 u). Subsequently, the formation of the fragment ion at *m/z* 334 was caused by the additional loss of C14:0 (or C12:0 for PHAD-504 and *E. coli*) at the C-2' secondary position.

Moreover, each MS^2 mass spectrum also exhibited another inter-ring cleavage product with low intensity (at *m/z* 388, 598, and 614 in Fig 14a, b, and c-e, respectively) called the Y_1-type ion. Specifically, it was the Y_1 ion that lost its substituent at C-1. In the case of 3D(6-acyl)-PHAD (Fig. 14b), the loss of fatty acid at the secondary position at C-2 of

the Y_1 ion was also detected with a small fragment at *m/z* 370. In addition to the ions mentioned above, a high-intensity fragment due to water loss (18 u) from the C-1 position of the precursor ion appeared for all derivatives. On the other hand, the loss of phosphoric acid (98 u) could also be observed from the C-1 position (resulting in the peak at *m/z* 1620) but only for the *E. coli* lipid A. The ion, where the substituent at the C-1 position is lost, is referred to as the B_2 ion. In this sense, two B_2 ions were observed in the *E. coli* sample. Moreover, in a unique manner, for 3D(6-acyl)-PHAD, the cleavage of a C14:0 from the C-2 secondary position could also be observed from the B_2 ion by the low-intensity peak at *m/z* 1485. At this point, it should also be noted that the ion corresponding to the [Y_1–C-1 substituent] ion could be easily identified in each mass spectrum by subtracting the *m/z* value of B_1 from the *m/z* value of B_2 and then, adding the mass of a proton.

Thereafter, the fragmentation patterns of the intact B_1 ions selected as precursor ions using ESI-IT MS^3 measurements were examined. Within the MS^3 mass spectra of the B_1 ions of the standards (Fig. 15) and of 4'-monophosphorylated lipid A from *E. coli* (Fig. 16a), the base peak (*m/z* 887) resulted from the release of the C-2' secondary fatty acid as an acid. Besides, a low-intensity peak occurred at *m/z* 905, which resulted from the loss of the same fatty acid as a ketene. Subsequently, two low-intensity peaks were formed by the losses of phosphoric acid (98 u) and metaphosphoric acid (80 u) from the non-intact B_1 ion at *m/z* 887. Furthermore, from the same (triacylated) B_1 ion, the C-3' secondary fatty acid was removed both as an acid (*m/z* 659) and a ketene (*m/z* 677). Other cleavage products were formed by the release of the residual C-3' primary fatty acyl chain (C14:1) as an acid (*m/z* 433) and a ketene (*m/z* 451). Losses of phosphoric acids (98u) from the di- and monoacylated B_1 ions led to peaks at *m/z* 561 and 335, respectively.

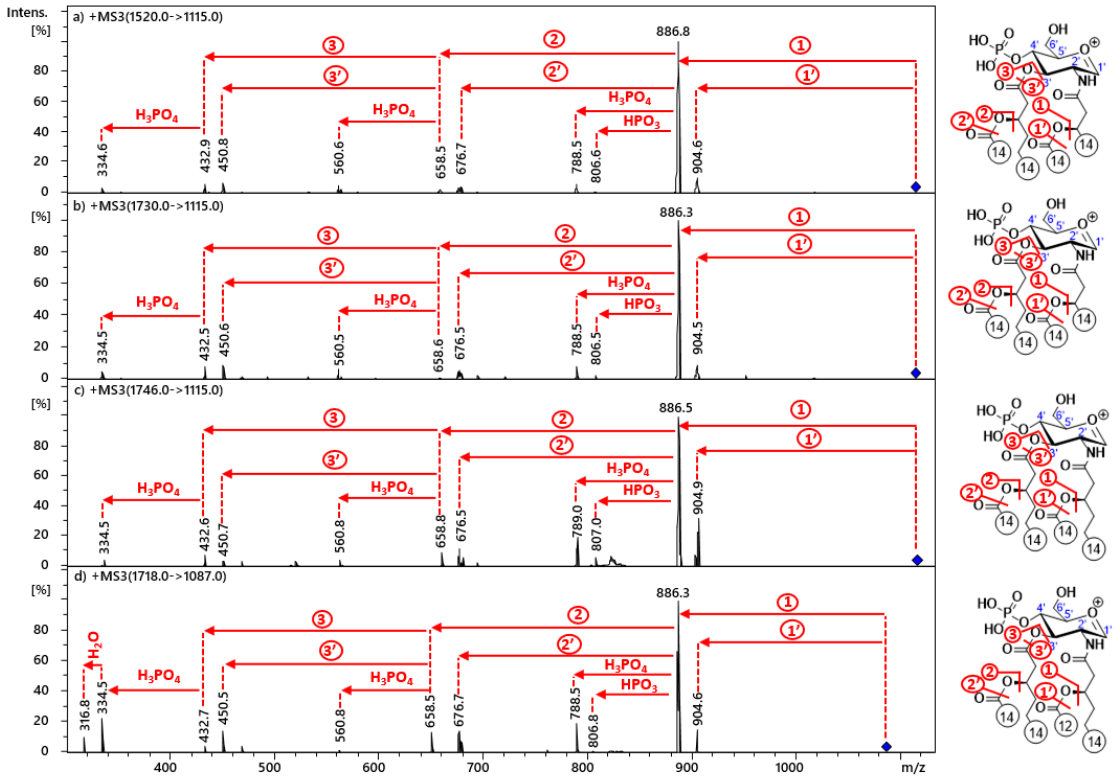

Figure 15. ESI-ion trap MS^3 mass spectra of the intact $[B_1 + H]^+$ ion selected as a precursor at *m/z* 1115 of a) 3D-PHAD, b) 3D(6-acyl)-PHAD, c) PHAD, and d) at *m/z* 1087 of PHAD-504 with the indication of cleavage sites in the structures (Aissa et al., 2022).

The MS^3 mass spectrum of the B_1 ion at *m/z* 1007 of the 1-monophosphorylated lipid A from *E. coli* O83 (Fig. 16b) was characterized by the same set of fatty acyl losses and intensity ratios as observed for the 4'-monophosphorylated species, except that the removal of the C14:1 residue in the form of ketene from the C-3' position was not detected. In addition, there was a lack of signals due to the removal of the phosphate group (in the form of phosphoric acid and metaphosphoric acid), evidently, as the non-reducing GlcN II subunit (representing the precursor ion in this case) was not phosphorylated at the C-4' position.

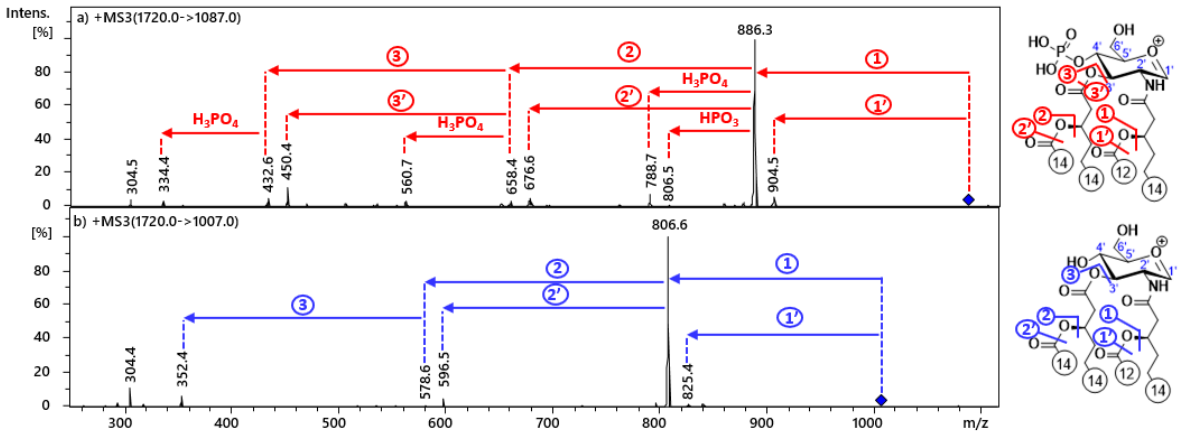

Figure 16. ESI-ion trap MS^3 mass spectra of the intact $[B_1 + H]^+$ ion selected as a precursor at a) *m/z* 1087 for the 4'-monophosphoryl species and b) *m/z* 1007 for the 1-monophosphoryl species from *E.coli* O83 lipid A. Cleavage sites are indicated in the structures (Aissa et al., 2022).

5.1.4. CID fragmentation pattern of the $[M + Na]^+$ lipid A precursor ions

The ESI-Q-TOF MS/MS mass spectra of the monosodium adducts $[M + Na]^+$ of the lipid A analytes (Fig. 17) presented a similar, but slightly more complex fragmentation pattern, than that observed for the $[M + H]^+$ precursor ions (Fig. 14).

Here, as well, both the intact B_1 fragment (at *m/z* 1137 in Fig. 17a-c and *m/z* 1109 in Fig. 17d and e) and the triacylated (at *m/z* 909) – resulting from the loss of the C-2' secondary acyl chain – B_1 fragment ions appeared, However, it was not the intact but the triacylated one being the base peak in the mass spectra of the $[M + Na]^+$ precursor (for $[M + H]^+$ precursor ions it was the intact one).

It should be noted that in Fig. 17e of the native sample of *E. coli* lipid A, two sets of B ions could be detected reflecting the simultaneous presence of two phosphorylation isomers. However, no further loss from the B_1 ion at *m/z* 1029 originating from the 1-monophosphoryl isomer was observed (any loss from this ion was only detected by MS^3 measurements).

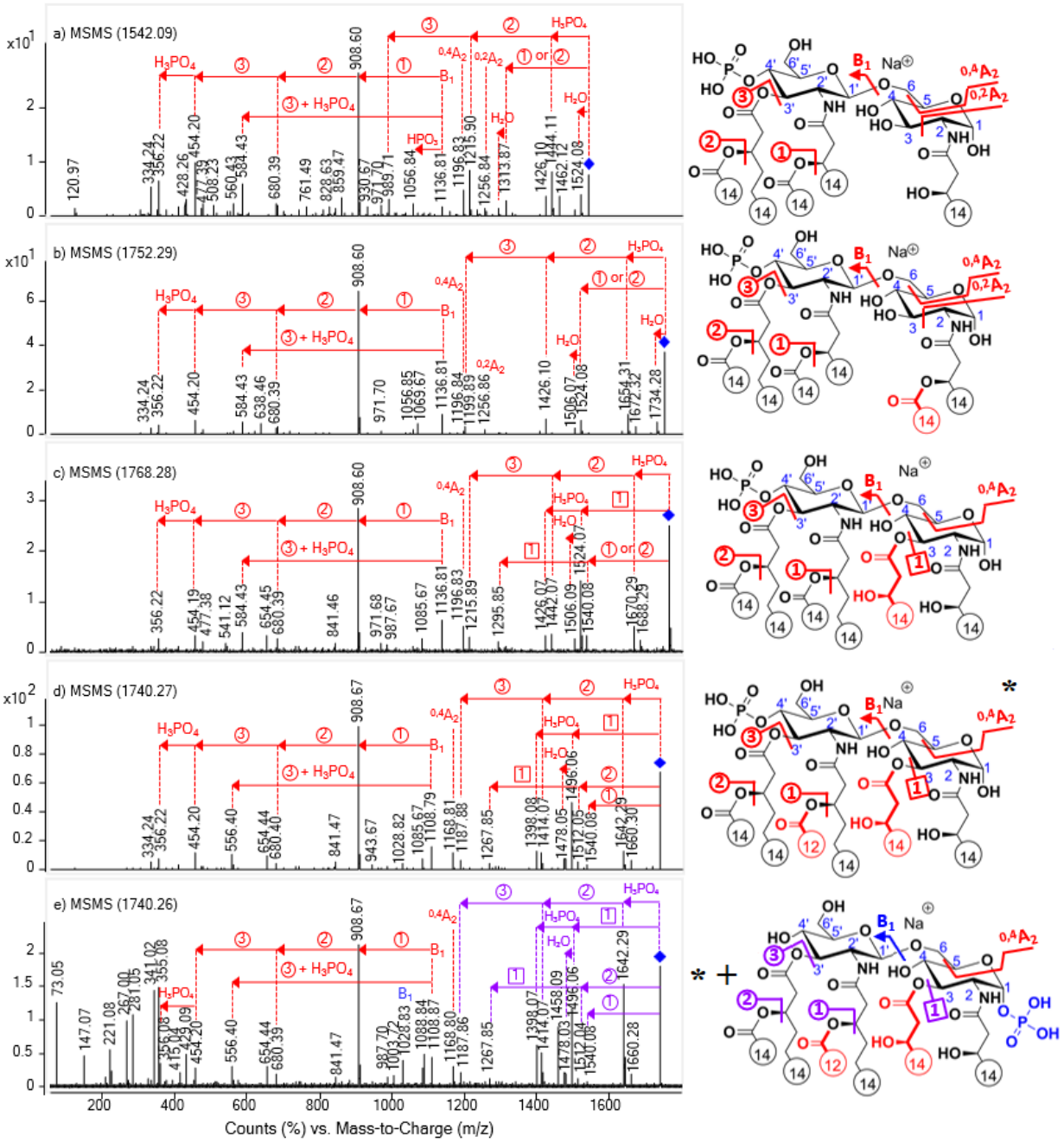

Figure 17. ESI-Q-TOF MS/MS mass spectra of $[M + Na]^+$ lipid A precursor ions of a) 3D-PHAD (*m/z* 1542), b) 3D(6-acyl)-PHAD (*m/z* 1752), c) PHAD (*m/z* 1768), d) PHAD-504 (*m/z* 1740) and ESI-ion trap MS/MS mass spectrum of e) *E. coli* O83 (*m/z* 1740), with showing cleavage locations in the structure. Red signs match with 4'-monophosphoryl species, blue signs with 1-monophosphoryl species, and purple signs refer to both isomeric species. Fatty acyl chain lengths are given by numbers, and the colored parts of the structure show the differences among the four lipid congeners (Aissa et al., 2022).

In addition to the B ions, another intense peak was observed only for the 3-acyl lipid A compounds (at *m/z* 1524 in Fig. 17c and *m/z* 1496 in Fig. 17d and e), coming from the removal of a C14:0(3-OH) (244 u) at the C-3 primary position from the precursor ion.

Each MS/MS mass spectrum showed signals due to water loss or removal of the phosphate group (in the form of phosphoric acid and metaphosphoric acid) from the precursor ion. The release of secondary fatty acids at the C-3' or C-2' position from the precursor led to a single low-intensity peak (at *m/z* 1314, 1524, and 1540 in Fig. 17a,b, and c, respectively) for the lipid A species with the same type of secondary fatty acids; and pairs of peaks (*m/z* 1512 and 1540 in Fig. 17d and e) for those having different substituents at these positions. A third generation fragment was also produced by the loss of the C-3' primary acyl residue (*m/z* 990, 1200, 1216, and 1188 in Fig. 17a,b,c, and d/e, respectively). Cross-ring fragments, such as a $^{0,4}A_2$ ion (at *m/z* 1197 in Fig. 17a and b for the 3-deacyl, and at *m/z* 1169 in Fig. 17c-e for the 3-acyl species) and a $^{0,2}A_2$ ion (at *m/z* 1257 only for the 3-deacyl species) came out with moderate intensities.

Subsequently, the intact B_1 ions present in the samples of PHAD-504 standard and *E. coli* O83 bacterium were subjected to MS^3 measurements. As shown in Fig. 18, fragmentation patterns looked quite similar for the synthetic and bacterial lipid A samples with C-4' phosphorylation (Fig. 18a and b). However, the fragmentation pattern of the 1-monophosphoryl lipid A from *E. coli* (Fig. 18c) was different from the two previously described, as the relative intensities of the fragments formed by secondary fatty acyl loss (as an acid) from the C-2' and C-3' positions, respectively, were inverted. Another difference was that (evidently) no signal because of the removal of the phosphate group (in the form of phosphoric acid and metaphosphoric acid) appeared.

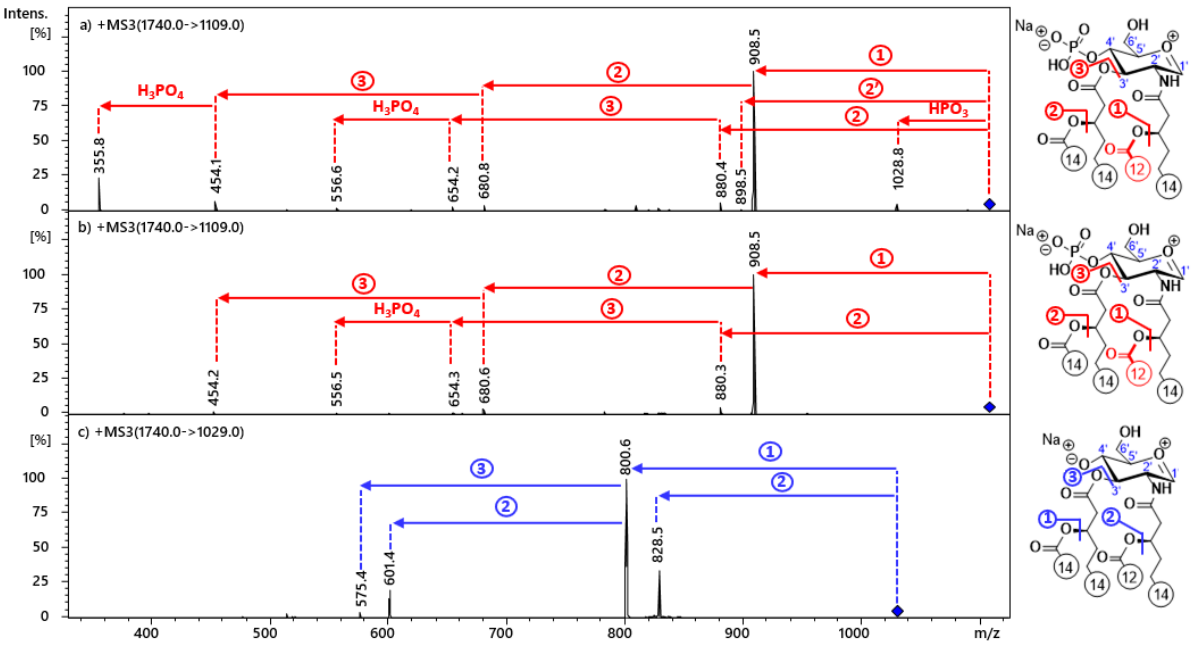

Figure 18. ESI-ion trap mass spectra of the $[B_1 + Na]^+$ ion obtained at MS^3 stage of the selected ion at a) *m/z* 1109 for PHAD-504, b) *m/z* 1109 for the 4'-monophosphoryl and c) *m/z* 1029 for the 1-monophosphoryl species from *E.coli* O83 lipid A, with the indication of cleavage sites in the structures. Red signs match with 4'-monophosphoryl, and blue signs with 1-monophosphoryl species. Fatty acyl chain lengths are given by numbers (Aissa et al., 2022).

5.1.5. CID fragmentation pattern of the $[M - H + 2Na]^+$ lipid A precursor ions

MS/MS measurements of the $[M - H + 2Na]^+$ precursor ions provided a very complex fragmentation pattern (Fig. 19), having many differences from that observed for the protonated molecule (Fig. 14) and the monosodium lipid A (Fig. 17).

For example, products of ring cleavage (type B and Y ions) have not been observed at all. For each sample, an intense peak in the MS/MS mass spectrum (*i.e.*, at *m/z* 1336 for 3D-PHAD, 1546 for 3D-(6-acyl)-PHAD, 1562 for PHAD, and 1534 for PHAD-504 and *E. coli*) was generated when the fatty acid (C14:0, 228 u) was released from the C-3' secondary position. From this latter, an additional loss of a C14:1 fatty acyl residue at C-3' (226) produced a clearly visible peak, while the loss of water (18 u) from the same fragment and the precursor ion could only be observed for the 3-deacyl standards.

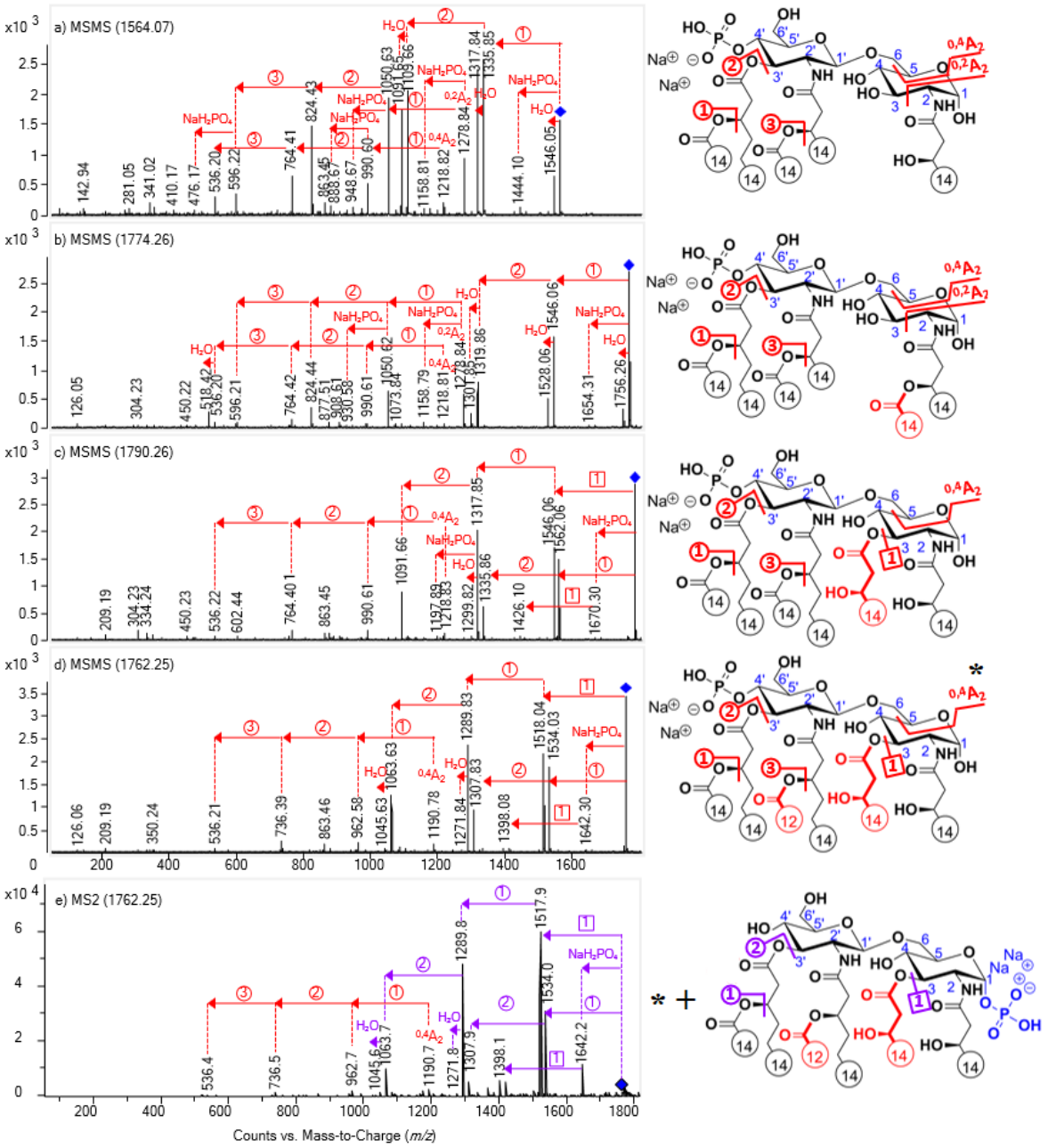

Figure 19. ESI-Q-TOF MS/MS mass spectra of $[M - H + 2Na]^+$ lipid A precursor ions of a) 3D-PHAD (*m/z* 1564), b) 3D(6-acyl)-PHAD (*m/z* 1774), c) PHAD (*m/z* 1790), d) PHAD-504 (*m/z* 1762) and ESI-ion trap MS/MS mass spectrum of e) *E. coli* O83 (*m/z* 1762), with showing cleavage locations in the structure. Red signs match with 4'-monophosphoryl species, blue signs with 1-monophosphoryl species, and purple signs refer to both isomeric species. Fatty acyl chain lengths are given by numbers, and the colored parts of the structure show the differences among the four lipid congeners (Aissa et al., 2022).

For the 3-acyl lipid A (Fig. 19c and d/e), the loss of the C-3 primary substituent (244 u) from the precursor ion led to a high-intensity fragment ion signal (*m/z* 1546 and 1518,

respectively), A further loss of secondary fatty acid at the C-3' resulted in an abundant peak, as well (*m/z* 1092 and 1064, respectively). This was followed by the loss of a C14:1 fatty acyl residue at C-3' (226 u), yielding a relatively high-intensity peak (*m/z* 1092 and 1064, respectively).

Moreover, in the MS/MS mass spectra of lipid A disodium adducts, intact $^{0,2}A_2$ and $^{0,4}A_2$ cross-ring fragments showed up with moderate intensities, from which further fragments were formed by sequential losses of the C-3' secondary, C-3' primary, and C-2' secondary acyl residues. Note that the $^{0,2}A_2$ ion series was only detected for the 3-deacyl (Fig. 19a and b), whereas the $^{0,4}A_2$ ion series appeared for all samples, apart for the 1-monophosphoryl species in the *E. coli* sample (Fig. 19e). In fact, given that no phosphate-free $^{0,4}A_2$ ions were detected in Fig. 19c-e, it could be assumed that the $^{0,4}A_2$ ion series detected in the *E. coli* sample in Fig. 19e derived only from the 4'-monophosphoryl isomer. In addition, multiple signals due to water loss (18 u) and eliminations of the monosodium phosphate (NaH_2PO_4, 120 u) from the precursor or other product ions contributed to the complexity of the fragmentation pattern of disodium adducts.

5.2. NACE–ESI-MS/MS separation of lipid A from *P. aeruginosa* PAO1

The lipid A isolate from *P. aeruginosa* PAO1 was analyzed using the newly developed NACE-MS/MS method with CID fragmentation in both positive and negative ion modes. Our main goal was to search for previously undiscovered structural isomers, specifically related to C-1 and C-4' monophosphorylated compounds, for which we can demonstrate the complementary role of the positive and negative ion CID mass spectra for their reliable differentiation and structural characterization.

The representative extracted ion electropherogram (EIE) of the tetra-, penta-, and hexaacylated lipid A, which appeared in more isomeric forms than that seen by the previous chromatographic separation (Buré et al., 2021) of the PAO1 isolate, can be seen in Figure 20. The electropherograms could be divided into two distinct migration zones, depending on the location of the phosphate group, i.e., C-1 phosphorylated lipid A (C-1P) moved more quickly toward the anode (MS detection) than those having the phosphate group at the C-4' position (C-4'P). Furthermore, ions within the two migration areas. were, in some cases, resolved into even more electrophoretic peaks matching with various acyl chain positional isomers. The exact composition of the separated species is summarized in Table 1

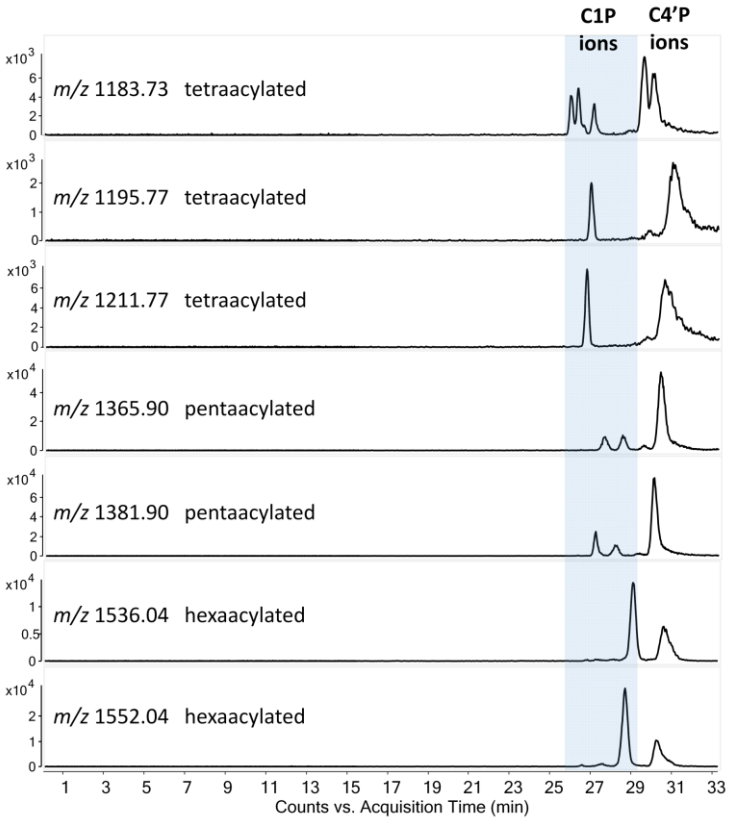

Figure 20. NACE-MS extracted ion electropherograms (EIEs) of some representative deprotonated ions from the tetra-, penta-, and hexa-acylated lipid A families presented in the *P. aeruginosa* PAO1 extract (Sandor et al., 2023). Notations: C1P refers to C1-monophosphorylated, and C4′P refers to C4′-monophosphorylated lipid A species. Confirmation of the phosphorylation site was based on the positive ion CID mass spectra of lipid A.

Table 1 Lipid A structures identified from the *P. aeruginosa* PAO1 isolate by NACE–ESI-QTOF MS/MS analysis (t_m: migration time; P: phosphate group) (Sandor et al., 2023)

t_m (min)	*m*calc. (Da)	Position on the diglucosamine backbone						reported by
		C4'	C3'	C2'	C3	C2	C1	Buré et al. (2021)
25.91	**1184.73**	H	H	C12:0(3-OH)	C10:0(3-OH)	C12:0(3-O(C12:0(2-OH)))	P	no
26.25	**1184.73**	H	H	C12:0(3-O(C12:0(2-OH)))	C10:0(3-OH)	C12:0(3-OH)	P	no
26.68	**1212.76**	H	H	C12:0(3-O(C12:0(2-OH)))	H	C12:0(3-O(C12:0(2-OH)))	P	no
26.89	**1196.77**	H	H	C12:0(3-O(C12:0))	H	C12:0(3-O(C12:0(2-OH)))	P	no
27.02	**1184.73**	H	C10:0(3-OH)	C12:0(3-OH)	H	C12:0(3-O(C12:0(2-OH)))	P	no
27.02	**1184.73**	H	C10:0(3-OH)	C12:0(3-O(C12:0(2-OH)))	H	C12:0(3-OH)	P	no
27.10	**1382.89**	H	H	C12:0(3-O(C12:0(2-OH)))	C10:0(3-OH)	C12:0(3-O(C12:0(2-OH)))	P	no
27.53	**1366.90**	H	H	C12:0(3-O(C12:0))	C10:0(3-OH)	C12:0(3-O(C12:0(2-OH)))	P	no
28.08	**1382.89**	H	C10:0(3-OH)	C12:0(3-O(C12:0(2-OH)))	H	C12:0(3-O(C12:0(2-OH)))	P	no
28.42	**1366.90**	H	C10:0(3-OH)	C12:0(3-O(C12:0))	H	C12:0(3-O(C12:0(2-OH)))	P	no
28.51	**1553.02**	H	C10:0(3-OH)	C12:0(3-O(C12:0(2-OH)))	C10:0(3-OH)	C12:0(3-O(C12:0(2-OH)))	P	no
29.01	**1537.03**	H	C10:0(3-OH)	C12:0(3-O(C12:0))	C10:0(3-OH)	C12:0(3-O(C12:0(2-OH)))	P	no
29.52	**1184.73**	P	C10:0(3-OH)	C12:0(3-O(C12:0(2-OH)))	H	C12:0(3-OH)	H	yes
30.03	**1184.73**	P	C10:0(3-OH)	C12:0(3-OH)	H	C12:0(3-O(C12:0(2-OH)))	H	yes
30.03	**1382.89**	P	C10:0(3-OH)	C12:0(3-O(C12:0(2-OH)))	H	C12:0(3-O(C12:0(2-OH)))	H	yes
30.16	**1553.02**	P	C10:0(3-OH)	C12:0(3-O(C12:0(2-OH)))	C10:0(3-OH)	C12:0(3-O(C12:0(2-OH)))	H	yes
30.37	**1366.90**	P	C10:0(3-OH)	C12:0(3-O(C12:0))	H	C12:0(3-O(C12:0(2-OH)))	H	yes
30.50	**1537.03**	P	C10:0(3-OH)	C12:0(3-O(C12:0))	C10:0(3-OH)	C12:0(3-O(C12:0(2-OH)))	H	yes
30.59	**1212.76**	P	H	C12:0(3-O(C12:0(2-OH)))	H	C12:0(3-O(C12:0(2-OH)))	H	yes
31.02	**1196.77**	P	H	C12:0(3-O(C12:0))	H	C12:0(3-O(C12:0(2-OH)))	H	no
31.02	**1196.77**	P	H	C12:0(3-O(C12:0(2-OH)))	H	C12:0(3-O(C12:0))	H	no

5.2.1. Mass spectrometric determination of phosphorylation site and acylation profile

The structural assessment of all of the separated lipid A isomers was based on MS/MS of the positively charged triethylammonium adducts $[M + H + Et_3N]^+$ and the negatively charged deprotonated $[M – H]^–$ lipid A precursor ions.

The most demonstrative example for determining both phosphorylation and acyl chain positional isomers in PAO1 is shown in Fig. 21. This figure presents the separation and structural verification of six tetraacylated lipid A isomers (two of them co-migrating), all having *m/z* 1184 in negative ESI mode (as seen in the first EIE in Fig. 21) and *m/z* 1287 in positive ESI mode. In the positive ion mode CID, the major cleavage sites of the $[M + H + Et_3N]^+$ precursor of all isomers are the glycosidic bond cleavages, giving B_2 and B_1 ions. These are indicated by the cleavages of the 1α and 1'α bonds, respectively, in Fig. 21b and d. Since the 1α bond is a potential phosphorylation site, the B_2 ion formed by its cleavage (following the loss of the adduct-forming Et_3N) is highly characteristic for the phosphorylation pattern of lipid A. Consequently, the B_2 ion peak at *m/z* 1088 in the MS/MS mass spectra of the first three isomers (compounds 1,2 and 3) was due to the loss of $Et_3N + H_3PO_4$ (199 u), stating the C-1 location of the phosphate group, whereas for compounds 4 and 5, the B_2 ion at *m/z* 1168 resulted by the loss of $Et_3N + H_2O$ (119 u) exposing the phosphorylation site at C-4'.

Cleavage of the 1'α bond gave rise to two fragments in the CID mass spectra (Fig. 21b), such as the high-intensity B_1 and the low-intensity Y_1–1α ions (Note that this latter can be identified by subtracting the *m/z* value of B_1 from that of B_2 and then, adding the mass of a proton.) From the masses of the B_1 and Y_1-1α ions, preliminary information can be obtained on the distribution of the acyl chains among the non-reducing and reducing glucosamines of each of the isomers. So, the B_1-type fragment (*m/z* 360) of the first

tetraacylated isomer (compound 1) is a non-phosphorylated, monoacylated non-reducing glucosamine part bearing an amide-linked C12:0(3-OH) likely at the C-2' primary position (since amide bonds are more stable than ester bonds under CID conditions). Therefore, the ion at *m/z* 728 is the Y_1–1α ion bearing three hydroxylated fatty acids, one with 10 and two with 12 carbon atoms (At this stage, it is not possible to determine the location of these fatty acids). Similarly, a non-phospholated , diacylated B_1 at *m/z* 558, bearing two 12-carbon hydroxy fatty acids, and a diacylated Y_1–1α ion (*m/z* 530), bearing one 10-carbon and one 12-carbon hydroxy fatty acids, are observed for compound 2.

Similarly, such ions B_1 and Y_1-1α ions are observed for compound 3, as well, at *m/z* 530, bearing one 10-carbon and one 12-carbon hydroxy fatty acids, and at *m/z* 558, bearing two 12-carbon hydroxy fatty acids, respectively. However, for Compound 3, fragments of a co-migrating isomer (Compound 3') were also found at *m/z* 728 and 360. These masses could only be related to a non-phosphorylated, triacylated B_1 ion, bearing one 10-carbon and two 12-carbon hydroxy fatty acids, and a mono-acylated Y_1–1α ion, bearing a C12:0(3-OH) certainly at the C2 primary position. As only one B_2 ion is seen in the chimera mass spectrum, we can verify that the compound 3 and the co-migrating compound 3', as well, contain a non-phosphorylated non-reducing part.

In the case of C-4'P isomers (compounds 4 and 5), only phosphorylated B_1 ions were detected (Fig. 21b). The peak at *m/z* 808 for compound 4 can be related with a phosphorylated, triacylated B_1, bearing one 10-carbon and two 12-carbon hydroxy fatty acids, and that at *m/z* 360 is a monoacylated Y_1–1α ion bearing an amide-linked C12:0(3-OH) likely at C-2. In compound 5, the peak at *m/z* 610 corresponds to a phosphorylated, diacylated B_1, bearing one 10-carbon and one 12-carbon hydroxy fatty acids, and that at *m/z* 558 to a diacylated Y_1–1α ion, bearing two hydroxy fatty acids with 12 carbon atoms.

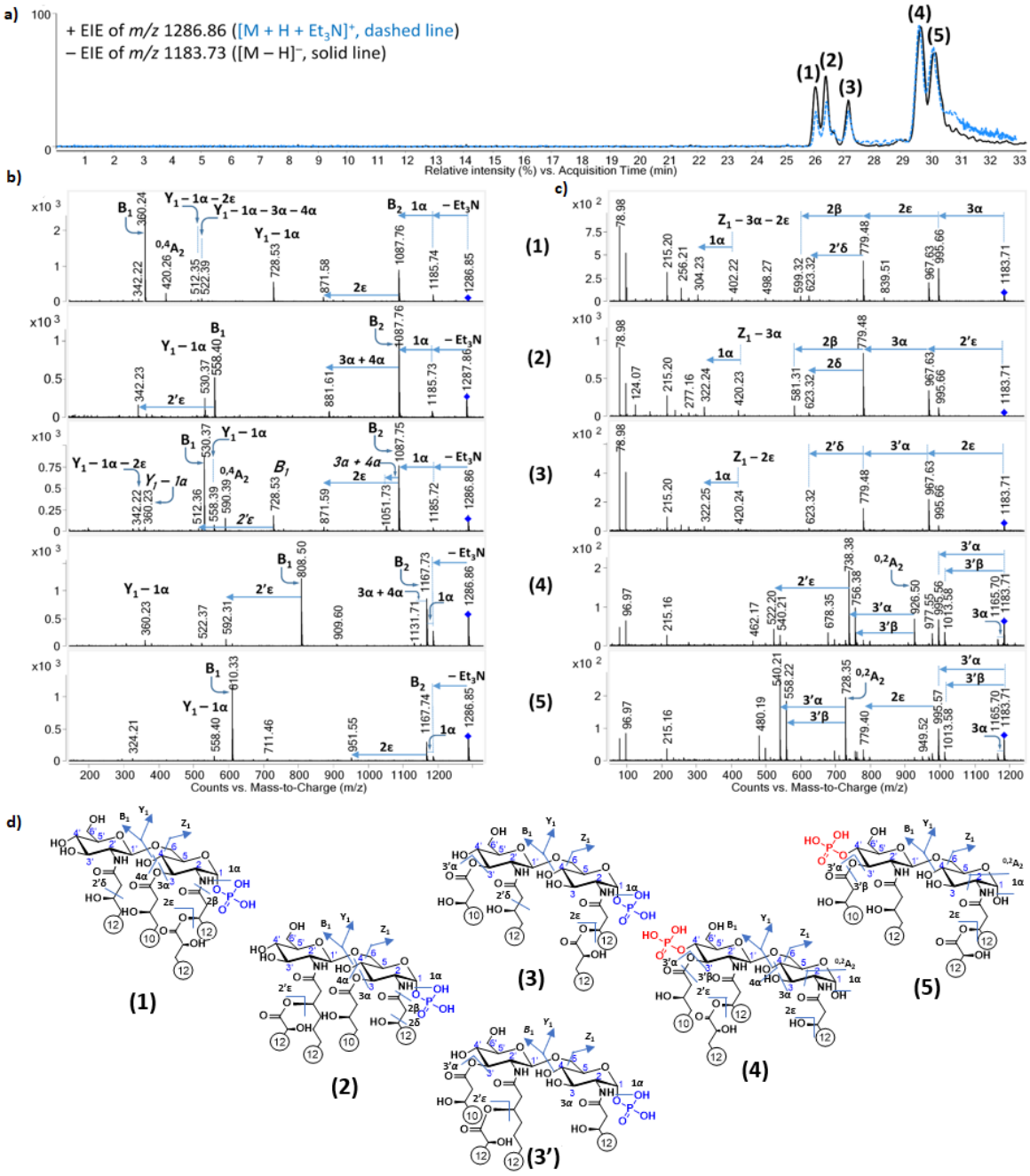

Figure 21. Structural characterization of tetra-acylated lipid A isomers from *P. aeruginosa* PAO1 (Sandor et al., 2023). The overlaid electropherograms of the $[M + H + Et_3N]^+$ (*m/z* 1286.86) and $[M – H]^-$ ions (*m/z* 1183.73) obtained by NACE–ESI-QTOF MS analysis in positive and negative ionization modes are shown in a), whereas MS/MS mass spectra of the observed isomers (compounds 1 – 5) achieved by positive and negative ion CID are shown in b) and c), respectively. Proposed structures of the separated isomers with all cleavage sites corresponding to both positive and negative ion CID experiment are shown in d). Italic labels correspond to a co-migrating isomer (compound 3').

For Et_3N-lipid A adducts, it is known that loss of secondary fatty acid at C-2' position (*i.e.*, cleavage of the 2'ε bond) can be determined by the difference in mass between the B_1 ion and an adjacent fragment. If an adjacent fragment is not present, then most probably no secondary substituent is linked to the C-2' primary acyl chain (Sándor et al., 2018). Therefore, a fragment resulting from the loss of a fatty acid (216 Da) from the B_1 ion has only been seen in the MS/MS mass spectra of compound 2 (at *m/z* 342), 3' (at *m/z* 512) and 4 (at *m/z* 592), indicating a C12:0(2-OH) in the C-2' secondary position for these isomers (note that this secondary fatty acid is typical for *P. aeruginosa* lipid A (Buré et al., 2021). Based on what has been elucidated so far, the acylation profile of the non-reducing part of compound 2 could be inferred: a C12:0(3-O-C12:0(2-OH)) is at C-2' and the –OH at C-3' is free.

For Et_3N-lipid A adducts,, it is also known that when primary fatty acid at C-2 is substituted, there is a loss of the secondary fatty acid from the B_2 ion (*i.e.*, cleavage of the 2ε bond) , but when C-2 secondary acyl chain is absent, then the parallel cleavages of the 3α + 4α bonds is most frequently visible (Sándor et al., 2018). Using this rule, the presence of a C12:0(2-OH) in the C-2 secondary position could be verified for compounds 1, 3, and 5 by the small-intensity peaks at *m/z* 872, 872, and 952, respectively, derived from the same type of loss (216 u) from the corresponding B_2 ions. For compound 2, the fragment seen by 206 u mass difference from the B_2 ion could be attributed to the parallel losses of a C10:0(3-OH) (188 u) from the C-3 primary position and a water molecule (18 u) from the C-4 position, hence, the C-2 primary substituent has to be a C12:0(3-OH). Loss of two water molecules (36 u) from the C-3 and C-4 positions from the B_2 ion was observed for compounds 3' and 4 by the peaks at *m/z* 1052 and 1132, respectively, involving their free C-3 primary position.

Overall, the positive ion CID experiments enabled the complete structural assignment of compound 2, and the determination of fatty acids on the non-reducing part of compound 1 and on the reducing parts of compounds 3, 3', 4, and 5 (Fig. 21d).

Subsequently, an assessment of the negative ion mode tandem mass spectra of the deprotonated tetra-acyl isomers at *m/z* 1184 (Fig. 21c) is required to check the remaining acylation patterns of all six isomers. For the three separated and one co-migrating C-1P isomers, very similar fragmentation patterns were seen, showing the same fragment ions at *m/z* 996 (produced by the loss of a 10-carbon hydroxy fatty acid, 188 u), *m/z* 968 (produced by the loss of 12-carbon hydroxy fatty acid, 216 u), and *m/z* 780 (produced by the loss of both of these fatty acids, 404 u), only the relative intensities of the ion peaks differed. Knowing that only ester-linked fatty acids are released under low energy CID conditions, the peak at *m/z* 996 for compound 1 could only come from the loss of a C10:0(3-OH) related to the C-3 primary position, and the peak at *m/z* 780 came from an additional loss of C-2 secondary C12:0(2-OH) linked to a C12:0(3-OH) at the C-2 primary position. Therefore, the full structure of Compound 1 could also be disclosed (Fig. 21d). The entire structure of compound 2 has already been determined from positive ion CID, whereas peaks at *m/z* 968 and 780 obtained by negative ion MS/MS confirmed that a C12:0(2-OH) substituent is connected at the C-2' secondary, and a C10:0(3-OH) is related at the C-3 primary positions. In the negative mode CID mass spectrum of compound 3 (having a C-2 secondary C12:0(2-OH) on the reducing sugar part) and of the co-migrating isomer, compound 3' (having a C-2' secondary C12:0(2-OH) on the non-reducing sugar part), the two with a free C-3 position, the peak at *m/z* 968 has to come from the loss of a C10:0(3-OH) at C-3' for both isomers, and that at *m/z* 780 resulted from the loss of a secondary C12:0(2-OH) at C-2, or at C-2' for compound 3'. It is also worth

mentioning that for the three C-1P isomers, cleavages of the 2'δ or 2δ bonds produced the small fragment at *m/z* 623 through the loss of a C9:0(CHO) aliphatic aldehyde from the unbranched amide-linked fatty acid at the C-2' or C-2 primary positions.

The negative ion mode tandem mass spectra of the C-4'P isomers (compounds 4 and 5 in Fig. 21c) exhibited different fragmentation patterns than the C1-P isomers (compounds 1–3) since different rules have regulated their gas phase fragmentation. The diagnostic acid/ketene loss of the C-3' primary fatty acid, and the presence of $^{0,2}A_2$ and $^{0,4}A_2$-type cross-ring fragments in their CID mass spectrum (Madalinski et al., 2006) were of big help for their structural identification. The loss of a C10:0(3-OH) as an acid and as a ketene from position C-3' resulted in ions at *m/z* 996 and 1014 for both compounds. The same pair of acid/ketene loss was also found from the $^{0,2}A_2$ ions for both compounds, yielding fragments at *m/z* 738/756 for compound 4, and at *m/z* 540/558 for compound 5. Additional loss of a C12:0(2-OH) secondary fatty acid C-2' was seen for compound 4 because of the $^{0,2}A_2$-type ion at *m/z* 522. In addition, from the mass of the mono-acylated $^{0,2}A_2$ ion at *m/z* 522 for compound 4, it could be concluded that a C12:1 residue is attached (produced in a CID process from the C12:0(3-O(C12:0(2-OH) at this position), whereas the mono-acylated $^{0,2}A_2$ ion at *m/z* 540 for compound 5 showed a C12:0(3-OH) connected at the C-2' primary position.

6. Discussion

6.1. Utility of fragmentation pathways of positively charged precursor ions

Ionization of lipid A molecules in negative mode ESI is usually more favored over the positive mode ESI due to the presence of acidic phosphoryl groups in the lipid A structures. Therefore, the formation of anions is preferred for these compounds. However, the detection of lipid A with negative ionization from a native sample still presents a challenge for scientists, because the simultaneous presence of phosphate positional isomers, *i.e.*, monophosphoryl lipid A compounds with the phosphate group at either C-1 or C-4', produces a chimera mass spectrum upon MS^2 analysis, which, in the case of lipid A compounds, makes their precise structural identification difficult due to overlapping mass spectral peaks (Fig. 13e). Moreover, since the fragmentation pattern of a chimeric spectrum of lipid A highly resembles that of the 4'-phosphorylated isomer alone, the presence of the 1-phosphorylated analog usually remains hidden.

To find out whether ionization of lipid A molecules in positive mode ESI combined with tandem MS can be used for a better distinction of phosphorylation isomers, we carried out a systematic MS/MS study of sodiated adducts and the protonated molecule of lipid A using pure lipid A samples and a mixture of phosphoisomers.

The greatest advantage is that the combined analysis of at least two of these three types of the positively charged precursors discussed above provides additional structural information on the acyl linkages at the C-2/ C-3/C-3′ primary and C-2/C-2′/C-3 secondary positions. In addition, assignment of the phosphorylation site (i.e., C-1 or C-4′) is highly facilitated by the fragmentation pattern of $[M + H]^+$ or $[M+Na]^+$. Particularly, the B_2 ion formed from the $[M + H]^+$ precursor ion is of great importance, as it directly points out the position of the phosphate group in lipid A.

6.2. Comparison of the fragmentation behavior of lipid A precursor ions

There are some similarities between the fragmentation mass spectrum of the single sodium ion adduct and the protonated molecular ion. Figure 21 shows the principal similarities and differences between the two fragmentation patterns. As already mentioned, the cleavage between the glucosamine units of the precursor ion resulting in a B_1 ion occurs in both mass spectra. Also, the parallel losses of C14:0(3 O-C14:0) at C-3' position and phosphoric acid elimination were observed in both mass spectra. A difference was found in the intensity of the precursor ion, which was higher for the single sodium adduct compared to the protonated molecular ion, when using the same collision energy (40 eV). This suggests that the adduct ion is more stable. Indeed, even at higher fragmentation energy (80 eV instead of 40 eV) the $[M + Na]^+$ precursor ion was still relatively abundant (results not shown). Moreover, the phosphoric acid loss was observed only from the single sodium adduct ion, but not from the protonated molecular ion.

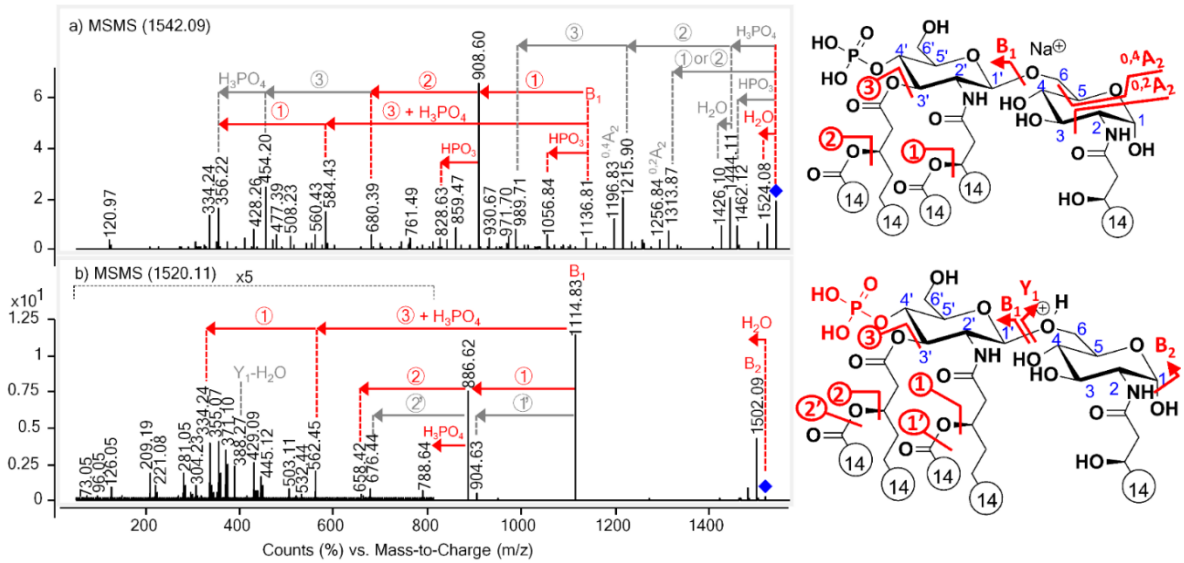

Figure 22. Comparison of ESI-Q-TOF MS/MS mass spectra of a) the $[M + Na]^+$ (*m/z* 1542) and b) the $[M + H]^+$ (*m/z* 1564) precursor ions of 3D-PHAD (Aissa et al., 2022). The similarities between the two fragmentation patterns are indicated in red, and the differences are shown in gray.

One of the main advantages of the fragmentation mass spectrum of the $[M - H + 2Na]^+$ is that it closely resembles that of a $[M - H]^-$ of 4'-monophosphorylated lipid A. The main similarities and differences between the two fragmentation patterns are demonstrated in Fig. 23. Both MS/MS mass spectra show the same type of cross-ring cleavages and serial fatty acid cleavages from the precursor ion, although there are fewer cross-ring fragments appearing from the series in the case of the $[M - H]^-$ precursor. Moreover, the characteristic loss of the C-3' fatty acyl chain in the form of acid and ketene can only be observed during the dissociation of the deprotonated form, whereas eliminations specific to the phosphate group and of water from the precursor ion are only seen during the fragmentation of the disodiated form. Another difference is that in the case a $[M - H + 2Na]^+$ precursor, the CID fragmentation of 4'-monophosphorylated lipid A containing also the C-3 fatty acyl substituent will not result in the formation of $^{0,2}A_2$ ions, only in the case of the $[M - H]^-$ precursor.

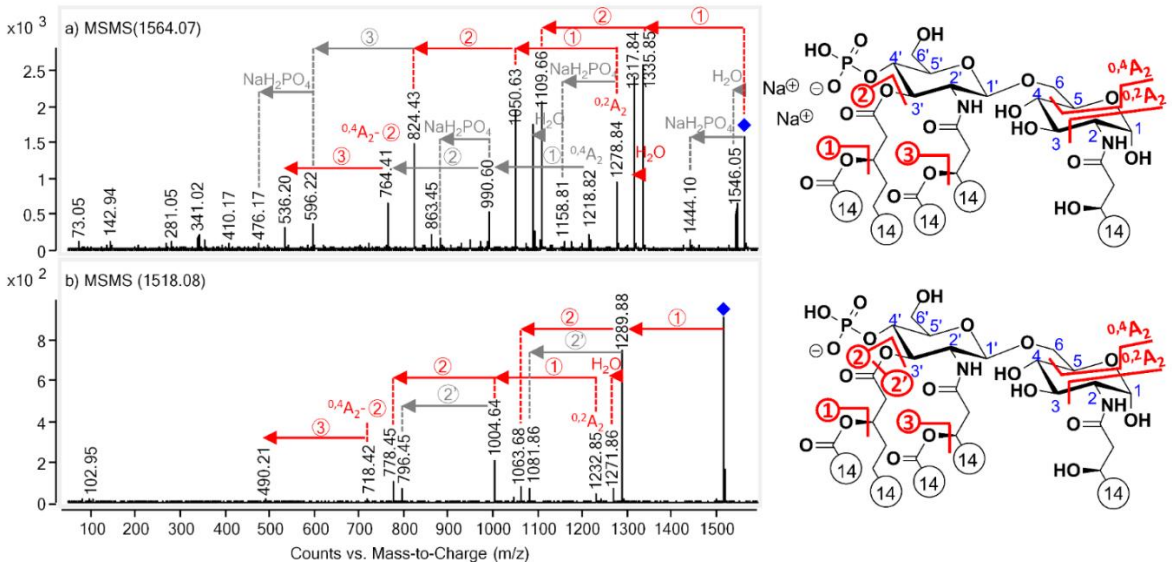

Figure 23. Comparison of ESI-Q-TOF MS/MS mass spectra of 3D-PHAD measured a) in positive-ion mode as the $[M - H + 2Na]^+$ (*m/z* 1564) precursor ion or b) in negative-ion mode as the $[M - H]^-$ (*m/z* 1518) precursor ion (Aissa et al., 2022). Similarities between the two fragmentation patterns are indicated in red, and the differences are shown in gray.

6.3. Structural elucidation of unknown monophosphorylated lipid A

We collected information from the positive mode ESI tandem MS analyses of the three ion types of lipid A disscussed above, namely the protonated molecule and the two singly-charged sodiated adducts, in order to formulate guidelines that can be applied for the proper structural elucidation of an unknown monophosphorylated lipid A even from complex samples containing phosphorylation isomers. Accordingly, based on the combined data from the CID fragmentation patterns of the $[M + H]^+$, $[M + Na]^+$ and $[M – H + 2Na]^+$ ions, a flowchart was developed (Fig. 24). The flowchart describes the steps for identifying the lipid A constituents. The first step is the determination of the phosphorylation site, and this is followed by the identification of the fatty acyl chains bound at specific sites. It can be applied for the structural characterization of unknown monophosphorylated lipid A molecules with higher acylation degrees (*i.e.*, penta-, hexa- or hepta-acylation).

In detail. The lipid A sample (containing a small amount of ammonium formate and NaCl) is initially ionized with positive-ion ESI to generate protonated, mono and disodium-cationized precursor ion signals (each differing by 22 u in mass). Thereafter, the first peak ($[M + H]^+$ ion) is subjected to CID to generate product ions that provide information on the complexity of the lipid A sample, *i.e.*, if more than one phosphorylation isomer is present. Phosphorylation locations can be determined by the occurrence of one or two B_2 ion peaks in the MS/MS mass spectrum of the $[M + H]^+$ precursor ion, *i.e*, one formed by removal of phosphoric acid (98 u) – showing C-1 phosphorylation. – and a second resulting from a loss of water (18 u) – showing C-4' phosphorylation. The occurence of two B_2 ions shows that the sample is a mixture of C-

1 and C-4’ phosphorylated lipid A; but the occurrence of a single B_2 peak confirms that the sample contains a single phosphorylation isomer.

Then, the type of secondary fatty acid at the C-2’ position (if present) can be identified by the mass difference between the B_1 ion and a prominent fragment beside it., caused by the loss of that fatty acid (Note that this loss of secondary fatty acyl produces the base peak during the CID of the $[M + Na]^+$ precursor, or using higher collision energies, such as CE ≥ 50 eV, during the CID of the $[M + H]^+$ precursor). Furthermore, the composition of the C-2’ secondary fatty can be confirmed with the lastly generated product ion from the A-type ions in the MS/MS mass spectrum of the disodiated lipid A.

At this stage, further structural information can be otained from the MS/MS analysis of the sodiated ions, $[M + Na]^+$ and $[M – H + 2Na]^+$ lipid A precursor ion subjected to CID. To find out if the lipid A molecule has any acyl chain at the C-3 position, the MS/MS mass spectrum should be examined for an abundant peak formed by water loss (18 u) from (any of) the sodiated precursor ions. Detection of this fragment indicates that the C-3 primary acyl chain is not present, while the absence of this fragment in the MS/MS mass spectrum defines a lipid A compound containing the C-3 acyl chain. In the case of this latter, the next step is to seek out for three abundant fragment peaks consecutively coming from the $[M – H + 2Na]^+$ precursor with mass differences in accordance with C-3 primary, C-3’ secondary (if present), and C-3’ primary fatty acyl losses. The first and second fragments of these dominant peaks can have concurrent peaks as a result of the sequential loss of the C-3’ secondary and primary substituents from the precursor ion. In the case of the $[M + Na]^+$ precursor, the C-3 primary fatty acyl loss-fragment is normally seen, but peaks of the other two losses (from the C-3’ secondary and primary positions) should be sought only from the phosphate-depleted fragment of the precursor ion.

For a 3-deacyl compound, only two abundant peaks – each followed by water loss – need to be sought, resulting from the serial release of the C-3' secondary (if present) and C-3' primary fatty acids from the $[M - H + 2Na]^+$ precursor ion, or from the phosphate-depleted fragment of the $[M + Na]^+$ precursor ion. In addition, the distribution of the C-3' secondary, C-3' primary, and also the C-2' secondary fatty acids can also be verified by the existence of cross-ring cleavage fragments, such as $^{0,2}A_2$ (for 3-deacyl) and $^{0,4}A_2$ (for 3-deacyl and 3-acyl lipid A) from the $[M - H + 2Na]^+$ precursor ion.

For assignment of the C-2 substitution, search for the Y_1-type ion (which already lost the C-1 substituent) in the MS/MS mass spectrum of the $[M + H]^+$ precursor ion (*i.e.*, calculate the mass difference between the B_2 and B_1 ions and add the mass of a proton). In case the C-2 primary fatty acid is further substituted (forming an acyloxyacyl group), also the composition of the C-2 secondary fatty acid can be determined by the same mass difference between i) the Y_1-type ion and one small peak near to the Y_1-type ion, and ii) the B_2 ion peak and a small peak beside the B_2 ion.

After identifying all the fatty acyl chains mentioned above by analysing the three positively charged precursor ions, also the C-2' primary fatty acid can be (indirectly) inferred, by calculation of the mass difference between the precursor ion and the sum of the identified sugar, fatty acid, and phosphate substituents.

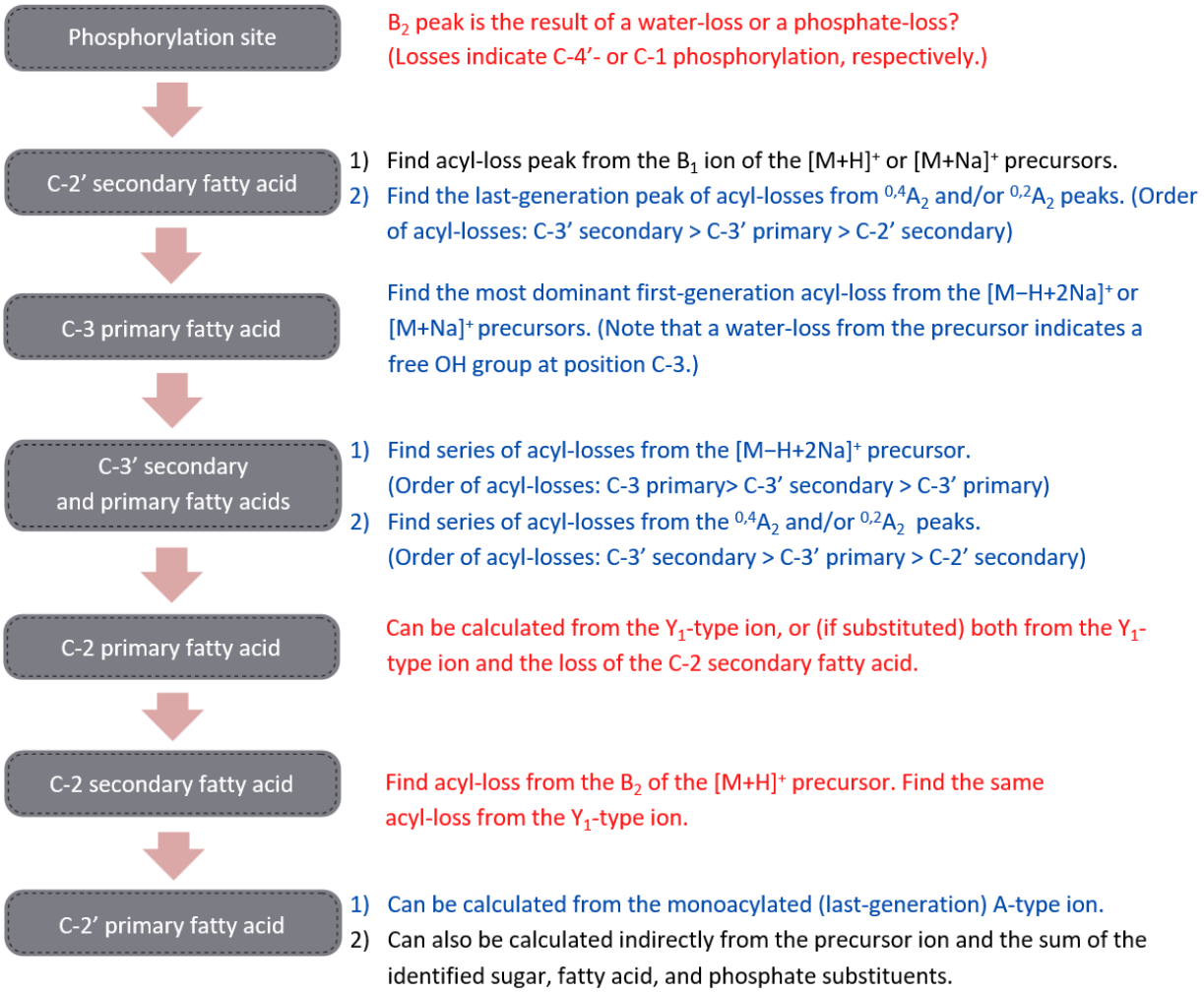

Figure 24. Guidelines for the structure elucidation of unknown 4'-monophosphorylated lipid A by the combined analysis of MS/MS mass spectra of its $[M + H]^+$, $[M + Na]^+$ and $[M – H + 2Na]^+$ precursor ions. Information obtained from the CID pattern of the $[M + H]^+$ precursor is indicated by red, whereas information gained from the $[M – H + 2Na]^+$ and $[M + Na]^+$ precursors is indicated by blue.

6.4. Mechanistic study of the fragment ion formation in the gas phase

There are relatively few studies found on the dissociation processes of 4'-monophosphoryl lipid A upon low-energy collisional activation. In those studies, two possible mechanisms are indicated for the elimination of acyloxy esters from lipid A, a charge remote process (Kussak and Weintraub, 2002; Lee et al., 2004; El-Aneed and Banoub, 2005) , and a charge-driven process (Madalinski et al., 2006). Meanwhile, the

underlying mechanisms of cross-ring fragment formations, or the elimination of the acyloxy amides or the phosphate group are barely described in the literature.

This section is intended to examine particular product ions resulting from the gas-phase fragmentation of the four synthetic lipid A compounds through MS^n analyses (n = 2 – 6) in both negative and positive ion modes. A detailed mechanistic study regarding the fragment ion formation through CID MS^n is important for a better insight of ion chemistry and to help identify lipid A derivatives and fragmentation dependence on specific linkages.

6.4.1. Mechanisms suggested for the release of the secondary fatty acids from deprotonated 4'- monophosphoryl lipid A molecules

The elimination of secondary fatty acid at C-3' position (as free fatty acid) contiguous to the phosphate group was the first dominant dissociation process for all the studied lipid A standards (Fig. 11). The mechanism was originally described by Madalinski et al. (Madalinski et al., 2006) involving a charge-driven dissociation through the formation of an anion-molecule complex (Scheme 3). This means that the negative charge located on the phosphate group (basic site) eliminates a proton from the α position (acidic site) of the primary fatty acyl chain linked at the C-3' position. Next, an anion–molecule complex is produced by the α–β elimination with neutralization of the negatively charged phosphate group in an intermediate structure, and then the loss of the C-3' acyloxy chain by removal of a proton from the phosphate group and formation of an α,β-unsaturated carboxylic ester stabilized by resonance.

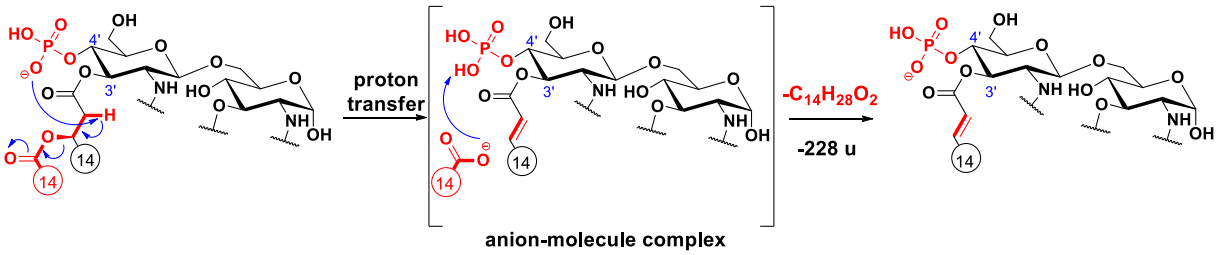

Scheme 3. Suggested fragmentation mechanism for the loss of the C-3’ secondary acyl chain as an acid (Madalinski et al., 2006).

The release of the secondary fatty acid at C-2’ from the precursor was not seen at the MS^2 stage (otherwise there would be a peak at *m/z* 1516 in Fig. 13d). Only the upper MS^n stages (n = 4, 5, 6) displayed anion species due to cleavages of secondary fatty acids at C-2' (200 u for C12:0 in PHAD-504) and at C-2 (228 u for C14:0 in 3D(6-acyl) PHAD), after the liberation of the other labile ester-bound fatty acids and mostly after cross-ring fragmentation had taken place. For illustrative mass spectra showing the release of these fatty acids, see Fig. A2 in the Appendix. For both cleavage mechanisms, we proposed charge-driven processes (Schemes 4 and 5, respectively), where the proton is removed (by the weak basic phosphate group) from the acidic site in the α position of the corresponding amide group.

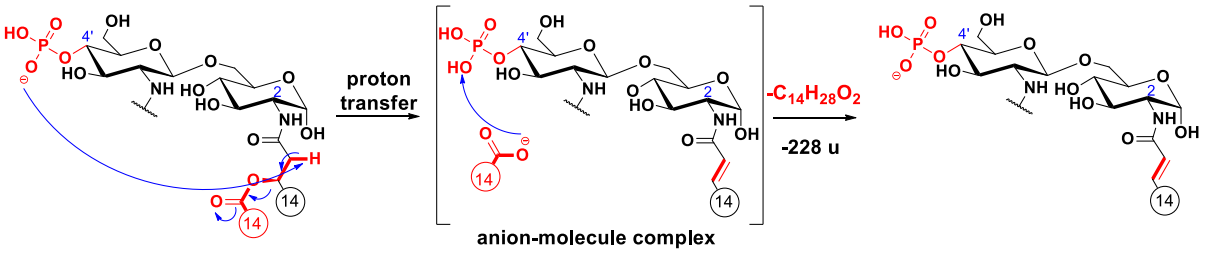

Scheme 4. Suggested fragmentation mechanism for the loss of the C-2 secondary acyl chain as an acid (Aissa et al., 2021).

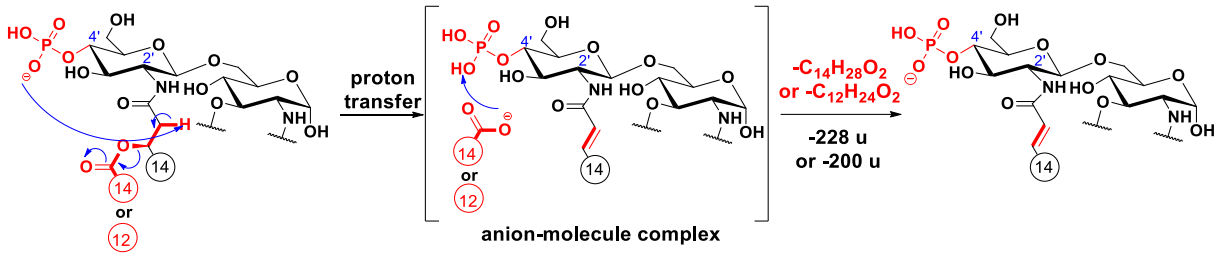

Scheme 5. Suggested fragmentation mechanism for the loss of the C-2’ secondary acyl chain as an acid (Aissa et al., 2021).

In addition, based on MS^n measurements, the C-2' secondary fatty acid was also cleaved in the form of a ketene (182 u or 210 seen in Fig. A3). This type of cleavage process may be due to intra-molecular hydrogen transfer from the α-carbon of the ester group and direct O–CO bond cleavage (Scheme 6).

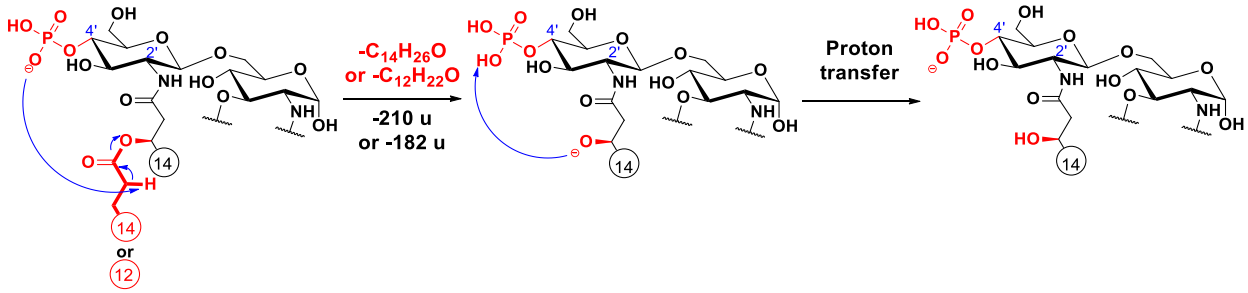

Scheme 6. Suggested fragmentation mechanism for the loss of the C-2’ secondary acyl chain as a ketene (Aissa et al., 2021).

6.4.2. Mechanisms proposed for the release of the C-3’ primary fatty acid

The primary fatty acid was removed from the C-3' position as an unsaturated primary fatty acid (C14:1) in all standards (observe that the previous removal of the ramified chain at C-3' leaves behind a double bond). As already presented in Schemes 1 and 2, the loss of a C-3’ primary substituent occurs in two forms, as a ketene and an acid, through two rival processes. Concerning the loss of the C14:1 as a ketene, the suggested process is initiated by a proton removal (captured by the anionic charge of the phosphate group)

from the allylic position of the unsaturated chain, and then, the conjugated carbanion induces the direct O–CO bond cleavage leading to the release of C14:1 in the form of ketene (Scheme 7). Also, we assumed that a second proton transfer would happen, and the negative charge is retained by the phosphate group.

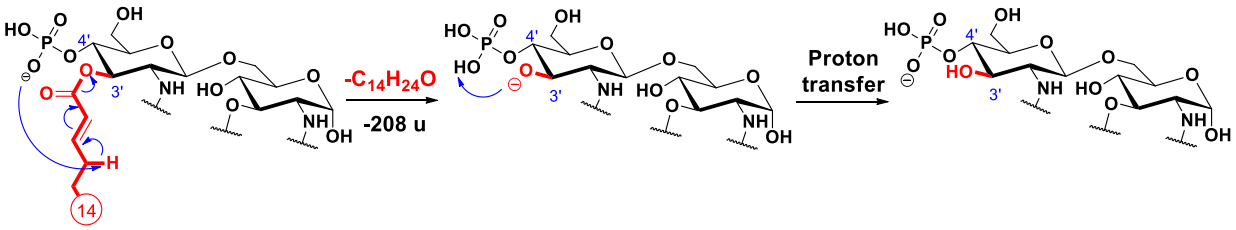

Scheme 7. Suggested fragmentation mechanism for the loss of the C-3’ primary acyl chain as a ketene, along with a proton transfer (Aissa et al., 2021).

For loss of the C-3’ primary chain as a free fatty acid, a charge-remote fragmentation process has already been suggested (Kussak and Weintraub, 2002), where the elimination of a hydrogen atom at C-4' resulted in the formation of a double bond between the C-3' and C-4' carbon atoms (Scheme 2). Besides, we proposed here an alternative, charge-driven dissociation pathway. Namely, a five-membered cyclic phosphate is generated in a process initiated by the attack of the anionic charge site of the phosphate group on the carbon C-3’, leading to the removal of the unsaturated alkyl chain as a free fatty acid (Scheme 8). This assumption was based on a previous report (Hsu and Turk, 2000) demonstrating the formation of a cyclic phosphate derivative (a six-membered ring) from diacyl glycerophosphoethanolamine through the release of a primary fatty acid.

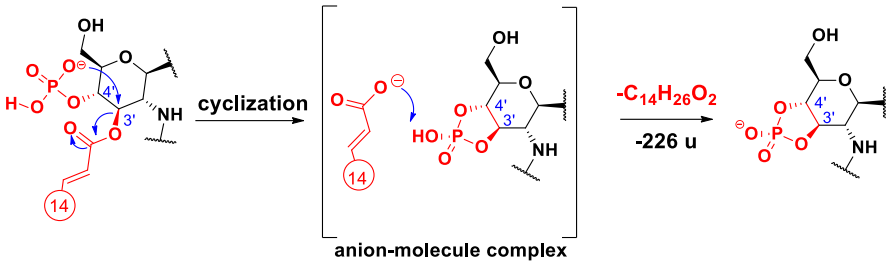

Scheme 8. proposed fragmentation mechanism for the loss of the C-3' primary fatty acyl chain as an acid, leading to the formation of a cyclic phosphate derivative (Aissa et al., 2021).

6.4.3. Mechanisms proposed for the release of the C-2' and C-2 primary fatty acids

We examined the elimination process of the amide-linked primary fatty acid at C-2'. In fact, such release was observed only in the case of 3D-PHAD (this has the smallest molecular weight) and only at higher MS stages (Fig. 25). Here, a fragment ion at *m/z* 282 was formed by eliminating a C14:1 as a ketene from the C-2' position of the $^{0,4}A_2$ cross-ring fragment. The proposed mechanism begins with a proton transfer from the allylic position of the unsaturated acyl amide chain to the phosphate group (Scheme 9). Then, the conjugated carbanion facilitates the direct N–CO bond cleavage.

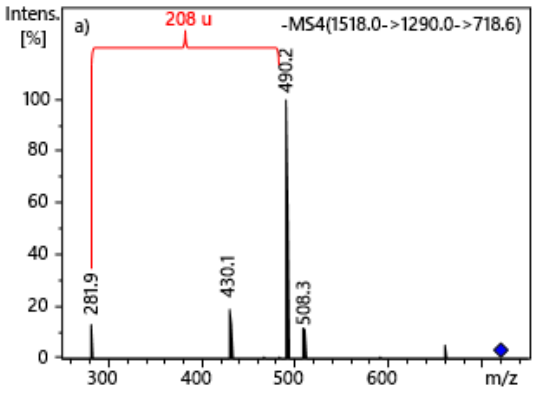

Figure 25. ESI-IT MS^4 mass spectrum of the selected ion at *m/z* 718 for 3D-PHAD, displaying the release of an unsaturated myristic acid (208 u) as a ketene from the C-2' primary position (Aissa et al., 2021).

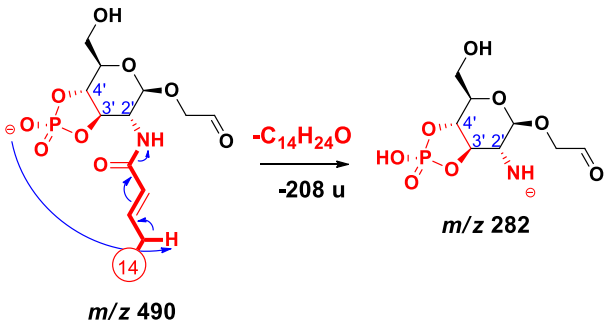

Scheme 9. Suggested fragmentation mechanism leading to the release of the C-2' primary fatty acyl chain as a ketene (Aissa et al., 2021).

On the contrary, we have seen the cleavage of the C-2 primary fatty acyl chain for all standards. An example is shown for PHAD-504 (Fig. 26), where the fragment at *m/z* 774 was formed through the removal of the hydroxymyristic acid amide (Δm = 243 u) from the ion at *m/z* 1017. The first step of this charge-driven process (due to a long proton transfer) is the creation of a reactive alkoxide group at the C-1 position. Next, a ketone derivative is established *via* a hydride transfer through the formation of an intermediate anion–molecule complex (Scheme 10).

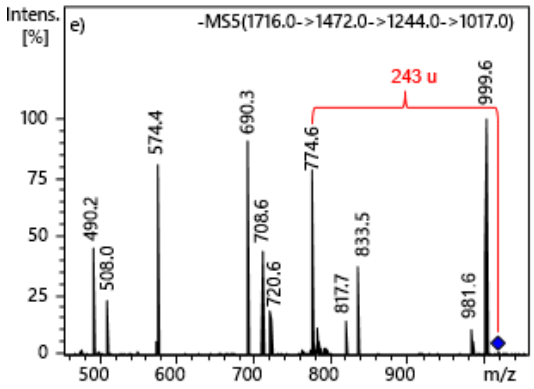

Figure 26. ESI-IT MS^5 mass spectrum of the selected ion at *m/z* 1017 for PHAD-504, indicating the loss of hydroxymyristic acid amide from the C-2 primary position (243 u) (Aissa et al., 2021).

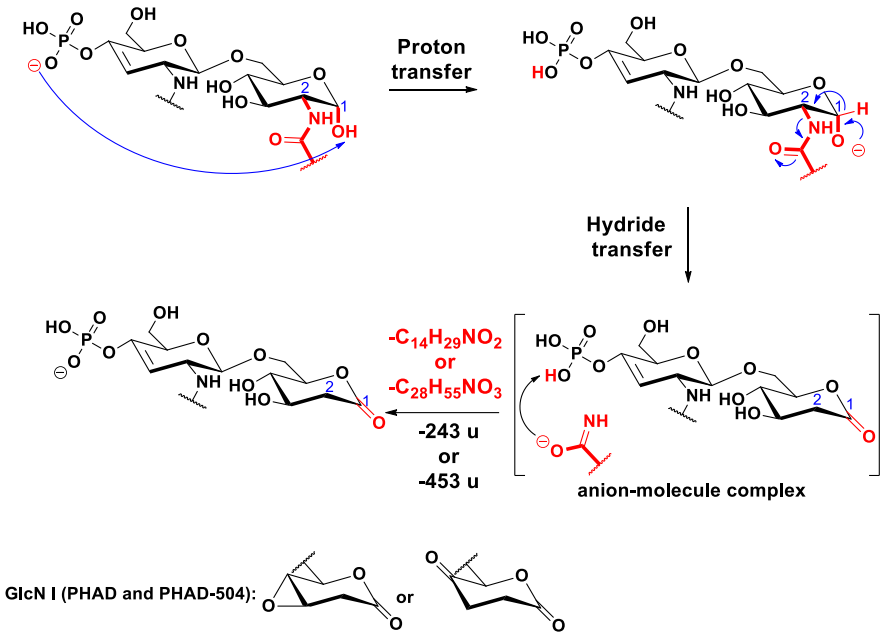

Scheme 10. Suggested fragmentation mechanism for the loss of the C-2 primary fatty acyl chain, leading to the formation of a ketone group in the sugar ring (Aissa et al., 2021).

6.4.4. Mechanisms proposed for the release of the C-3 primary fatty acid

The cleavage of the C-3 linked primary fatty acyl chain was evidently only observed for the two 3-acyl standards (PHAD and PHAD-504), by the intensive peaks at *m/z* 1500 and *m/z* 1472, respectively, in Fig. 13. A charge-driven process has already been suggested for this release (Madalinski et al., 2006), induced by a long proton transfer, followed by the creation of a reactive alkoxide group at C-4. Then, a hydride transfer takes place between C-4 and C-3, promoting release of the C-3 fatty acid anion, which, through an anion-molecule complex, can remove a proton from the phosphate group. The product ion of this process is a ketone derivative (Scheme 12).

However, we suggest here another pathway where the product ion will be an epoxide derivative (note that that epoxide sugars are multipurpose intermediates in organic synthesis (Wang et al., 2005)) as a result from the anti-attack of the alkoxide ion at C-4 on the hydroxymyristic acid chain at C-3 (Scheme 13).

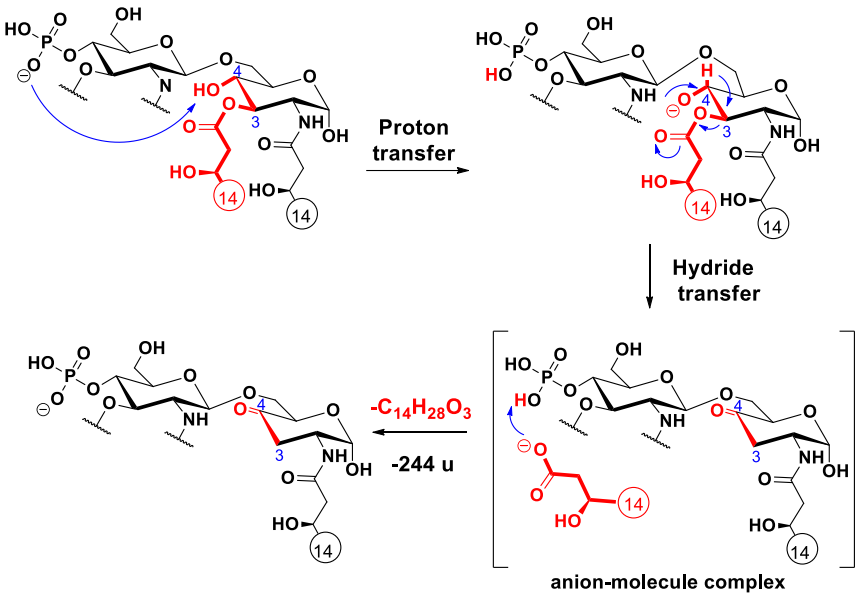

Scheme 12. Suggested fragmentation mechanism for the loss of the C-3 primary fatty acyl chain as an acid, leading to the formation of a ketone group in the sugar ring (Madalinski et al., 2006).

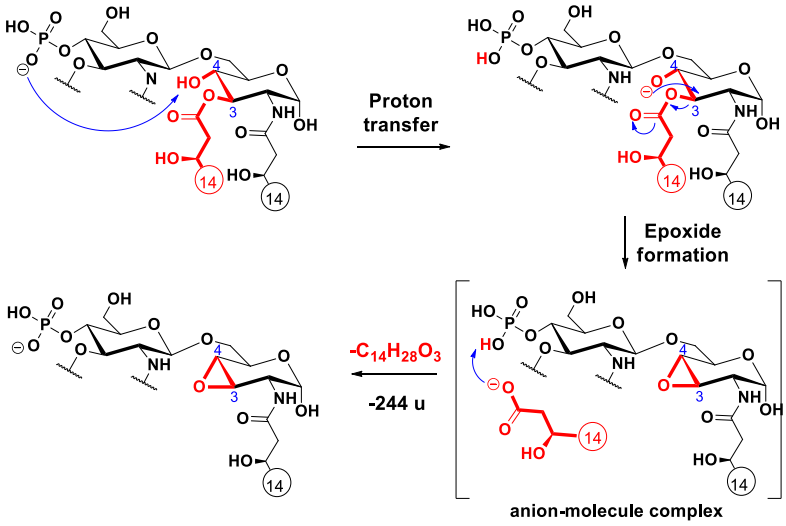

Scheme 13. Suggested fragmentation mechanism for the loss of the C-3 primary fatty acyl chain as an acid, leading to the formation of a sugar-derived epoxide (Aissa et al., 2021).

6.4.5. Mechanisms proposed for cross-ring fragmentations

Cross-ring cleavage products, such as $^{0,2}A_2$ ions, appeared already at the MS^2 stage for all standards (Fig. 13), but $^{0,4}A_2$ cross-ring fragments appeared only at higher MS

stages. Since the mechanisms of cross-ring fragment formations for lipid A are not fully discussed in the literature, we took a closer look at these fragmentations.

The formation of both types of cross-ring fragments can easily be followed by sequential CID measurements. For example, the MS^3 mass spectrum of the selected first-generation fragment ion at *m/z* 1500 for 3D(6-acyl)-PHAD (Fig. 27a) showed a high-intensity peak at *m/z* 1005. This peak resulted from $^{0,2}A_2$ cross-ring cleavage. When looking at the MS^4 mass spectrum of this ion, then a fragment ion at *m/z* 945 (60 u) was seen, corresponding to $^{0,4}A_2$ cross-ring cleavage (Fig. 27b). This observation infers that there is a structural relationship between the two cross-ring fragments (The same ions, *m/z* 1005 and *m/z* 945, were observed for 3D-PHAD, when the first-generation fragment at *m/z* 1290 was selected for MS^n; Fig. A4).

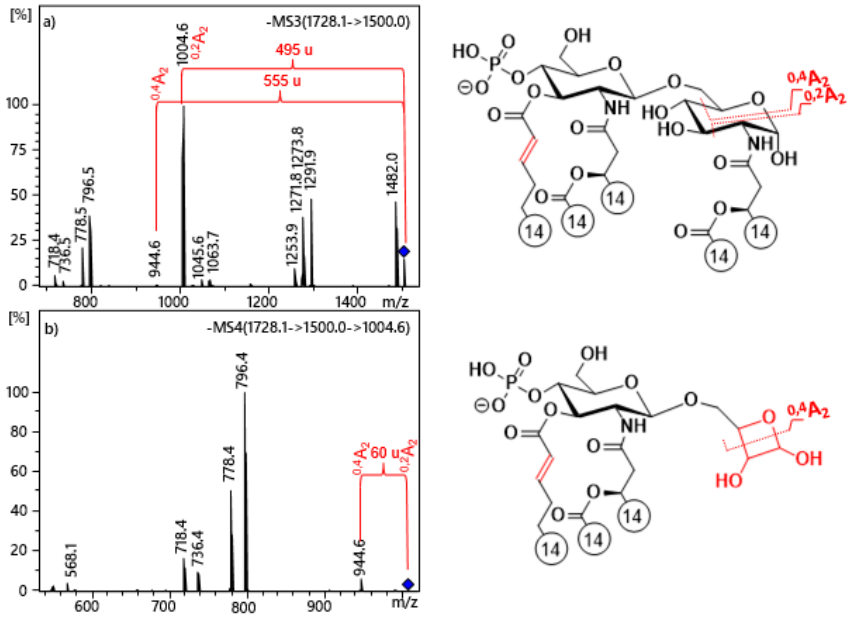

Figure 27. ESI-ion trap mass spectra obtained at MS^3 and MS^4 stages of selected ions at a) *m/z* 1500 and b) *m/z* 1005 for 3D(6-acyl)PHAD, demonstrating the structural relationship between $^{0,2}A_2$ and $^{0,4}A_2$ cross-ring fragment ions in 3-deacyl lipid A (Aissa et al., 2021).

In order to elucidate details on the mechanistic origin of these ions, first it should be pointed out that $^{0,2}A_2$ and $^{0,4}A_2$ cross-ring fragments are usually typically seen in the

tandem mass spectra of non-phosphorylated (Sándor et al., 2016) or such monophosphorylated lipid A species (Kussak and Weintraub, 2002; Post et al., 2002), where the phosphate group is connected to the C-4' position, and the C-1 position is free (Kilár et al., 2018). Based on this observation, we can consider a ring-opening (Spengler et al., 1990) of the reducing sugar as the first step of the mechanism, assuming that there is an equilibrium amount of the open-chain aldehyde and the closed-chain form. The open-chain form is then able to act like a reducing agent. Hence, this form catalyzes a retro-aldol reaction (Chiu et al., 2019) to produce a smaller α,β-dihydroxy aldehyde, *i.e.*, an $^{0,2}A_2$ fragment, through the neutral loss of the anchored enol (Scheme 14). For the further decomposition of the $^{0,2}A_2$ product ion, we suggest two ways: either a second retro-aldol reaction occurs which leads directly to the $^{0,4}A_2$ fragment ion through loss of an ethane-1,2-diol (60 u), or the hydroxyl group at C-5 reacts with the formed aldehyde, which, by a second hemiacetal-aldehyde equilibrium, forms a four-membered ring oxetanose (Hazelard and Compain, 2017), that may be subject to a [2 + 2] retrocycloaddition reaction (Popsavin et al., 2004) (Scheme 14). Taken together, the two pathways differ from each other by the presence or absence of the intermediate oxetanose ring, a motif that creates a straightforward relationship between $^{0,2}A_2$ and $^{0,4}A_2$ cleavages. In sharp contrast to the prevalence of furanose and pyranose sugar derivatives in nature, examples of four-membered ring analogues are only rarely described in the literature (Lee et al., 1994; Pistara et al., 2013).

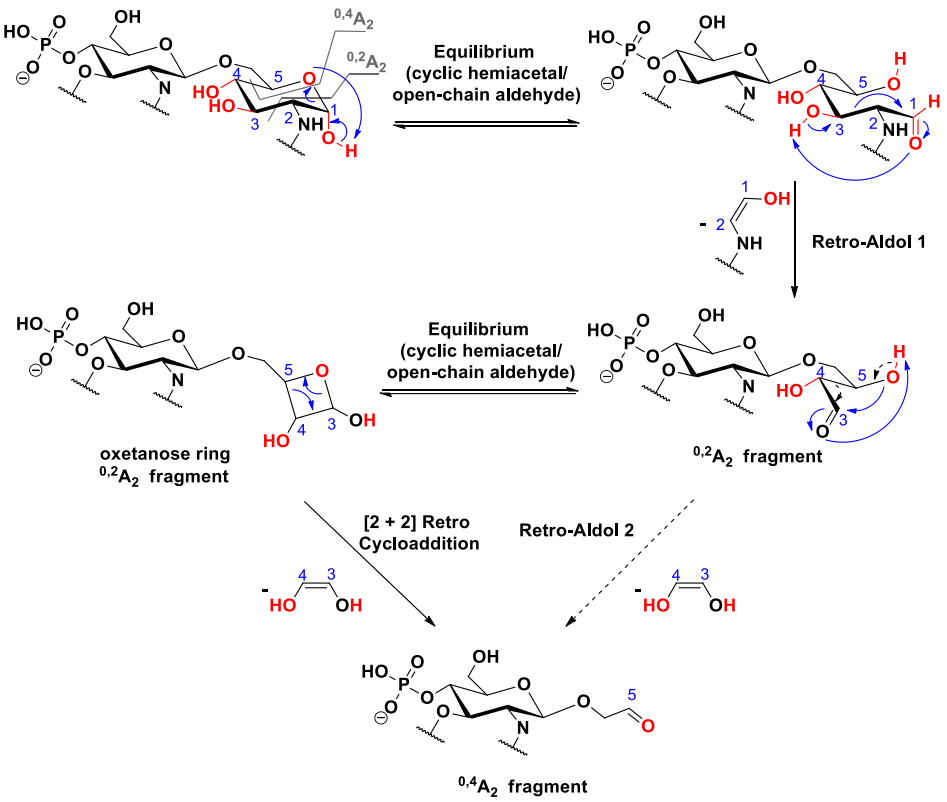

Scheme 14. Suggested mechanisms for the consecutive formation of $^{0,2}A_2$ and $^{0,4}A_2$ fragment ions in 3-deacyl lipid A (Aissa et al., 2021).

By selecting precursors at *m/z* 1488 of PHAD-504 (Fig. 13d) and *m/z* 1516 of PHAD (Fig. 9c) for further MS^n experiments, signals resulting from $^{0,2}A_2$ cross-ring fragmentation (*m/z* 1203 and 917 for PHAD-504 in Fig. 28, and *m/z* 1231 and 945 for PHAD in Fig. A5, respectively) appeared, as well. Again, a relationship between the $^{0,2}A_2$ and $^{0,4}A_2$ ions was observed in the MS^4 spectrum of the selected $^{0,2}A_2$ precursor ion. Because of the presence of an extra chain C14:0(3-OH) at C-3 in the reducing sugar of these molecules, the proposed mechanism of cross-ring cleavages has a different step from the one described above for the 3-deacyl lipid A derivatives. That is, after the first step (*i.e.*, ring-opening of the reducing sugar), an intramolecular transesterification (Prian et al., 2019) takes place between the hydroxyl group at C-4 and the ester chain at C-3,

resulting in a derivative which may be susceptible to a retro-aldol reaction. As a result, it is suggested that the $^{0,4}A_2$ fragment be formed either from a second retro-aldol or a [2 + 2] retro-cycloaddition reaction (Scheme 15).

In addition, a small signal appeared at *m/z* 959 in Figure 28b, resulting from the release of the fatty acyl chain from the oxetanose ring in the $^{0,2}A_2$ fragment. Indeed, the cleavage of this fatty acyl chain (originally linked at C-3 in lipid A) may occur from the $^{0,2}A_2$ fragment, but only with a small probability. Additionally, note that when the C-3 primary fatty acid had been eliminated (*i.e.*, preceding the cross-ring fragmentation), the $^{0,2}A_2$ fragment cannot be formed at all (Kussak and Weintraub, 2002).

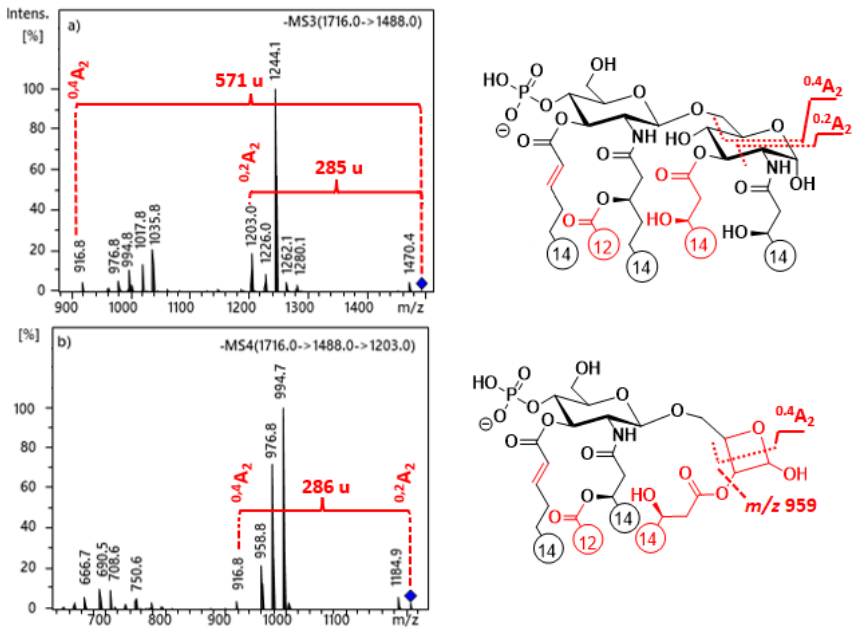

Figure 28. ESI-ion trap mass spectra obtained at MS^3 and MS^4 stages of selected ions at a) *m/z* 1488 and b) *m/z* 1203 for PHAD-504, demonstrating the structural relationship between $^{0,2}A_2$ and $^{0,4}A_2$ cross-ring fragment ions in 3-acyl lipid A (Aissa et al., 2021).

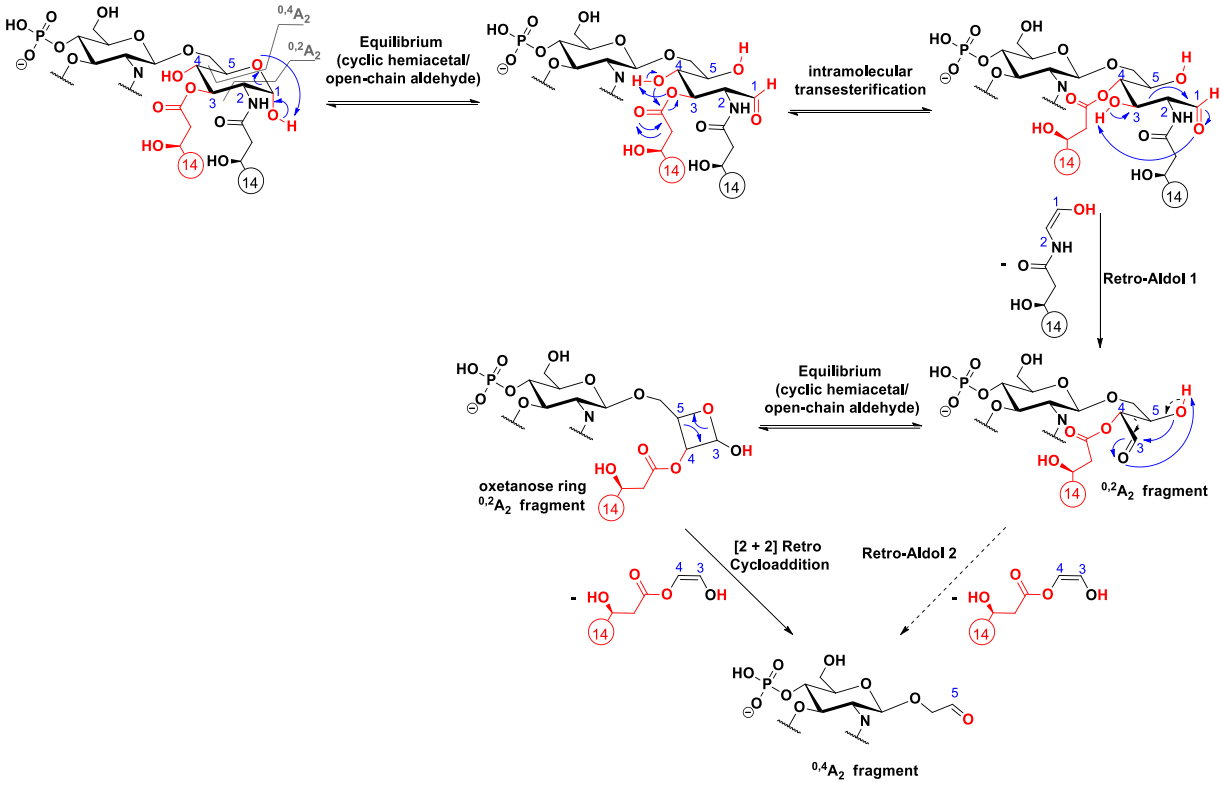

Scheme 15. Suggested mechanisms for the consecutive formation of $^{0,2}A_2$ and $^{0,4}A_2$ fragment ions in 3-acyl lipid A (Aissa et al., 2021).

6.4.6. Mechanisms suggested for dephosphorylation

In Scheme 16, two different routes are proposed for the formation of dihydrogen phosphate ion ($H_2PO_4^-$, *m/z* 97), which was considered based on the fragment seen at *m/z* 796 in Fig. 12. In one, an epoxidation occurs (Implying the antiperiplanar relationships between the formed oxide ion at C-3' and the phosphate group), and this will easily facilitate the removal of H_2PO_4 that will hold the negative charge. In the other, a hydride transfer occurs, causing the formation of the $H_2PO_4^-$ ion.

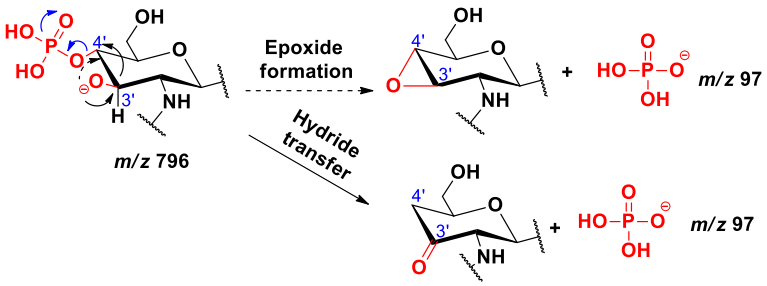

Scheme 16. Suggested mechanisms for the formation of dihydrogen phosphate ion $H_2PO_4^-$ (Aissa et al., 2021).

The formation of monometaphosphate ion (PO_3^-, *m/z* 79) was accounted for based on the fragment at *m/z* 778 in Fig. 12, using two main paths, both based on the cyclic phosphate derivative (Scheme 17), whom the monometaphosphate ion regarded as a good starting group which undergoes a hydride transfer or an epoxide formation. However, the route based on the non-cyclic phosphate derivative (Scheme 18) was ignored, as in that case, the formation of PO_3^- would happen by the removal of a proton from the detached neutral metaphosphoric acid (HPO_3), which would make it possible to detect the intermediate fragmentation product, *i.e.*, the negatively charged lipid A without the C-4' phosphate group; although such an ion without a phosphate group (virtually appearing at *m/z* 698) was not observed in the MS^n mass spectra.

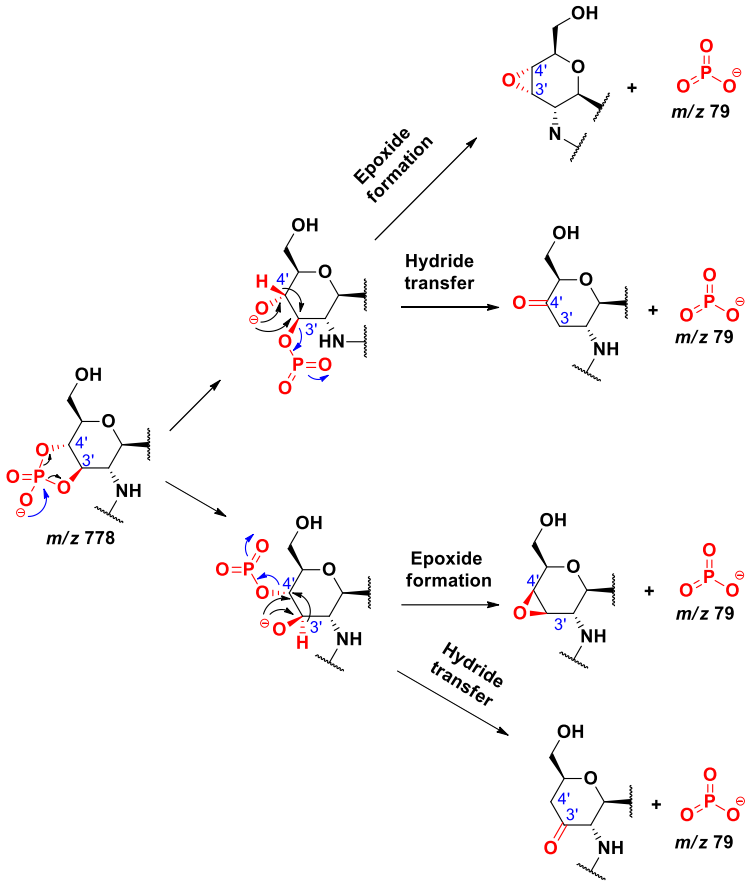

Scheme 17. Suggested alternative routes for the formation of metaphosphate ion, PO_3^-, from the cyclic phosphate lipid A derivative (Aissa et al., 2021).

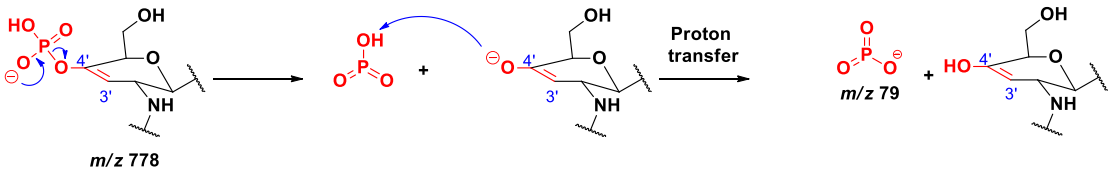

Scheme 18. An unlikely mechanism for the formation of metaphosphate ion, PO_3^-, from the noncyclic phosphate lipid A derivative (Aissa et al., 2021).

6.4.7. Formation of the B1 fragment from protonated and sodium cationized species

During the gas-phase fragmentation of the protonated or sodiated molecules, the glycosidic bond cleavage could be initiated either by a proton or a sodium cation. Traditionally, it has been argued that direct coordination of the metal to the glycosidic

oxygen was a prerequisite for bond cleavage. However, Bythell et al. (Bythell et al., 2017) showed that the cleavage occurred for cationized carbohydrates, as well. In the case of protonated lipid A standards, we proposed either an oxonium derivative can be formed (Scheme 19) or a bicyclic derivative may develop (Scheme 20).

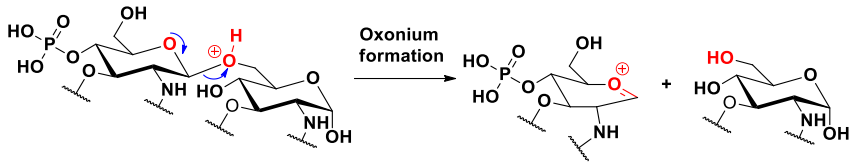

Scheme 19. Suggested mechanism for a B_1 fragment from the $[M+H]^+$ precursor ion, leading to the formation of an oxonium derivative.

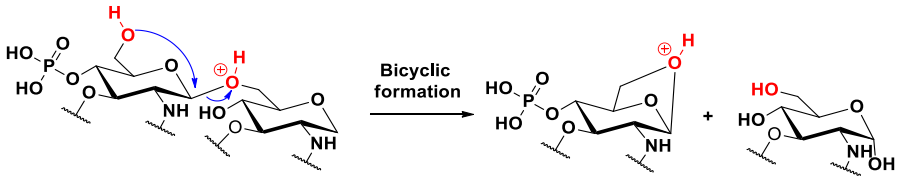

Scheme 20. Suggested mechanism for a B_1 fragment from the $[M+H]^+$ precursor ion, leading to the development of a bicyclic derivative.

In the case of sodiated lipid A, it is proposed that the sodium is located between the two oxygens bonded to the phosphorus atom, but not the glycosidic oxygen. A proton is then mobilized to the glycosidic bond to facilitate its cleavage (Schemes 21 and 22).

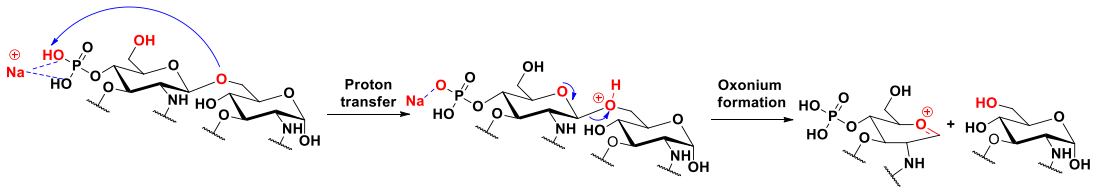

Scheme 21. Suggested mechanism for a B_1 fragment from the $[M+Na]^+$ precursor ion, leading to the formation of an oxonium derivative.

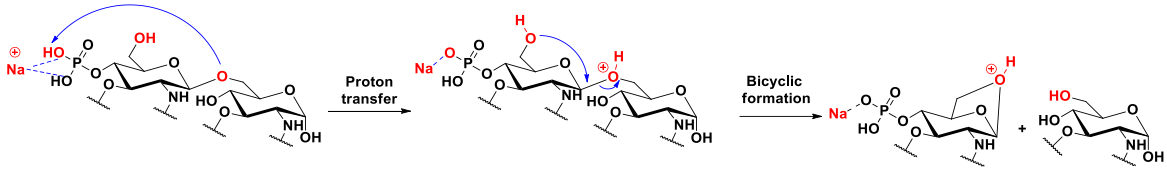

Scheme 22. Suggested mechanism for a B_1 fragment from the $[M+Na]^+$ precursor ion, leading to the development of a bicyclic derivative.

6.4.8. Suggested dehydration pathways

In the case of disodiated 3-deacyl PHAD compounds (Fig. 19), the better leaving ability of the hydroxyl group bound to the carbon atom at C-3 of the reducing sugar residue seems to be favorable to promote dehydration reaction. Mechanistically, three plausible pathways for dehydration process can be proposed considering structural and electronic effects. In the first assumption, the hydroxyl group splits off from C-3 to form a water molecule with the neighboring hydrogen at C-4 (scheme 23). In a different way, the H_2O-elimination could proceed in favor of epoxide formation *via* C–O coupling involving vicinal hydroxyl groups at C-3 and C-4 (scheme 24). Finally, the elimination of H_2O could also take place from the C-3 position, while the oxygen-bridging C-1–O–C-3 leads to an Oxetanose moiety (scheme 25).

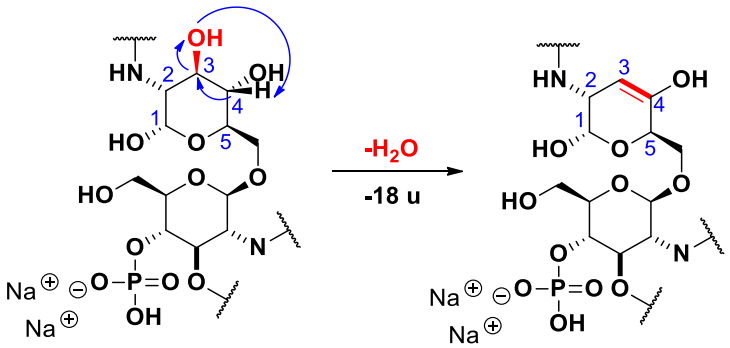

Scheme 23. Possible double bond formation C_3=C_4 *via* dehydration mechanism.

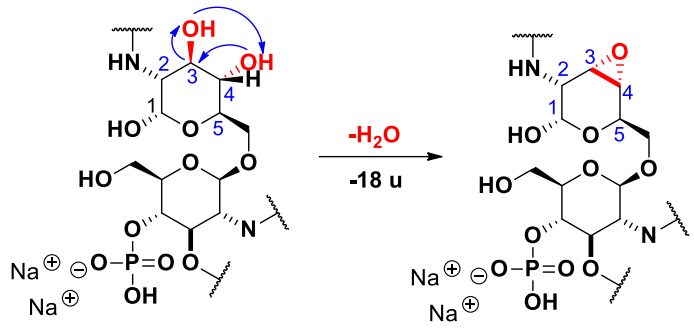

Scheme 24. Suggested dehydration mechanism leading to the formation of an epoxide on the sugar moiety.

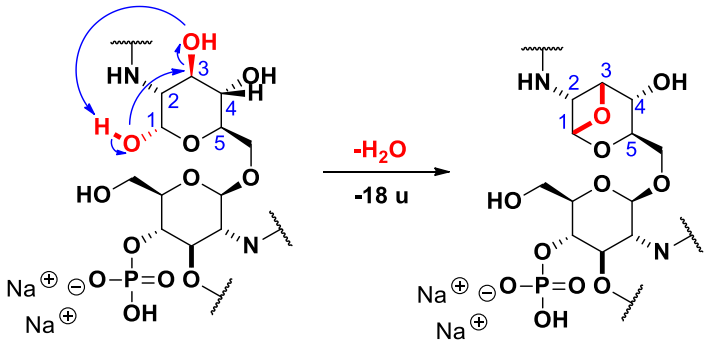

Scheme 25. Proposed dehydration mechanism followed by oxygen-bridge formation on the sugar ring.

6.5. Characterization of isomeric lipid A species in *Pseudomonas aeruginosa* PAO1 by NACE-MS/MS

A recent investigation by LC-MS/MS in the negative ion mode revealed significant structural heterogeneity for the *P. aeruginosa* PAO1 isolate (Buré et al., 2021). In that study, only monophosphorylated compounds were detected, and the acylation degree ranged from tri- to hexaacylation. In addition, structures of isomers were also elucidated, meaning that within each of the tri-, tetra-, and pentaacylated lipid A families, two acyl chain positional isomers were identified, although no isomers were confirmed with hexaacylation.

Information on the structure and unique modification of lipid A is of profound significance for understanding the survival and virulence of pathogens, such as *P. aeruginosa*. However, a remaining complicating factor for lipid A identification in complex mixtures is the recognition of phosphorylation isomers that cannot be identified through direct MS measurements or traditional reversed-phase LC-MS strategies. As phosphorylation positional isomers of lipid A (meaning that the phosphate group is either at C-1 or C-4') are usually chromatographically unresolved, their MS/MS analysis in the negative ion mode will give a chimera mass spectrum. On the other hand, with the recently developed NACE-MS/MS technology, phosphoisomers can be baseline separated, and their structures can be confidently identified by MS/MS applying both negative and positive ESI modes.

Here, a modified NACE-(CID) MS/ MS method for the analysis of lipid A phosphorylation and acylation isomers was applied to reveal the *P. aeruginosa* PAO1 lipid A heterogeneity. Although with a newly developed HPLC-(HCD/ UVPD)MS/MS method (Buré et al., 2021), several previously unreported lipid A acyl chain positional isomers had been explored in the PAO1 strain, this unique orthogonal separation system allowed the recognition of additional lipid A structures, identified as C1-monophosphorylated species.

It must be noted that the direct infusion MS strategy (discussed above) used for the identification of phosphorylation isomers through the sodiated and protonated forms of lipid A could not be applied, because for the coupled MS measurements, such as NACE-MS, further development would be required for the detection of the three positively charged ion types that we have not carried out at yet. Therefore, we used the well-established Et_3N-adduct strategy for the positive mode NACE-ESI-MS/MS.

Briefly, the combined interpretation of CID fragmentation patterns in positive and negative ion modes of the five separated and one co-migrating tetra-acyl lipid A isomers made it possible to assign the structures represented in Fig. 21d. Among them, the two tetra-acylated C-4'P isomers were already discovered in the previous study of Buré et al (Buré et al., 2021)., but the four C-1P compounds have not previously been identified in PAO1. In fact, C-1 monophophorylated lipid A species have not been discovered at all in *P. aeruginosa*.

We must emphasize that to differentiate the structure of various C-1P isomers, first they must be separated by electrophoresis and then analyzed first with positive ion MS/MS and only then with negative ion MS/MS. Without the knowledge previously obtained from the positive mode CID, the acyl chain positional isomers of C-1 phosphorylated lipid A cannot be distinguished according to their CID mass spectra in the negative ion mode. This is especially true for higher acylation degrees of C-1 phosphorylated acyl chain positional isomers.

7. Conclusion

Negative mode ESI MS/MS has generally been preferred for the structural analysis of bacterial lipid A molecules, nevertheless, these approaches are not capable of identifying chimera mass spectra that might arise during a shotgun MS analysis or an LC–MS separation. In our studies, we found that positive mode ESI MS/MS is an even better option owing to its potential to not only locate the acylation sites, but also the phosphate group in monophosphorylated lipid A. The combined evaluation of three positively charged precursor ions, such as $[M + H]^+$, $[M + Na]^+$ and $[M – H + 2Na]^+$, provides complementary structural data, because it increases the diversity of possible cleavage sites using the classical CID technique. Typically, cleavages of the protonated form of lipid A give information on the acyl linkages at the C-2 primary and C-2/C-2′ secondary positions, while cleavages of sodiated lipid A precursors identify fatty acids at the C-3′ secondary and C-3/C-3′ primary positions. In particular, the phosphorylation site (*i.e.*, at C-1 or C-4′) can be assigned from the protonated lipid A, as the B_2 ion formed from the $[M + H]^+$ precursor directly points out the position of the phosphate group. On the other hand, such a distinctive fragment ion is fully absent in the common negative mode MS/MS mass spectrum of deprotonated lipid As.

Altogether, our proposed strategy (Fig. 24), based on the observed fragmentation regularities of positively charged precursor ions, can now be applied for the fast and accurate structural elucidation of 4’-monophosphorylated lipid A present in native, heterogeneous lipid A samples, using only positive ionization mode MS/MS.

Furthermore, it can shed light on chimeric mass spectra, without the need for prior separation of phosphoisomers. However, further studies are required to describe the

cleavage rules related to a 1-monophosphorylated lipid A species, for which synthetic C-1 phosphoryl lipid A standards would be needed.

The MS^n analyses of deprotonated, protonated and some sodiated 4'-monophosphoryl lipid A led to the following proposed dissociation mechanisms in the gas phase:

(i) cleavage of the C-3 primary fatty acid (as an acid) leaves behind an epoxide group attached to the reducing sugar;

(ii) cleavage of the C-3' primary fatty acid (as an acid) generates a cyclic phosphate connected to the nonreducing sugar;

(iii) cleavage of the C-2' secondary fatty acid occurs both in acid and ketene forms;

(iv) the C-2 and C-2' primary fatty acids are eliminated as an amide and ketene, respectively;

(v) the $^{0,2}A_2$ cross-ring fragment contains a four-membered ring (oxetanose);

(vi) the $^{0,4}A_2$ ion is consecutively formed from the $^{0,2}A_2$ ion by retro-aldol, retro-cycloaddition, and transesterification;

(vii) formations of $H_2PO_4^-$ and PO_3^- are associated with the formation of sugar epoxide

(viii) formation of the B_1 ion is associated with the formation of a bicyclic sugar derivative.

Besides a better understanding of fragmentation mechanisms, our findings can also have applications in the interpretation of mass spectra of unknown lipid A compounds detected as $[M - H]^-$ precursors. For instance, the preferential loss of the secondary acyl group at C-3' over that at C-2' provides important information on the structure of a 4'-monophosphoryl lipid A, carrying the same secondary fatty acids at these positions.

Moreover, as the first-generation product ion formed by the liberation of the C-2' secondary acyl chain is not favored in 4-monophosphoryl lipid A (unlike 1-monophosphoryl lipid A); thus, the detection of two first-generation fragments that individually lack the C-2' and C-3' secondary fatty acids, indicates the presence of phosphorylation isomers in the sample. Finally, the detection of peak-pairs with 18 u apart, in combination with relatively high-intensity $^{0,2}A_2$ fragments, indicates the presence of a 3'-acyl, 3-deacyl lipid A compound in the sample. Without applying these "rules", misleading information of some product ions in complex lipid A mixtures may be obtained, and some low abundance, but biologically important isomers can remain unexplored.

For a deeper understanding of subtle chemical variations of lipid A in relation to biological properties, the structural elucidation of lipid A species within a bacterial strain is of crucial importance. By comparing the NACE approach combined with positive and negative ion (CID)MS/MS with a previous HPLC–(UVPD)MS/MS approach developed by other researchers for assessing the lipid A content of *P. aeruginosa* PAO1, we could demonstrate the presence of 1-monophosphoryl components in PAO1 for the first time. Moreover, we could characterize several acyl chain positional isomers of 1-monophosphorylated species owing to the application of both ionization modes (*i.e.*, triethylamine adducts and deprotonated lipid A were fragmented in parallel). In the wider context of the biological significance of lipid A modifications, it is possible that many other Gram-negative bacteria also produce phosphorylation isomers; however, as already mentioned, the C-1 phosphorylated compounds next to the C-4' phosphorylated ones cannot easily be recognized with direct MS measurements or with conventional LC–MS strategies.

This suggests that important details concerning the lipid A isomeric composition of known Gram-negative pathogens need to be re-examined, for which the NACE–(CID) MS/MS approach can be a useful tool in the future.

8. Thesis points

1. We conclude that the combined analysis with low-energy CID of the $[M + H]^+$, $[M + Na]^+$ and $[M – H + 2Na]^+$ precursor ions allow for the full structural characterization of 4’-monophosphorylated lipid A compounds in natural mixtures of bacterial lipid A. Our approach is capable to distinguishing phosphorylation isomers and identifying chimera mass spectra.

2. There is a high degree of similarity between the fragmentation pattern of lipid A as a disodium adduct and as a deprotonated molecule; meanwhile, the fragmentation pattern of monosodiated lipid A shows similarity with the protonated and deprotonated molecule, as well.

3. New alternative mechanisms explaining the gas-phase dissociation routes of deprotonated, protonated and sodiated 4'-monophosphoryl lipid A species have been suggested, regarding the release of the different ester- or amide-linked fatty acyl chains and the phosphate group, as well as ring cleavages. By applying low-energy CID conditions, mainly charge-induced processes were considered.

4. The NACE method coupled with positive and negative ion (CID)MS/MS revealed hitherto unknown C-1 phosphate positional isomeric compounds among three acylation families (tetra-, penta-, and hexa-acylated species), and thus, it expanded the structural information obtained by chromatographic characterization of the lipid A composition of *Pseudomonas aeruginosa* PAO1 bacterium. Therefore, the NACE–MS/MS strategy using CID fragmentation in the complementary positive and negative ion modes can replace commonly used HPLC–MS/MS approaches for monitoring bacterial lipid A compositions.

9. References

Aissa, I., Dornyei, A., Sandor, V. and Kilar, A., 2022. Complete structural elucidation of monophosphorylated lipid A by CID fragmentation of protonated molecule and singly charged sodiated adducts. *Journal of the American Society for Mass Spectrometry*. 34, 92 - 100. https://doi.org/10.1021/jasms.2c00269

Aissa, I., Kilár, A. and Dörnyei, A., 2021. Study on the CID Fragmentation Pathways of Deprotonated 4'-Monophosphoryl Lipid A. *Molecules*. 26, 5961. https://doi.org/10.3390/molecules26195961

Alexander, C. and Rietschel, E.T., 2001. Bacterial lipopolysaccharides and innate immunity. Journal of Endotoxin Research. 7, 167-202. https://doi.org/10.1179/096805101101532675

Arenas, J., 2012. The Role of bacterial lipopolysaccharides as immune modulator in vaccine and drug developement. *Endocrine, Metabolic & Immune Disorders - Drug Targets*. 12, 221-235.

Aussel, L., Brisson, J.R., Perry, M.B. and Caroff, M., 2000. Structure of the lipid A of *Bordetella hinzii* ATCC 51730. *Rapid Communications in Mass Spectrometry*. 14, 595-599. https://doi.org/10.1002/(sici)1097-0231(20000415)14:7<595::aid-rcm919>3.0.co;2-4

Backhed, F., Normark, S., Schweda, E.K.H., Oscarson, S. and Richter-Dahlfors, A., 2003. Structural requirements for TLR4-mediated LPS signalling: A biological role for LPS modifications. Microbes and Infection. 5, 1057-1063. https://doi.org/10.1016/s1286-4579(03)00207-7

Baldridge, J.R., McGowan, P., Evans, J.T., Cluff, C., Mossman, S., Johnson, D. and Persing, D., 2004. Taking a Toll on human disease: Toll-like receptor 4 agonists as vaccine adjuvants and monotherapeutic agents. Expert Opinion on Biological Therapy. 4, 1129-1138. https://doi.org/10.1517/14712598.4.7.1129

Basheer, S.M., Guiso, N., Tirsoaga, A., Caroff, M. and Novikov, A., 2011. Structural modifications occurring in lipid A of B*ordetella bronchiseptica* clinical isolates as demonstrated by matrix-assisted laser desorption/ionization time-of-flight mass spectrometry. Rapid Communications in Mass Spectrometry. 25, 1075-1081. https://doi.org/10.1002/rcm.4960

Beasley, A.S., Cotter, R.J., Vogel, S.N., Inzana, T.J., Qureshi, A.A. and Qureshi, N., 2012. A variety of novel lipid A structures obtained from *Francisella tularensis* live vaccine strain. Innate Immunity. 18, 268-278. https://doi.org/10.1177/1753425911401054

Beutler, B. and Rietschel, E.T., 2003. Innate immune sensing and its roots: the story of endotoxin. *Nature Reviews Immunology*. 3, 169-176. https://doi.org/10.1038/nri1004

Bobbala, S., McDowell, A. and Hook, S., 2015. Quantitation of the immunological adjuvants, monophosphoryl lipid A and Quil A in poly (lactic-co-glycolic acid) nanoparticles using high performance liquid chromatography with evaporative light scattering detection. Journal of Chromatography B-Analytical Technologies in the Biomedical and Life Sciences. 975, 45-51. https://doi.org/10.1016/j.jchromb.2014.11.006

Boue, S.M. and Cole, R.B., 2000. Confirmation of the structure of lipid A from *Enterobacter agglomerans* by electrospray ionization tandem mass spectrometry. *Journal of Mass Spectrometry*. 35, 361-368. https://doi.org/10.1002/(sici)1096-9888(200003)35:3<361::aid-jms943>3.0.co;2-d

Buré, C., Le Senechal, C., Macias, L., Tokarski, C., Vilain, S. and Brodbelt, J.S., 2021. Characterization of isomers of lipid A from *Pseudomonas aeruginosa* PAO1 by liquid chromatography with tandem mass spectrometry with higher-energy collisional dissociation and ultraviolet photodissociation. Analytical Chemistry. 93, 4255-4262. https://doi.org/10.1021/acs.analchem.0c05069

Bythell, B.J., Abutokaikah, M.T., Wagoner, A.R., Guan, S.S. and Rabus, J.M., 2017. Cationized carbohydrate gas-phase fragmentation chemistry. Journal of the American Society for Mass Spectrometry. 28, 688-703. https://doi.org/10.1007/s13361-016-1530-x

Caroff, M. and Karibian, D., 2003. Structure of bacterial lipopolysaccharides. Carbohydrate Research. 338, 2431-2447. https://doi.org/10.1016/j.carres.2003.07.010

Caroff, M. and Novikov, A., 2020. Lipopolysaccharides: Structure, function and bacterial identification. *OCL: Oilseeds Fats, Crops Lipids*. 27, https://doi.org/10.1051/ocl/2020025

Casella, C.R. and Mitchell, T.C., 2008. Putting Endotoxin to work for us: Monophosphoryl lipid A as a safe and effective vaccine adjuvant. Cellular and Molecular Life Sciences. 65, 3231-3240. https://doi.org/10.1007/s00018-008-8228-6

Cavaillon, J.M., 2018. Exotoxins and endotoxins: Inducers of inflammatory cytokines. Toxicon. 149, 45-53. https://doi.org/10.1016/j.toxicon.2017.10.016

Chan, S. and Reinhold, V.N., 1994. Detailed structural characterization of lipid-A - electrospray-ionization coupled with tandem mass-spectrometry. Analytical Biochemistry. 218, 63-73. https://doi.org/10.1006/abio.1994.1141

Chiu, C.C., Huynh, H.T., Tsai, S.T., Lin, H.Y., Hsu, P.J., Phan, H.T., Karumanthra, A., Thompson, H., Lee, Y.C., Kuo, J.L. and Ni, C.K., 2019. Toward closing the gap between hexoses and N-acetlyhexosamines: Experimental and computational studies on the collision-induced dissociation of hexosamines. Journal of Physical Chemistry A. 123, 6683-6700. https://doi.org/10.1021/acs.jpca.9b04143

Coats, S.R., Berezow, A.B., To, T.T., Jain, S., Bainbridge, B.W., Banani, K.P. and Darveau, R.P., 2011. The lipid A phosphate position determines differential host toll-like receptor 4 responses to phylogenetically related symbiotic and pathogenic bacteria. *Infection and Immunity*. 79, 203-210. https://doi.org/10.1128/iai.00937-10

Coats, S.R., Jones, J.W., Do, C.T., Braham, P.H., Bainbridge, B.W., To, T.T., Goodlett, D.R., Ernst, R.K. and Darveau, R.P., 2009. Human Toll-like receptor 4 responses to P-gingivalis are regulated by lipid A 1-and 4'-phosphatase activities. *Cellular Microbiology*. 11, 1587-1599. https://doi.org/10.1111/j.1462-5822.2009.01349.x

Coler, R.N., Bertholet, S., Moutaftsi, M., Guderian, J.A., Windish, H.P., Baldwin, S.L., Laughlin, E.M., Duthie, M.S., Fox, C.B., Carter, D., Friede, M., Vedvick, T.S. and Reed, S.G., 2011. Development and characterization of synthetic glucopyranosyl lipid adjuvant system as a vaccine adjuvant. Plos One. 6, https://doi.org/10.1371/journal.pone.0016333

Domon, B. and Costello, C.E., 1988. A systematic nomenclature for carbohydrate fragmentations in FAB-MS/MS spectra of glycoconjugates. *glycoconjugate journal*. 5, 397-409. https://doi.org/10.1007/bf01049915

El-Aneed, A. and Banoub, J., 2005. Elucidation of the molecular structure of lipid A isolated from both a rough mutant and a wild strain of *Aeromonas Salmonicida* lipopolysaccharides using electrospray ionization quadrupole time-of-flight tandem mass spectrometry. *Rapid Communications in Mass Spectrometry*. 19, 1683-1695. https://doi.org/10.1002/rcm.1971

Ernst, R.K., Hajjar, A.M., Tsai, J.H., Moskowitz, S.M., Wilson, C.B. and Miller, S.I., 2003. Pseudomonas aeruginosa lipid A diversity and its recognition by Toll-like receptor 4. Journal of Endotoxin Research. 9, 395-400. https://doi.org/10.1179/096805103225002764

Ernst, R.K., Yi, E.C., Guo, L., Lim, K.B., Burns, J.L., Hackett, M. and Miller, S.I., 1999. Specific lipopolysaccharide found in cystic fibrosis airway *Pseudomonas aeruginosa*. Science. 286, 1561-1565. https://doi.org/10.1126/science.286.5444.1561

Fox, C.B., Carter, D., Kramer, R.M., Beckmann, A.M. and Reed, S.G., 2017. Current status of Toll-Like Receptor 4 ligand vaccine adjuvants. Immunopotentiators in Modern Vaccines, 2nd Edition. 105-127. https://doi.org/10.1016/b978-0-12-804019-5.00006-2

Fox, C.B., Friede, M., Reed, S.G. and Ireton, G.C., 2010. Synthetic and natural TLR4 agonists as safe and effective vaccine adjuvants. Endotoxins: Structure, Function and Recognition. Dordrecht, Springer Netherlands: 303-321.

Galanos, C. and Delves, P.J., 1998. Endotoxin (Lipopolysaccharide (LPS)). Encyclopedia of Immunology (Second Edition). Oxford, Elsevier: 806-809.

Galanos, C., Luderitz, O., Rietschel, E.T., Westphal, O., Brade, H., Brade, L., Freudenberg, M., Schade, U., Imoto, M., Yoshimura, H., Kusumoto, S. and Shiba, T., 1985. Synthetic and natural *Escherichia-coli* free lipid-A express identical endotoxic activities. *European Journal of Biochemistry*. 148, 1-5. https://doi.org/10.1111/j.1432-1033.1985.tb08798.x

Gehring, U., Wijga, A.H., Koppelman, G.H., Vonk, J.M., Smit, H.A. and Brunekreef, B., 2020. House dust endotoxin, asthma and allergic sensitization through childhood into adolescence. *Clinical and Experimental Allergy*. 50, 1055-1064. https://doi.org/10.1111/cea.13705

Hagen, S.R., Thompson, J.D., Snyder, D.S. and Myers, K.R., 1997. Analysis of a monophosphoryl lipid A immunostimulant preparation from *Salmonella minnesota* R595 by high-performance liquid chromatography. Journal of Chromatography A. 767, 53-61. https://doi.org/10.1016/s0021-9673(97)00041-1

Hamdy, S., Haddadi, A., Somayaji, V., Ruan, D. and Samuel, J., 2007. Pharmaceutical analysis of synthetic lipid A-based vaccine adjuvants in poly (D,L-lactic-co-glycolic acid) nanoparticle formulations. Journal of Pharmaceutical and Biomedical Analysis. 44, 914-923. https://doi.org/10.1016/j.jpba.2007.03.010

Hankins, J.V., Madsen, J.A., Giles, D.K., Brodbelt, J.S. and Trent, M.S., 2012. Amino acid addition to Vibrio cholerae LPS establishes a link between surface remodeling in Gram-positive and Gram-negative bacteria. Proceedings of the National Academy of Sciences of the United States of America. 109, 8722-8727. https://doi.org/10.1073/pnas.1201313109

Harrata, A.K., Domelsmith, L.N. and Cole, R.B., 1993. Electrospray mass-spectrometry for characterization of lipid-A from *Enterobacter-agglomerans*. *Biological Mass Spectrometry*. 22, 59-67. https://doi.org/10.1002/bms.1200220108

Hazelard, D. and Compain, P., 2017. Square sugars: Challenges and synthetic strategies. Organic & Biomolecular Chemistry. 15, 3806-3827. https://doi.org/10.1039/c7ob00386b

Henderson, J.C., O'Brien, J.P., Brodbelt, J.S. and Trent, M.S., 2013. Isolation and chemical characterization of lipid A from Gram-negative bacteria. *Journal of Visualized Experiments*. https://doi.org/10.3791/50623

Hitchcock, P.J. and Brown, T.M., 1983. Morphological heterogeneity among *salmonella* lipopolysaccharide chemotypes in silver-stained polyacrylamide gels. *Journal of Bacteriology*. 154, 269-277. https://doi.org/10.1128/jb.154.1.269-277.1983

Hopkins, M., Lees, B., Richardson, D.G., Woroniecki, S.R. and Wheeler, A.W., 2001. Standardisation of glutaraldehyde-modified tyrosine-adsorbed tree pollen vaccines containing the Th1-inducing adjuvant, monophosphoryl lipid A (MPL). Allergol Immunopathol. 29: 245-254.

Hsu, F.F. and Turk, J., 2000. Charge-remote and charge-driven fragmentation processes in diacyl glycerophosphoethanolamine upon low-energy collisional activation: A mechanistic proposal. *Journal of the American Society for Mass Spectrometry*. 11, 892-899. https://doi.org/10.1016/s1044-0305(00)00159-8

Jones, J.W., Cohen, I.E., Turecek, F., Goodlett, D.R. and Ernst, R.K., 2010. Comprehensive structure characterization of lipid A extracted from *Yersinia Pestis* for determination of its Phosphorylation configuration. *Journal of the American Society for Mass Spectrometry*. 21, 785-799. https://doi.org/10.1016/j.jasms.2010.01.008

Kabanov, D.S. and Prokhorenko, I.R., 2010. Structural analysis of lipopolysaccharides from Gram-negative bacteria. Biochemistry-Moscow. 75, 383-404. https://doi.org/10.1134/s0006297910040012

Karibian, D., Brunelle, A., Aussel, L. and Caroff, M., 1999. Cf-252-plasma desorption mass spectrometry of unmodified lipid A: Fragmentation patterns and localization of fatty acids. Rapid Communications in Mass Spectrometry. 13, 2252-2259. https://doi.org/10.1002/(sici)1097-0231(19991130)13:22<2252::aid-rcm783>3.0.co;2-g

Kilár, A., Dörnyei, Á. and Kocsis, B., 2013. Structural characterization of bacterial lipopolysaccharides with mass spectrometry and on- and off-line separation techniques. *Mass Spectrometry Reviews*. 32, 90-117. https://doi.org/10.1002/mas.21352

Kilár, A., Dörnyei, Á., Sándor, V., Kilár, F. and Kocsis, B., 2018. Phosphoglycolipid profiling of bacterial endotoxins. *Hungarian Journal of Industry and Chemistry*. 46, 7-11. https://doi.org/10.1515/hjic-2018-0003

King, J.D., Kocincova, D., Westman, E.L. and Lam, J.S., 2009. Lipopolysaccharide biosynthesis in Pseudomonas aeruginosa. Innate Immunity. 15, 261-312. https://doi.org/10.1177/1753425909106436

Kondakov, A. and Lindner, B., 2005. Structural characterization of complex bacterial glycolipids by Fourier transform mass spectrometry. European Journal of Mass Spectrometry. 11, 535-546. https://doi.org/10.1255/ejms.721

Kumada, H., Haishima, Y., Umemoto, T. and Tanamoto, K.I., 1995. Structural study on the free lipid-A isolated from lipopolysaccharide of *Porphyromonas gingivalis*. *Journal of Bacteriology*. 177, 2098-2106. https://doi.org/10.1128/jb.177.8.2098-2106.1995

Kussak, A. and Weintraub, A., 2002. Quadrupole ion-trap mass spectrometry to locate fatty acids on lipid A from Gram-Negative bacteria. *Analytical Biochemistry*. 307, 131-137. https://doi.org/10.1016/s0003-2697(02)00004-0

Lee, C.S., Kim, Y.G., Joo, H.S. and Kim, B.G., 2004. Structural analysis of lipid A from *Escherichia coli* O157:H7:K- using thin-layer chromatography and ion-trap mass spectrometry. Journal of Mass Spectrometry. 39, 514-525.

Lee, J.W., Lewin, N.E., Blumberg, P.M. and Marquez, V.E., 1994. Conformationally constrained analogs of diacylglycerol .9. The effect of side-chain orientation on the protein-kinase-c (Pk-c) binding-affinity of delta-lactones. *Bioorganic & Medicinal Chemistry Letters*. 4, 2405-2410. https://doi.org/10.1016/s0960-894x(01)80399-1

Luderitz, O., Freudenberg, M.A., Galanos, C., Lehmann, V., Rietschel, E.T. and Shaw, D.H., 1982. Lipopolysaccharides of Gram-Negative bacteria. Current Topics in Membranes and Transport. 17, 79-151.

Lukasiewicz, J., Dzieciatkowska, M., Niedziela, T., Jachymek, W., Augustyniuk, A., Kenne, L. and Lugowski, C., 2006. Complete lipopolysaccharide of *Plesiomonas shigelloides* O74 : H5 (strain CNCTC 144/92). 2. Lipid A, its structural variability, the linkage to the core oligosaccharide, and the biological activity of the lipopolysaccharide. Biochemistry. 45, 10434-10447. https://doi.org/10.1021/bi060774d

Madala, N.E., Leone, M.R., Molinaro, A. and Dubery, I.A., 2011. Deciphering the structural and biological properties of the lipid A moiety of lipopolysaccharides from *Burkholderia cepacia* strain ASP B 2D, in *Arabidopsis thaliana*. Glycobiology. 21, 184-194. https://doi.org/10.1093/glycob/cwq146

Madalinski, G., Fournier, F., Wind, F.L., Afonso, C. and Tabet, J.C., 2006. Gram-negative bacterial lipid A analysis by negative electrospray ion trap mass spectrometry: Stepwise dissociations of deprotonated dpecies under low energy CID conditions. *International Journal of Mass Spectrometry*. 249, 77-92. https://doi.org/10.1016/j.ijms.2005.12.049

Madsen, J.A., Cullen, T.W., Trent, M.S. and Brodbelt, J.S., 2011. IR and UV photodissociation as analytical tools for characterizing lipid A structures. *Analytical Chemistry*. 83, 5107-5113. https://doi.org/10.1021/ac103271w

Mayer, H., Bhat, U.R., Masoud, H., Radziejewskalebrecht, J., Widemann, C. and Krauss, J.H., 1989. Bacterial lipopolysaccharides. Pure and Applied Chemistry. 61, 1271-1282. https://doi.org/10.1351/pac198961071271

Mbongue, J.C., Vanterpool, E., Firek, A. and Langridge, W.H.R., 2022. Lipopolysaccharide-Induced Immunological Tolerance in Monocyte-Derived Dendritic Cells. *Immunology*. 2, https://doi.org/10.3390/immuno2030030

Moradali, M.F., Ghods, S. and Rehm, B.H.A., 2017. *Pseudomonas aeruginosa* lifestyle: A paradigm for adaptation, survival, and persistence. *Frontiers in Cellular and Infection Microbiology*. 7, 39. https://doi.org/10.3389/fcimb.2017.00039

Moran, A.P., Zahringer, U., Seydel, U., Scholz, D., Stutz, P. and Rietschel, E.T., 1991. Structural-analysis of the lipid-a component of campylobacter-jejuni ccug 10936 (serotype o-2) lipopolysaccharide - description of a lipid-A containing a hybrid backbone of 2-amino-2-deoxy-d-glucose and 2,3-diamino-2,3-dideoxy-d-glucose. European Journal of Biochemistry. 198, 459-469. https://doi.org/10.1111/j.1432-1033.1991.tb16036.x

Neidhart, J., Allen, K.O., Barlow, D.L., Carpenter, M., Shaw, D.R., Triozzi, P.L. and Conry, R.M., 2004. Immunization of colorectal cancer patients with recombinant baculovirus-derived KSA (Fp-CAM) formulated with monophosphoryl lipid A in liposomal emulsion, with and without granulocyte-macrophage colony-stimulating factor. Vaccine. 22, 773-780. https://doi.org/10.1016/j.vaccine.2003.08.021

Nichols, F.C., Bajrami, B., Clark, R.B., Housley, W. and Yao, X.D., 2012. Free lipid A isolated from *Porphyromonas gingivalis* lipopolysaccharide is contaminated with phosphorylated dihydroceramide lipids: Recovery in diseased dental samples. *Infection and Immunity*. 80, 860-874. https://doi.org/10.1128/iai.06180-11

Novem, V., Shui, G.H., Wang, D.L., Bendt, A.K., Sim, S.H., Liu, Y.C., Thong, T.W., Sivalingam, S.P., Ooi, E.E., Wenk, M.R. and Tan, G., 2009. Structural and biological diversity of lipopolysaccharides from *Burkholderia pseudomallei* and *Burkholderia thailandensis*. Clinical and Vaccine Immunology. 16, 1420-1428. https://doi.org/10.1128/cvi.00472-08

O'Brien, J.P., Needham, B.D., Henderson, J.C., Nowicki, E.M., Trent, M.S. and Brodbelt, J.S., 2014. 193 nm ultraviolet photodissociation mass spectrometry for the structural elucidation of lipid A compounds in complex mixtures. Analytical Chemistry. 86, 2138-2145. https://doi.org/10.1021/ac403796n

Park, B.S., Song, D.H., Kim, H.M., Choi, B.S., Lee, H. and Lee, J.O., 2009. The structural basis of lipopolysaccharide recognition by the TLR4-MD-2 complex. Nature. 458, 1191-U1130. https://doi.org/10.1038/nature07830

Peri, F. and Calabrese, V., 2014. Toll-like Receptor 4 (TLR4) modulation by synthetic and natural compounds: An update. Journal of Medicinal Chemistry. 57, 3612-3622. https://doi.org/10.1021/jm401006s

Phillips, N.J., Adin, D.M., Stabb, E.V., McFall-Ngai, M.J., Apicella, M.A. and Gibson, B.W., 2011. The Lipid A from vibrio fischeri lipopolysaccharide A unique structure bearing a phosphoglycerol moiety. *Journal of Biological Chemistry*. 286, 21203-21219. https://doi.org/10.1074/jbc.M111.239475

Phillips, N.J., Schilling, B., McLendon, M.K., Apicella, M.A. and Gibson, B.W., 2004. Novel modification of lipid A of *Francisella tularensis*. *Infection and Immunity*. 72, 5340-5348. https://doi.org/10.1128/iai.72.9.5340-5348.2004

Pistara, V., Corsaro, A., Rescifina, A., Catelani, G., D'Andrea, F. and Guazzelli, L., 2013. Prevalence of oxetanose forms in the tautomeric equilibrium of beta-hydroxy-1,5-dicarbonyl monosaccharides. Journal of Organic Chemistry. 78, 9444-9449. https://doi.org/10.1021/jo400953s

Popsavin, V., Radic, L., Popsavin, M. and Cirin-Novta, V., 2004. Unexpected cycloreversion of a tosylated tugar oxetane under E2 conditions. The facile formation of 2-(2-furanyl)-1,3-dioxolane from a novel 2,5 : 4,6-dianhydro-L-idose derivative. *Journal of the Serbian Chemical Society*. 69, 117-122. https://doi.org/10.2298/jsc0402117p

Post, D.M.B., Phillips, N.J., Shao, J.Q., Entz, D.D., Gibson, B.W. and Apicella, M.A., 2002. Intracellular survival of Neisseria gonorrhoeae in male urethral epithelial cells: Importance of a hexaacyl lipid A. Infection and Immunity. 70, 909-920. https://doi.org/10.1128/iai.70.2.909-920.2002

Potron, A., Poirel, L. and Nordmann, P., 2015. Emerging broad-spectrum resistance in *Pseudomonas aeruginosa* and *Acinetobacter baumannii*: Mechanisms and epidemiology. *International Journal of Antimicrobial Agents*. 45, 568-585. https://doi.org/10.1016/j.ijantimicag.2015.03.001

Prian, K., Aloui, I., Legros, V. and Buchmann, W., 2019. Study of the gas-phase decomposition of multiply lithiated polycaprolactone, polytetrahydrofurane and their copolymer by two different activation methods: Collision-Induced Dissociation and Electron Transfer Dissociation. *Analytica Chimica Acta*. 1048, 85-95. https://doi.org/10.1016/j.aca.2018.10.003

Pupo, E., Lindner, B., Brade, H. and Schromm, A.B., 2013. Intact rough- and smooth-form lipopolysaccharides from *Escherichia coli* separated by preparative gel electrophoresis exhibit differential biologic activity in human macrophages. Febs Journal. 280, 1095-1111. https://doi.org/10.1111/febs.12104

Qureshi, N., Honovich, J.P., Hara, H., Cotter, R.J. and Takayama, K., 1988. Location of fatty-acids in lipid-A obtained from lipopolysaccharide of *Rhodopseudomonas sphaeroides* ATCC-17023. Journal of Biological Chemistry. 263, 5502-5504.

Qureshi, N., Mascagni, P., Ribi, E. and Takayama, K., 1985. Monophosphoryl lipid-A obtained from lipopolysaccharides of *Salmonella minnesota* r595 - purification of the dimethyl derivative by high-performance liquid-chromatography and complete structural determination. Journal of Biological Chemistry. 260, 5271-5278.

Qureshi, N., Takayama, K., Heller, D. and Fenselau, C., 1983. position of ester groups in the lipid-A backbone of lipopolysaccharides obtained from *Salmonella typhimurium*. *Journal of Biological Chemistry*. 258, 2947-2951.

Rego, A., Viana, S.D., Ribeiro, C.A.F., Rodrigues-Santos, P. and Pereira, F.C., 2016. Monophosphoryl lipid-A: A promising tool for alzheimer's disease toll. Journal of Alzheimers Disease. 52, 1189-1202. https://doi.org/10.3233/jad-151183

Ribi, E., Cantrell, J.L., Takayama, K., Qureshi, N., Peterson, J. and Ribi, H.O., 1984. lipid-A and immunotherapy. Reviews of Infectious Diseases. 6, 567-572.

Rietschel, E.T. and Brade, H., 1992. Bacterial-Endotoxins. *scientific american*. 267, 54-61. https://doi.org/10.1038/scientificamerican0892-54

Rietschel, E.T., Brade, H., Holst, O., Brade, L., MullerLoennies, S., Mamat, U., Zähringer, U., Beckmann, F., Seydel, U., Brandenburg, K., Ulmer, A.J., Mattern, T., Heine, H., Schletter, J., Loppnow, H., Schonbeck, U., Flad, H.D., Hauschildt, S., Schade, U.F., DiPadova, F., Kusumoto, S. and Schumann, R.R., 1996. Bacterial endotoxin: Chemical constitution, biological recognition, host response, and immunological detoxification. Pathology of Septic Shock. 216: 39-81.

Rietschel, E.T., Kirikae, T., Schade, F.U., Mamat, U., Schmidt, G., Loppnow, H., Ulmer, A.J., Zahringer, U., Seydel, U., Dipadova, F., Schreier, M. and Brade, H., 1994. Bacterial Endotoxin - Molecular relationships of structure to activity and function. *Faseb Journal*. 8, 217-225. https://doi.org/10.1096/fasebj.8.2.8119492

Sándor, V., Berkics, B.V., Kilár, A., Kocsis, B., Kilár, F. and Dörnyei, A., 2020. NACE-ESI-MS/MS method for separation and characterization of phosphorylation and acylation isomers of lipid A. *Electrophoresis*. 41, 1178-1188. https://doi.org/10.1002/elps.201900251

Sándor, V., Dörnyei, Á., Makszin, L., Kilár, F., Péterfi, Z., Kocsis, B. and Kilár, A., 2016. Characterization of complex, heterogeneous lipid A samples using HPLC-MS/MS technique I. Overall analysis with respect to acylation, phosphorylation and isobaric distribution. *Journal of Mass Spectrometry*. 51, 1043-1063. https://doi.org/10.1002/jms.3839

Sándor, V., Kilár, A., Kilár, F., Kocsis, B. and Dörnyei, Á., 2016. Characterization of complex, heterogeneous lipid A samples using HPLC-MS/MS technique II. Structural elucidation of non-phosphorylated lipid A by negative-ion mode tandem mass spectrometry. *Journal of Mass Spectrometry*. 51, 615-628. https://doi.org/10.1002/jms.3786

Sándor, V., Kilár, A., Kilár, F., Kocsis, B. and Dörnyei, Á., 2018. Characterization of complex, heterogeneous lipid A samples using HPLC-MS/MS technique III. Positive-ion mode tandem mass spectrometry to reveal phosphorylation and acylation patterns of lipid A. *Journal of Mass Spectrometry*. 53, 146-161. https://doi.org/10.1002/jms.4046

Sándor, V., Űrmös, B., Aissa, I., Dörnyei, Á. and Kilár, A., 2023. Characterization of isomeric lipid A species from P*seudomonas aeruginosa* PAO1 by non-aqueous capillary electrophoresis with positive and negative ion electrospray tandem mass spectrometry. Arabian Journal of Chemistry. 16, 104944. https://doi.org/10.1016/j.arabjc.2023.104944

Schilling, B., McLendon, M.K., Phillips, N.J., Apicella, M.A. and Gibson, B.W., 2007. Characterization of lipid A acylation patterns in *Francisella Tularensis*, *Francisella Novicida*, and *Francisella Philomiragia* using multiple-stage mass spectrometry and matrix-assisted laser desorption/ionization on an intermediate vacuum source linear ion trap. *Analytical Chemistry*. 79, 1034-1042. https://doi.org/10.1021/ac061654e

Silipo, A., De Castro, C., Lanzetta, R., Molinaro, A., Parrilli, M., Vago, G., Sturiale, L., Messina, A. and Garozzo, D., 2008. Structural characterizations of lipids A by MS/MS of doubly charged ions on a hybrid linear ion trap/orbitrap mass spectrometer. Journal of Mass Spectrometry. 43, 478-484. https://doi.org/10.1002/jms.1333

Smit, J., Kaltoshov, I.A., Cotter, R.J., Vinogradov, E., Perry, M.B., Haider, H. and Qureshi, N., 2008. Structure of a novel lipid A obtained from the lipopolysaccharide of *Caulobacter crescentus*. Innate Immunity. 14, 25-37. https://doi.org/10.1177/1753425907087588

Spengler, B., Dolce, J.W. and Cotter, R.J., 1990. lInfrared-Laser desorption mass-spectrometry of oligosaccharides - Fragmentation mechanisms and isomer analysis. *Analytical Chemistry*. 62, 1731-1737. https://doi.org/10.1021/ac00216a004

Tagliabue, A. and Rappuoli, R., 2008. Vaccine adjuvants - The dream becomes real. Human Vaccines. 4, 347-349. https://doi.org/10.4161/hv.4.5.6438

Therisod, H., Labas, V. and Caroff, M., 2001. Direct microextraction and analysis of rough-type lipopolysaccharides by combined thin-layer chromatography and MALDI mass spectrometry. Analytical Chemistry. 73, 3804-3807. https://doi.org/10.1021/ac010313s

Trent, M.S., Stead, C.M., Tran, A.X. and Hankins, J.V., 2006. Diversity of Endotoxin and its impact on pathogenesis. Journal of Endotoxin Research. 12, 205-223. https://doi.org/10.1179/096805106x118825

Ulrich, J.T. and Myers, K.R., 1995. Monophosphoryl lipid A as an adjuvant. Vaccine Design: The Subunit and Adjuvant Approach. M. F. Powell and M. J. Newman. Boston, MA, Springer US: 495-524.

Vekey, K., 2001. Mass spectrometry and mass-selective detection in chromatography. Journal of Chromatography A. 921, 227-236. https://doi.org/10.1016/s0021-9673(01)00825-1

Wang, R., Chen, L., Cotter, R.J., Qureshi, N. and Takayama, K., 1992. Fragmentation of lipopolysaccharide anchors in plasma desorption mass-spectrometry. *Journal of Microbiological Methods*. 15, 151-166. https://doi.org/10.1016/0167-7012(92)90037-5

Wang, Y., Li, Q., Cheng, S.H., Wu, Y.F., Guo, D.J., Fan, Q.H., Wang, X.F., Zhang, L.H. and Ye, X.S., 2005. Base-promoted rearrangement of sugar epoxides to unsaturated sugars. *Organic Letters*. 7, 5577-5579. https://doi.org/10.1021/ol052128x

Westphal, V.O., Lüderitz, O. and Bister, F., 1952. Über die Extraktion von Bakterien mit Phenol/Wasser. *Z Naturforschung B*. 7, 148-155.

Wu, D., Zhao, Z.M., Kim, J., Razmi, A., Wang, L.L.W., Kapate, N., Gao, Y.S., Peng, K., Ukidve, A. and Mitragotri, S., 2021. Gemcitabine and doxorubicin in immunostimulatory monophosphoryl lipid A liposomes for treating breast cancer. Bioengineering & Translational Medicine. 6, https://doi.org/10.1002/btm2.10188

Xuan, X.C., Hu, G.Q. and Li, D.Q., 2006. Joule heating effects on separation efficiency in capillary zone electrophoresis with an initial voltage ramp. Electrophoresis. 27, 3171-3180. https://doi.org/10.1002/elps.200500871

Youngner, J.S., Feingold, D.S. and Chen, J.K., 1973. Involvement of a chemical moiety of bacterial lipopolysaccharide in production of interferon in animals. *The Journal of Infectious Diseases*. 128, 227-231.

Zahringer, U., Lindner, B., Knirel, Y.A., van den Akker, W.M.R., Hiestand, R., Heine, H. and Dehio, C., 2004. Structure and biological activity of the short-chain lipopolysaccharide

from *Bartonella henselae* ATCC 49882(T). *Journal of Biological Chemistry*. 279, 21046-21054. https://doi.org/10.1074/jbc.M313370200

Zahringer, U., Lindner, B. and Rietschel, E.T., 1994. Molecular-structure of lipid-A, the endotoxic center of bacterial lipopolysaccharides. Advances in Carbohydrate Chemistry and Biochemistry, Vol 50. 50, 211-276. https://doi.org/10.1016/s0065-2318(08)60152-3

Zhou, Z.M., Ribeiro, A.A. and Raetz, C.R.H., 2000. High-resolution NMR spectroscopy of lipid A molecules containing 4-amino-4-deoxy-L-arabinose and phosphoethanolamine substituents - Different attachment sites on lipid A molecules from NH4VO3-treated *Escherichia coli* versus kdsA mutants of *Salmonella typhimurium*. Journal of Biological Chemistry. 275, 13542-13551. https://doi.org/10.1074/jbc.275.18.13542

Appendix

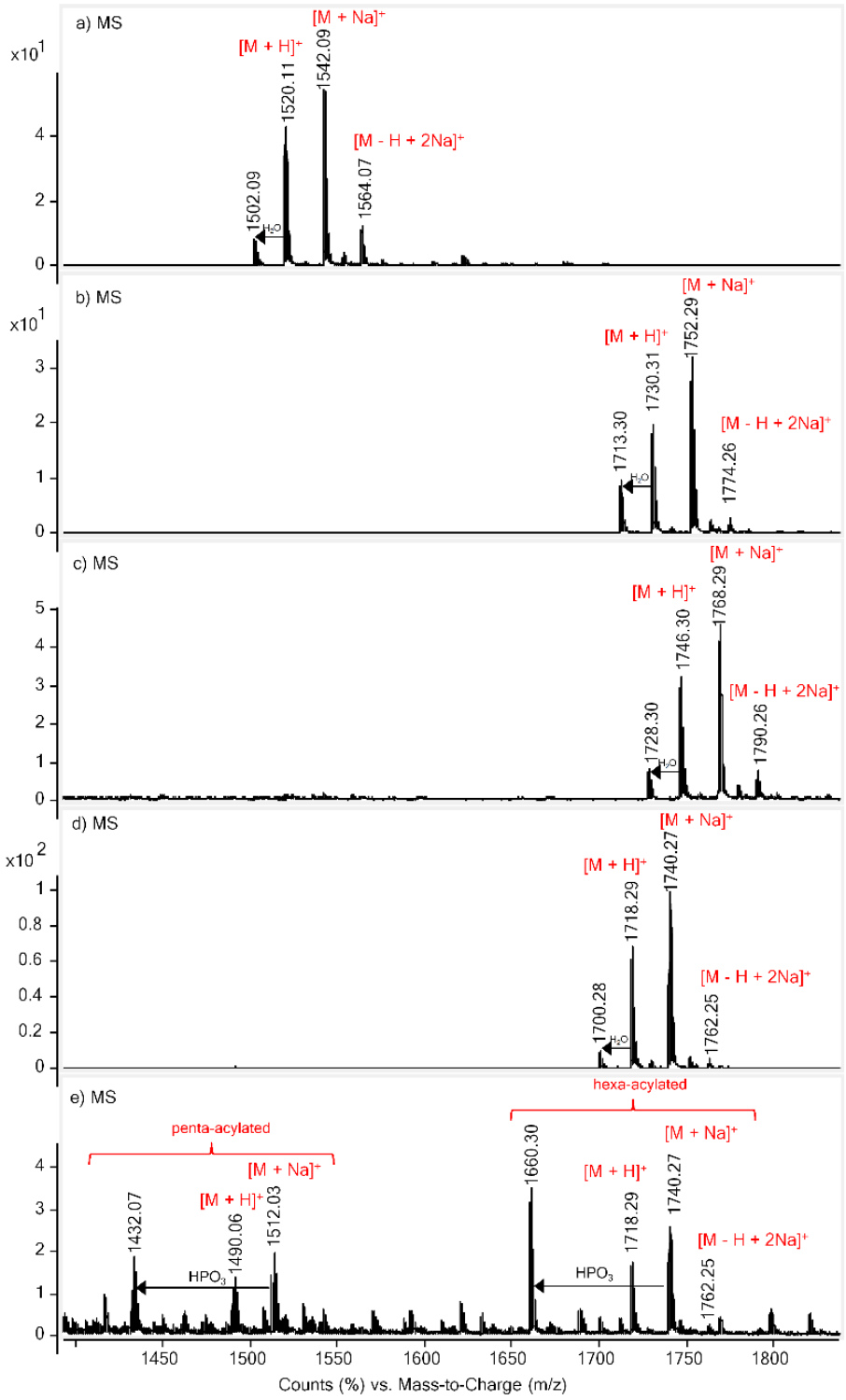

Figure A1. ESI-Q-TOF MS mass spectra of a) 3D-PHAD b) 3D(6-acyl)-PHAD, c) PHAD, d) PHAD-504 and e) lipid A extracted from *E. coli* O83 (as described in Materials and Methods, all samples were dissolved in MeOH/DCM 70/30 v/v, before addition of ammonium formate and NaCl).

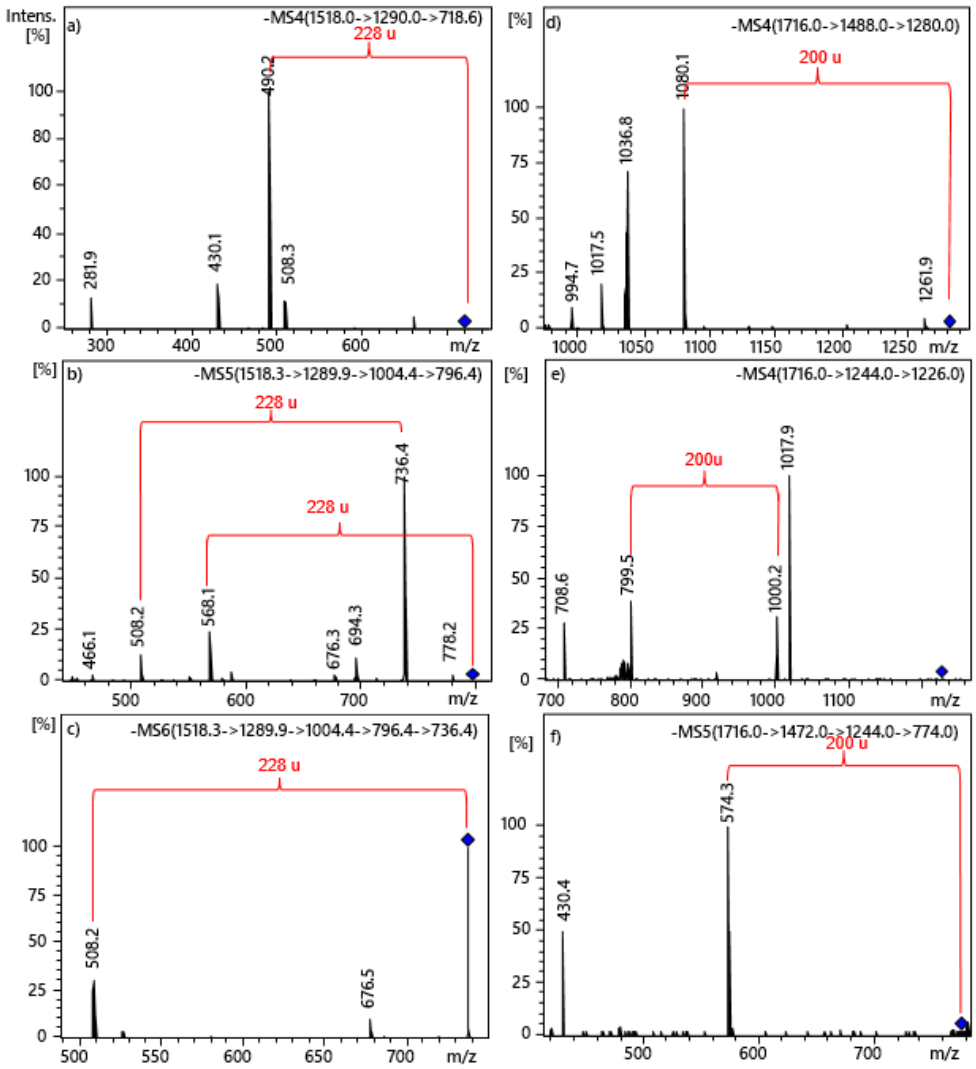

Figure A2. ESI-ion trap mass spectra obtained at MS^4, MS^5 and MS^6 stages for several fragment ions of 3D-PHAD (a, b, c) and of PHAD-504 (d, e, f), demonstrating the release of myristic acid (228u) as an acid or of lauric acid (200 u) as an acid from the C-2' secondary position.

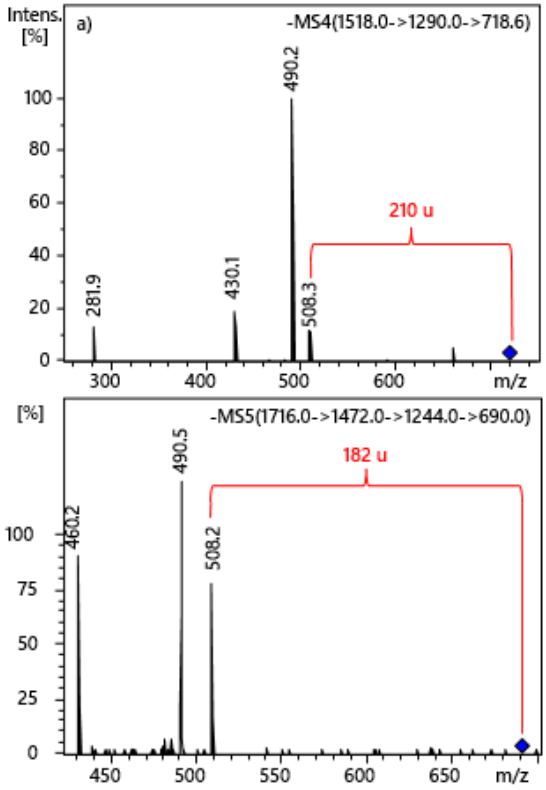

Figure A3. ESI-ion trap mass spectra obtained at a) MS^4 stage of the selected ion at *m/z* 718 for 3D-PHAD, demonstrating the release of myristic acid (210 u) as a ketene from the C-2' secondary position, and b) at MS^5 stage of the selected ion at *m/z* 690 for PHAD-504, demonstrating the release of lauric acid (182 u) as a ketene from the C-2' secondary position.

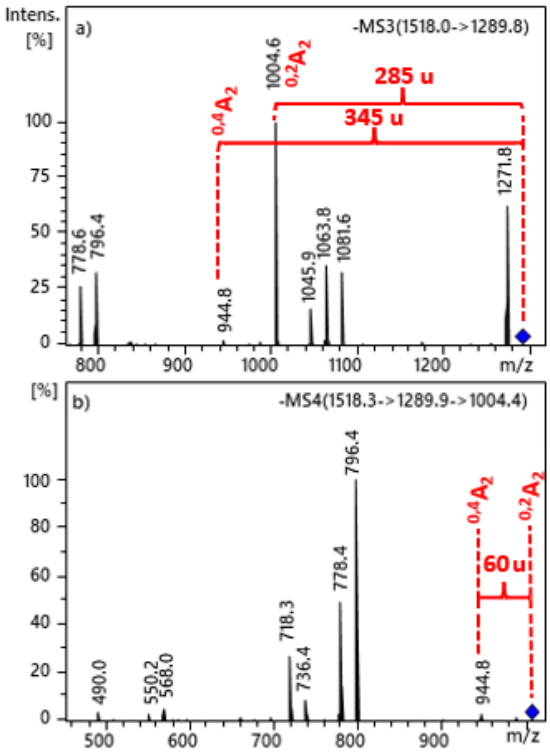

Figure A4. ESI-ion trap mass spectra obtained at MS^3 and MS^4 stages of selected precursor ions at a) *m/z* 1290 and b) *m/z* 1005 for 3D-PHAD, demonstrating the structural relationship between $^{0,2}A_2$ and $^{0,4}A_2$ cross-ring fragment ions in 3-deacyl lipid A.

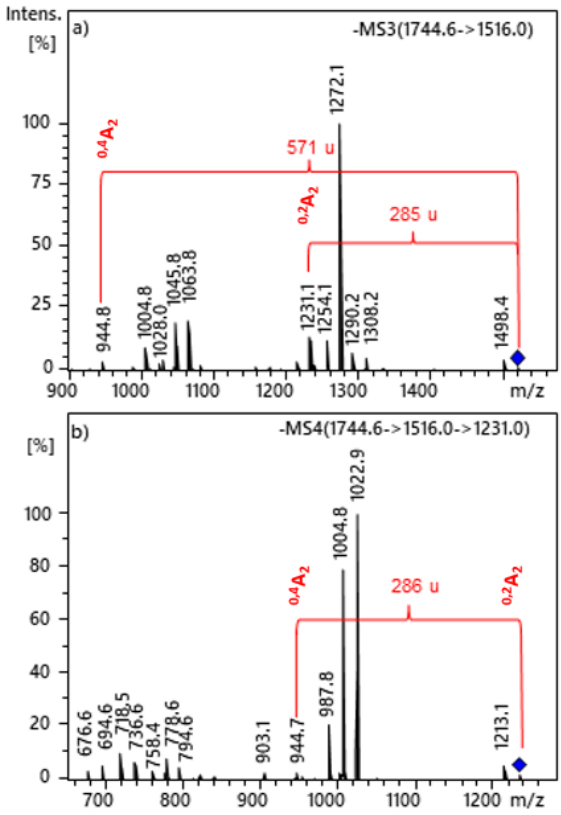

Figure A5. ESI-ion trap mass spectra obtained at MS^3 and MS^4 stages of selected precursor ions at a) *m/z* 1516 and b) *m/z* 1231 for PHAD, demonstrating the structural relationship between $^{0,2}A_2$ and $^{0,4}A_2$ cross-ring fragment ions in 3-acyl lipid A.

List of publications

Publications related to the PhD thesis

1. Study on the CID Fragmentation Pathways of Deprotonated 4'-Monophosphoryl Lipid A.
   Ibrahim Aissa, Anikó Kilár, Ágnes Dörnyei.
   Molecules **2021**, 26, 5961. (IF: 4.924, Q1)

2. Complete Structural Elucidation of Monophosphorylated Lipid A by CID Fragmentation of Protonated Molecule and Singly-Charged Sodiated Adducts.
   Ibrahim Aissa, Ágnes Dörnyei, Viktor Sándor, Anikó Kilár.
   Journal of the American Society for Mass Spectrometry **2022**, 34(1), 92–100. (IF: 3.262, Q2)

3. Characterization of Isomeric Lipid A Species from *Pseudomonas aeruginosa* PAO1 by Non-Aqueous Capillary Electrophoresis with Positive and Negative Ion Electrospray Tandem Mass Spectrometry.
   Viktor Sándor, Bettina Űrmös**, Ibrahim Aissa**, Ágnes Dörnyei, Anikó Kilár.
   Arabian Journal of Chemistry **2023**, 16(8), 104944 (IF: 6.212, Q1)

Publications not related to this thesis

4. Isocostic Acid, a Promising Bioactive Agent from The Essential Oil of *Inula Viscosa* (L): Insights from Molecular Docking and SAR Analysis.
   Ibrahim Aissa, Vijaykumar D Nimbarte, Afifa Zardi-Bergaoui, Mansour Znati, Guido Flamini, Roberta Ascrizzi, Hichem Ben Jannet.
   Chemistry & biodiversity **2019**, 16(4), e1800648 (IF: 2.03, Q3)

5. GC, GC-MS, and NMR Spectroscopy Integrated Analyses and *In Vitro* Antibacterial, Anticholinesterase, Anti-tyrosinase and Anti-5 lipoxygenase, Potential of *inula viscosa* (L) Root Fractionated Essential Oil.
   Ibrahim Aissa, Mansour Znati, Afifa Zardi-Bergaoui, Guido Flamini, Roberta Ascrizzi, Hichem Ben Jannet.
   South Africa Journal of Botany **2019**, 125, 386-392 (IF: 1.79, Q2)

Oral presentations related to the PhD thesis

1. Strategy for Structural Elucidation of Lipid A: Elucidation of Protonated and Disodiated Molecules using CID based MS/MS and MS^n Methods.
   Ibrahim Aissa, Ágnes Dörnyei, Viktór Sándor, Anikó Kilár.
   33rd International Symposium on Chromatography
   Budapest, Hungary, 2022.

2. Étude des Lipides A Monophosphorylés par Spectrométrie de Masse en Tandem (MS/MS et MS^n) et Exploitation de Nouveaux Processus de Fragmentation par des Calculs de Chimie Quantique Standards.
   Ibrahim Aissa, Anikó Kilár, Ágnes Dörnyei.
   REncontres de Chimie Organique Biologique 18^{éme} edition
   Aussois, France, 2022.

3. Structural characterization of isomeric lipid A species by NACE–ESI-MS/MS method.
   Ibrahim Aissa, Viktor Sándor, Bettina Űrmös, Anikó Kilár, Ágnes Dörnyei.
   Anakon
   Vienna, Austria, 2023.

Poster presentations related to the PhD thesis

4. Lipid-A Foszforilációs- és Acilációs Izomereinek Elválasztása és Szerkezeti Jellemzése NACE-ESI-MS/MS Módszerrel.
   Anikó Kilár, Viktor Sándor, Ágnes Dörnyei, **Ibrahim Aissa**, Béla Kocsis, Ferenc Kilár.
   „METT25" A Magyar Elválasztástudományi Társaság jubileumi konferenciája Egerszalók, Hungary, 2021.

5. Prediction of the Fragmentation Pathways of Deprotonated 4'-Monophosphoryl Lipid A by Using low Energy Collision Induced Dissociation (CID) Mass Spectrometry.
   Ibrahim Aissa, Anikó Kilár, Ágnes Dörnyei
   REncontres de Chimie Organique Biologique 18^{éme} edition
   Aussois, France, 2022.

6. Workflow for Structural Elucidation of Protonated and Disodiated Lipid A Molecules using Low Energy CID Tandem Mass Spectrometry.
   Ibrahim Aissa, Ágnes Dörnyei, Viktor Sándor, Anikó Kilár.
   20th International Symposium and Summer School on Bioanalysis
   Pécs, Hungary, 2022.

7. Characterization of Isomeric Lipid-A Species from *Pseudomonas Aeruginosa* by non-Aqueous CE-MS/MS with Collision-Induced Dissociation.
   Viktor Sándor, Anikó Kilár, Bettina Űrmös, **Ibrahim Aissa**, Ágnes Dörnyei.
   20th International Symposium and Summer School on Bioanalysis
   Pécs, Hungary, 2022.

8. NACE-ESI-MS/MS Method for the Separation and Characterization of Phosphate and Acyl Chain Positional Isomers of Bacterial Lipid A.

Anikó Kilár, Ágnes Dörnyei, **Ibrahim Aissa**, Viktor Sándor.
20th International Symposium and Summer School on Bioanalysis
Pécs, Hungary, 2022.

9. NACE-ESI-MS/MS Method for the Separation and Characterization of Phosphate and Acyl Chain Positional Isomers of Bacterial Lipid A.
Anikó Kilár, Ágnes Dörnyei, **Ibrahim Aissa**, Viktor Sándor.
APCE-CECE ITP-IUPAC
Siem Reap (Angkor Wat), Cambodia, 2022.

Poster presentations not related to the PhD thesis

10. Etude de la Composition Chimique et de l'Activité Antibactérienne de l'Huile Essentielle et de ses Fractions Extraite des Feuilles Fraîches d'*Inula viscosa*.
Ibrahim Aissa, Mansour Znati and Hichem Ben Jannet
International Gongress Of Applied Chemistry & Environment
Sousse, Tunisia, 2018.

11. Etude Chromatographique de l'Huile Essentielle des Feuilles d'*Inula viscosa* (L.): Accès à l'Acide Isocostique et sa Valorisation Biologique
Ibrahim Aissa and Hichem Ben Jannet.
The Second International Symposium: Medicinal Plants and Materials
Tozeur, Tunisia, 2019.

12. Etude de la Composition Chimique et des Activités Antibactérienne, Anticholinestérase, Anti-tyrosinase et Anti-5-lipoxygénase de l'Huile Essentielle et de ses Fractions Extraites des Racines d'*Inula viscosa* (L.).
Ibrahim Aissa and Hichem Ben Jannet.
The Second International Symposium: Medicinal Plants and Materials
Tozeur, Tunisia, 2019.

13. Novel 1,2,3-Triazoles Linked Isocostic Acid: Design, Microwave Assisted Synthesis and Evaluation as Antibacterial Agent.
Ibrahim Aissa and Hichem Ben Jannet.
Troisième Colloque Maghrébin sur la Chimie Hétérocyclique Monastir, Tunisia, 2019.